Master Thesis

Torsion in ZIP bridge system

Final version

Name: Evert van Vliet
21-1-2012
Student number: 1304356
E-mail: vvevert@gmail.com

Graduation committee

Chairman
Prof. dr. ir. J.C. Walraven
Department of Structural Engineering, Concrete Structures
Faculty of Civil Engineering and Geosciences
Delft University of Technology

Committee members
Dr.ir. C. van der Veen
Department of Structural Engineering, Concrete Structures
Faculty of Civil Engineering and Geosciences
Delft University of Technology

Dr. ir. P.C.J. Hoogenboom
Department of Structural Engineering, Structural Mechanics
Faculty of Civil Engineering and Geosciences
Delft University of Technology

External committee member
Ir. C. Quartel
Manager infra
Spanbeton B.V. at Koudekerk aan de Rijn

Secretary
Ir. L.J.M. Houben
Department of Structural Engineering, Road and Railway Engineering
Faculty of Civil Engineering and Geosciences
Delft University of Technology

Preface

This master thesis is written to finalize my study Civil Engineering at the department of Concrete Structures at the Delft, University of Technology. The work is done from April 2011 till January 2012 at the office of Spanbeton.

The study is related with the work done by Kassahun Minalu, which was done also at Spanbeton. This study is presented in the thesis 'Finite element modelling of skew slab-girder bridges'. In this study different models with and without end diaphragm beams, with different skew angles and different stiffnesses are studied with a number of finite element models.

The question that was still open after this research was the 'real behaviour' under torsion. Will cracks already appear in Serviceability Limit State or is crack forming delayed till Ultimate Limit State? Can torsion be used for equilibrium? These fundamental questions are studied with the program ATENA of Cervenka Consulting and checked with calculations of the principal stresses.

Without help of others I would not have reached the result presented in this report. First of all I thank Dobromil Pryl, employee of Cervenka Consulting for his help during making a working model in ATENA 3D. The help of Kees Quartel, Sander den Hertog, Dirk Post and Math Pluis at Spanbeton gave a good motivation to do the job, also the other colleagues always were interested and helpful. The advice of Joost Walraven, Cor van der Veen and Pierre Hoogenboom at Delft University was of great importance for the scientific level of the master thesis. Especially the debates with Pierre Hoogenboom about fundamental mechanical issues were very interesting. I will thank them all for their input and help.

For the Dutch reader a translation of the abstract, conclusions and recommendations is included in this report.

Evert van Vliet
Koudekerk aan den Rijn, January 2012

Samenvatting

In scheve bruggen treedt torsie op, wat leidt tot substantiële hoeveelheden wapeningsbeugels. Minalu heeft reeds onderzoek gedaan naar torsie in deze scheve brugdekken met behulp van verschillende typen eindige elementen modellen. De vraag die nog onbeantwoord is en de hoofdvraag van dit onderzoek vormt, is het moment waarop werkelijk torsiescheuren ontstaan en de wapening functioneel wordt.

De focus ligt op een scheef brugdek met een kruisingshoek van 45 graden omdat daarin de grootste torsiemomenten optreden. Zijdelings is ook een recht brugdek geanalyseerd, de torsiemomenten in een recht brugdek zijn namelijk altijd lager dan in een scheef brugdek. De belastingen volgens de Eurocode 1991-2 zijn gebruikt. Twee belangrijke belastingsconfiguraties voor torsie en dwarskracht zijn onderzocht: een configuratie die dagelijks bij Spanbeton wordt gebruikt en een configuratie ontwikkeld door Minalu.

Er is een poging gedaan om het gehele brugdek fysisch niet-lineair te modelleren met ATENA 3D om daarmee torsie-effecten te kunnen analyseren. Dat bleek met de huidige stand van de techniek onmogelijk. Daarom is een vereenvoudigde modellering ontwikkeld waarmee de spanningstoestand en scheurvorming in de eerste ZIP-ligger kunnen worden gesimuleerd. Bij het simuleren van torsiespanningen in een 3D model blijkt het belangrijk te zijn om kwadratische elementen te gebruiken om correcte schuifspanningen te verkrijgen. Uit dat model volgt, ondanks tekortkomingen in het model, duidelijk dat er een groot ongescheurd gebied in de ligger aanwezig is in de uiterste grenstoestand.

Om zekerheid te hebben over de juistheid van het computermodel kunnen de hoofdspanningen in de ligger worden gecontroleerd, dit is gedaan voor de uiterste grenstoestand. De spanningen door voorspanning, het eigen gewicht en het gewicht van het natte dek kunnen met handberekeningen worden bepaald. De spreidingsberekening kan worden uitgevoerd met eindige elementen methoden. Scia Engineer (orthotrope plaat) en ATENA 3D (volume elementen) zijn gebruikt voor deze berekening. Vooral de bepaling van de torsiemomenten uit ATENA door een analyse van de rotaties is interessant. Uit deze berekeningen volgen torsiemomenten, buigende momenten en dwarskrachten.

De hoofdconclusie van dit onderzoek is dat in uiterste grenstoestand geen scheurvorming optreedt in het einde van de beschouwde ligger in het scheve brugdek. Dat betekent dat alleen minimale wapening hoeft worden toegepast en dat de volledige torsiestijfheid in berekeningen kan worden gebruikt. Tot slot is er een praktische methode gepresenteerd om ook hoofdspanningen in andere ZIP brugdekken te controleren.

Conclusies

1. Het is onmogelijk om een gehele brug fysisch niet-lineair met volume-elementen te modelleren. Een grove schatting is dat dit over achttien jaar wel mogelijk is. Het is nu wel mogelijk om de brug lineair elastisch te modelleren met grove lineaire of kwadratische elementen. Door deze modellering is er slechts één element aanwezig over de dikte van het lijf. Torsieschuifspanningen worden in deze grove elementen niet correct berekend. Over de dikte van het lijf zijn minimaal drie kwadratische elementen nodig om accurate torsieschuifspanningen te verkrijgen (Hoofdstuk 4).

2. Het is mogelijk om voor één ligger een nauwkeurig fysisch niet-lineair model te ontwikkelen. In dit model kunnen scheurvorming en scheurwijdtes worden geanalyseerd. Het realistisch aanbrengen van de belasting op deze ligger is moeilijk. In theorie kunnen de elastische

vervormingen, gevonden met het lineair elastische model van de gehele brug, aangebracht worden op de ligger. Het accuraat aanbrengen van deze vervormingen vergt ten eerste veel tijd. Daarnaast ontstaan door het lokaal aanbrengen van de opgelegde vervormingen en onvolkomenheden in de modellering onjuiste spanningen in het model. Het ontwikkelde model geeft ondanks de onvolkomenheden een goede indruk van de aanwezige ongescheurde zone in de ligger (Hoofdstuk 5).

3. Het benaderen van de torsieschuifspanningen in de ligger ter hoogte van het zwaartepunt middels een grove handberekening leidt tot een overschatting in de orde van 40%. Dat komt doordat in de gebruikte doorsnede voor de handberekening de verdeling van de phi-heuvel anders is dan in de echte doorsnede. In de echte doorsnede heeft de phi-heuvel maxima in de verdikking in het lijf en in de onderflens waardoor schuifspanningen naar die zones wordt getrokken. Hierdoor wordt de schuifspanning ter hoogte van het zwaartepunt substantieel verlaagd. Scia Engineer kan gebruikt worden om de schuifspanningen te bepalen waarbij een voldoende fijn net moet worden gebruikt (Hoofdstuk 6).

4. Uit de bepaalde rotaties van de ligger in het lineair elastische volumemodel van de gehele brug kunnen de optredende torsiemomenten worden bepaald. Uit de analyse volgt dat het torsiemoment niet door verhinderde welving (normaalspanningen) maar vooral door zuivere torsie (schuifspanningen) wordt gedragen. Alleen in de zone rond de oplegging heeft verhinderde welving enige invloed, de grootte van de invloed is afhankelijk van de aanwezigheid van een einddwarsdrager (Hoofdstuk 7).

5. Voor de spreidingsberekening kunnen een orthotrope plaat model (Scia Engineer) en een volume model (ATENA 3D) worden gebruikt. Vergelijking van de uitkomsten uit deze modellen laat zien dat de dwarskrachten goed overeen komen, maar dat de torsiemomenten substantiële verschillen vertonen. Dit is opmerkelijk omdat het hier lineair elastische modellen betreft waarvan verwacht zou worden dat ze beter overeen zouden komen (Hoofdstuk 7).

6. In het rapport zijn twee belastingsgevallen parallel uitgewerkt. Het blijkt dat voor het doen van de plastische spanningscontrole beide belastingsgevallen vergelijkbare hoofdspanningen geven. Bij het uitvoeren van een elastische spanningscontrole geeft het belastingsgeval van Minalu de maatgevende hoofdspanningen (Hoofdstuk 7).

7. Uit de berekening van de hoofdtrekspanningen in de eerste ZIP ligger van het beschouwde scheve brugdek volgt dat er in de uiterste grenstoestand een grote ongescheurde zone aanwezig is. Belangrijk is dat hierbij de verstoorde aanhechtzone goed gecontroleerd dient te worden, afhankelijk van de toegestane hoeveelheid plastische herverdeling van de spanningen (Hoofdstuk 7). Impliciet betekent deze conclusie ook dat in de gebruikstoestand geen scheuren zullen optreden. Ook in de rechte brug zal er een soortgelijke ongescheurde zone zichtbaar zijn omdat daarin vergelijkbare dwarskrachten, maar lagere torsiemomenten optreden dan in een scheve brug (Hoofdstuk 5).

Aanbevelingen

A. Dit project is gestart met een tijdrovende fysisch niet-lineaire computermodellering. Het is belangrijk om bij een soortgelijk onderzoek eerst te starten met handberekeningen en lineair elastische computermodellen. Indien nodig kan daarna overgegaan worden naar fysisch niet-lineaire modellen.

B. De hoofdspanningen zijn in dit onderzoek vergeleken met de statische treksterktes van beton. Het aspect vermoeiing van beton is daarbij niet beschouwd. In het geval van een vermoeiingsberekening wordt de toelaatbare treksterkte gereduceerd en moeten ook andere belastingsconfiguraties worden gebruikt. Deze berekening moet nog worden uitgevoerd om te zien of ook daaruit geconcludeerd kan worden dat de ligger een grote ongescheurde zone bevat.

C. Het gepresenteerde onderzoek biedt toekomstperspectieven om de hoeveelheid wapening in de ongescheurde zone te reduceren tot het wettelijke minimum. Uit een onderzoek van één brug met bepaalde geometrische eigenschappen kan geen wetmatigheid worden ontleend. Wel kan een mogelijke procedure worden gepresenteerd om voor elke brug (gebruik makend van ZIP-liggers) te bepalen of het voordeel gebruikt kan worden.

   Mogelijke procedure:

   1) Er dient een <u>spreidingsberekening</u> uitgevoerd te worden waarbij de torsiestijfheid niet wordt gereduceerd. De in het rapport gepresenteerde belastingsgevallen dienen minimaal in beschouwing te worden genomen.
   2) De <u>voorspanning</u> kan berekend worden op de gebruikelijke wijze in de gebruikstoestand. Belangrijk is dat er daarbij in de einden van de ligger geen buigscheuren bovenin de ligger optreden.
   3) De <u>lengte van het ongescheurde gebied</u> in de uiterste grenstoestand kan bepaald worden door te bepalen bij welk buigend moment de treksterkte van beton wordt overschreden. Veilig is om geen trekspanningen toe te laten voor deze berekening. Het is mogelijk dat voor deze berekening het belastingsgeval om het maximale moment in de ligger te bepalen maatgevend is.
   4) De <u>schuifspanningsverdeling</u> door torsie in het profiel kan worden bepaald door met Scia Engineer de doorsnede te analyseren. Het is conservatief om dit met een handberekening te bepalen. De torsieschuifspanningen kunnen plastisch of elastisch verdeeld worden. De schuifspanningen door dwarskracht kunnen op de gebruikelijke manier worden uitgerekend. Deze spanningen kunnen elastisch of plastisch worden gecombineerd.
   5) De optredende <u>normaalspanningsverdeling</u> varieert over de hoogte van de ligger. Belangrijk is de normaalspanning ter hoogte van het zwaartepunt. De hoogte van het zwaartepunt varieert voor de enkele ZIP-ligger en het samengestelde systeem. De maatgevende hoogte ligt ergens tussen deze beide grenzen. Als gekozen wordt om te controle uit te voeren in het zwaartepunt van de ZIP ligger moet rekening gehouden worden met een reductie van de normaalspanning door buigende momenten die optreden in combinatie met het samengestelde zwaartepunt. Dit geldt ook als gekozen wordt om de controle uit te voeren in het samengestelde zwaartepunt Figure 10-17). In dit onderzoek was de reductie maximaal 6%. Daarnaast moet het gunstige effect van de voorspanning in de uiterste grenstoestand moet worden gereduceerd door het te vermenigvuldigen met een factor 0.9.
   6) In het ongescheurde gebied kunnen voor de gevonden schuifspanningen en normaalspanningen de <u>hoofdspanningen</u> worden berekend op de hoogte van het maatgevende zwaartepunt. Als de gevonden spanningen onder de gestelde grenzen liggen kan worden geconcludeerd dat de ligger inderdaad ongescheurd is en de aanname voor volledige torsiestijfheid in het orthotrope plaat model juist was. De minimale wapening voor dwarskracht en torsie dienen te worden toegepast volgens de Eurocode.

Abstract

In skew bridges torsion occurs. This leads to a substantial amount of reinforcement stirrups. Minalu already did research to torsion in bridge decks with different types of finite element models. The question when torsion cracks will really occur is still unanswered. This question is the main subject of this research.

The focus of the research is on a skew bridge with a skew angle of 45 degrees. In that bridge the largest torsional moments will occur. Beside that also a straight bridge is analysed, the torsional moments in a straight bridge are always lower than in a skew one under the same loading. The loads of Eurocode 1991-2 are used. Two important load configurations governing for torsional moments and shear force are used: a configuration which is used in daily practice at Spanbeton and a configuration developed by Minalu.

An attempt is made to model the whole bridge including physically non-linear behaviour with the program ATENA 3D to analyse the torsion effects. With the current state-of-the-art modelling technology that appeared to be impossible. For that reason a simplified model is developed to simulate the stress state and cracking in one ZIP girder. It was concluded that it is important to use more quadratic elements over the thickness of the web to obtain correct torsion shear stresses. From the simplified model it is concluded that, despite some shortcomings, clearly a substantial length at the ends of the girder is uncracked.

To be sure that the computer model is correct a calculation of the principal stresses is carried out at the ultimate limit state. The stresses due to prestressing, own weight and the weight of the fresh poured concrete can be calculated by hand. The calculation of the force distribution of the loads on the deck can be carried out using finite element methods. Scia Engineer (orthotropic plate model) and ATENA 3D (volume elements) are used for this calculation. Especially the determination of the torsional moments from ATENA by using an analysis of the rotations is interesting. This calculation results in the torsional moments, bending moments en shear forces acting on the ends of the girder.

The main conclusion of this research is that in ultimate limit state no cracking will occur in the end of the considered girder in the skew bridge. This means that only the minimal shear reinforcement must be applied and the full torsional stiffness can be used in finite element calculations. A practical method to check this for other bridges using ZIP-girders is proposed.

Contents

1 Introduction

1.1 Background

As mentioned in the preface the cracking behaviour of a ZIP girder is the main topic of this research. The loads in a ZIP bridge system are mainly carried by longitudinal and transverse bending moments but also torsion can also be used to satisfy the equilibrium. Normally in that case a high amount of torsion reinforcement must be applied. In daily practice Spanbeton uses an orthotropic two dimensional plate model to determine the load distribution in a bridge. An interesting question is which torsion stiffnesses are allowed and safe for Serviceability Limit State (SLS) and Ultimate Limit State (ULS).

Logical reasoning results in the following chain of events that occur during loading. In the beginning the beams are uncracked in SLS. In this stage the reinforcement stirrups are not stressed, so unnecessary. After this phase the cracking phase is reached. In this phase the stiffness is reduced and therefore the torsional moments (and related shear stress) will decrease. Depending on the amount of cracks the forces will be carried by longitudinal and transverse moments. It is safe to design the bridge using only bending moments, already stated by Minalu[1]. However, it will be beneficial to use the torsion for equilibrium when that is available.

So, fundamentally the real torsional stiffness is directly related to the amount of cracks present. When no cracks occur the entire stiffness will be available. If cracks do occur a reduction is necessary. ATENA 3D contains tools for physical non-linear modeling which can be used to analyze the reduced stiffness. A finite element model will be developed to analyze this.

Note: In the first stage of the research also investigation of Compressive Membrane Action (CMA) was intended, following a recommendation of Minalu. The work done for that topic is presented in Appendix A.

1.2 Approach

Main points of research are:

1. *Literature.* Some relevant points from the report of Minalu are presented. Also the fundamental theories about torsion in plain and cracked concrete are described.
2. *Finding a working model to simulate torsion effects in the girders.* First an attempt is done to model a whole bridge including physically non-linear behaviour. This appeared to be impossible. A simplification is developed. The occurring stresses and cracking behaviour will be presented and interpreted.
3. *An analytic analysis of the principal stresses in the first ZIP girder.* The stresses in the end of the girder are investigated in detail. Hand calculations are used when possible. When this was not possible calculations with orthotropic plate (Scia Engineer) and volume element (ATENA 3D) models are used.

[1] Minalu, Kassuhun K. (2010), *Finite element modelling of skew slab-girder bridges.* Page 114.

2 Torsion

2.1 Introduction

In bridges torsion occurs. The amount of torsion is dependent on many factors but the most important one for this thesis is the skew angle of the bridge which was investigated by Minalu. In his thesis a comparison was made between different types of FEM but also some conclusions were written about torsion effects.

2.2 Relevant parts from report of Minalu[2]

2.2.1 Considered cases

Minalu investigated the cases presented in Table 2-1 with different modelling techniques.

Number	End diaphragm beams	Girders
a.	Consider stiffness	Full torsional stiffness in SLS
b.	Consider stiffness	Reduced torsional stiffness in ULS
c.	Disregard stiffness	Full torsional stiffness in SLS
d.	Disregard stiffness	Reduced torsional stiffness in ULS
e.	Consider stiffness	Disregard torsional stiffness
f.	Disregarding stiffness	Disregard torsional stiffness

Table 2-1 Performed studies by Minalu

2.2.2 Relevant conclusions

The maximum torsional moment is near the obtuse corner. A governing load case is placing the first design lane load and the axle loads at the first notional lane and leaving the other lanes unloaded.

Ignoring the torsional stiffness of the girders had very little influence on the maximum bending moments. However, detailing rules to avoid excessive cracking should be consulted (Eurocode 1992-1-1).

A linear elastic 3D model gives tension normal force in the transverse direction of the deck. When cracking is included the tensile membrane force becomes a compressive force. Therefore linear elastic analysis is not appropriate to determine the CMA in the deck.

Live load moments in girders of skew bridges are generally smaller than those in straight bridges of the same span and deck width. On the contrary the torsional moments in the obtuse corner of the bridge and the transverse moments in the deck increases with skew angles.

End diaphragm beams decrease the bending and twisting moments in the girders and the deck. However, this reduction was insignificant as compared to the torsional moments occurring in the diaphragm beams.

2.2.3 Relevant recommendations

End diaphragm beams could be excluded from the finite element model. They can be designed with minimum reinforcement.

For small skew angles the presence of end diaphragm beams results only in a small reduction of the longitudinal bending moments and the torsions for vertical loading. The concrete diaphragms could be replaced by simple non-structural elements. Detailed investigation of the consequences is required.

[2] Minalu, Kassuhun K. (2010), *Finite element modelling of skew slab-girder bridges*

2.3 Theory[3,4]

2.3.1 Uncracked beam

In an uncracked beam stresses develop as shown in Figure 2-1. At the middle of the longitudinal edges the maximum stresses occur.

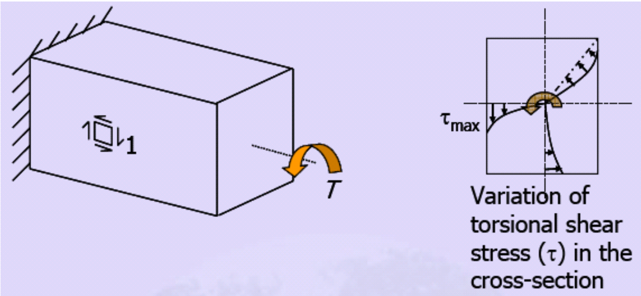

Figure 2-1 Stresses in uncracked beam subjected to torsion

The occurring shear stresses can be expressed in principal stresses using Mohr's circle as shown in Figure 2-2.

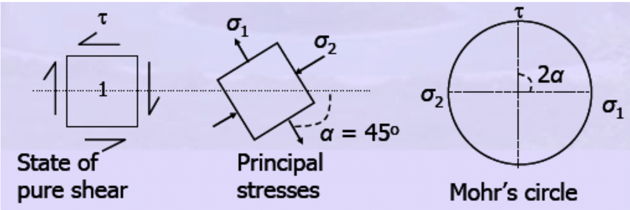

Figure 2-2 State of stresses

These principal stresses explain the crack pattern. Cracks occur perpendicular to the direction of the tensile stresses when the tensile strength is reached. In the uncracked state the stress carried by steel is negligible. After cracking there is redistribution of stresses between concrete and steel.

Saint Venant presented a theory for torsion. In this theory the cross-section rotates and warps (function ψ). There is a differential equation for warping available. A more practical method to calculate shear stresses and torsional stiffness in rectangular cross sections is to use the standardized table, Table 2-2.

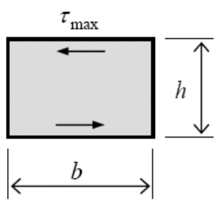

Figure 2-3 Rectangular cross section

[3] Sengupta, dr. Amlan K. et. al. *Prestressed concrete structures*
[4] Hoogenboom, P.C.J. (2010), *Aantekeningen over wringing*

$\frac{b}{h}$	$\frac{I_w}{bh^3}$	$\frac{I_p}{bh^3}$	$\frac{M_w}{\tau_{\max} bh^2}$	$1000\frac{C_w}{b^3h^3}$	$\frac{100\,B}{\sigma_{\max} b^2h^2}$
1,0	0,141	0,167	0,211	0,134	0,368
1,2	0,166	0,203	0,221	0,352	0,565
1,4	0,187	0,247	0,230	0,838	0,987
1,6	0,204	0,297	0,237	1,418	1,37
1,8	0,218	0,353	0,243	2,000	1,69
2,0	0,229	0,417	0,249	2,540	1,94
2,5	0,250	0,604	0,261	3,640	2,35
3,0	0,264	0,833	0,271	4,416	2,59
4,0	0,281	1,417	0,288	5,354	2,82
5,0	0,292	2,167	0,299	5,865	2,90
10,0	0,314	8,417	0,323	6,642	2,94
50,0	0,331	208,417	0,329	6,931	2,82
∞	0,333	∞	0,333	6,944	2,778

Table 2-2 Properties of rectangular cross-sections (Roark's formulas for stress and strain)

Is it allowed to resist torsion only with plain concrete when that's theoretically possible? In NEN-EN 1992-1-1 the following is stated in 6.3.1.2:
Where, in statically indeterminate structures, torsion arises from consideration of compatibility only, and the structure is not dependent on the torsional resistance for its stability, then it will normally be unnecessary to consider torsion at the ultimate limit state. In such cases a minimum reinforcement, given in Sections 7.3 and 9.2, in the form of stirrups and longitudinal bars should be provided in order to prevent excessive cracking.

2.3.2 Cracked beam

First cracks are visible at the longitudinal edge of the (rectangular) cross-section. Under pure torsion the cracks follow the stresses under 45˚. The formation of cracks is visualised in Figure 2-4. In a real structure always interaction occurs and the crack pattern is more complicated.

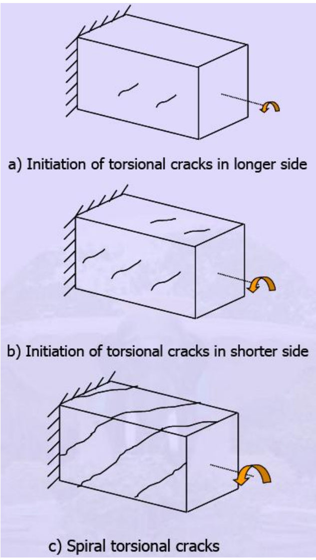

Figure 2-4 Development of cracks under torsion

When the girder is cracked it can be considered as an three-dimensional truss. The steel (longitudinal reinforcement and stirrups) forms the tension elements and the concrete compressive elements the struts (Figure 2-5). The maximum torsion capacity is bounded by the capacity of the concrete struts or the steel tensile elements.

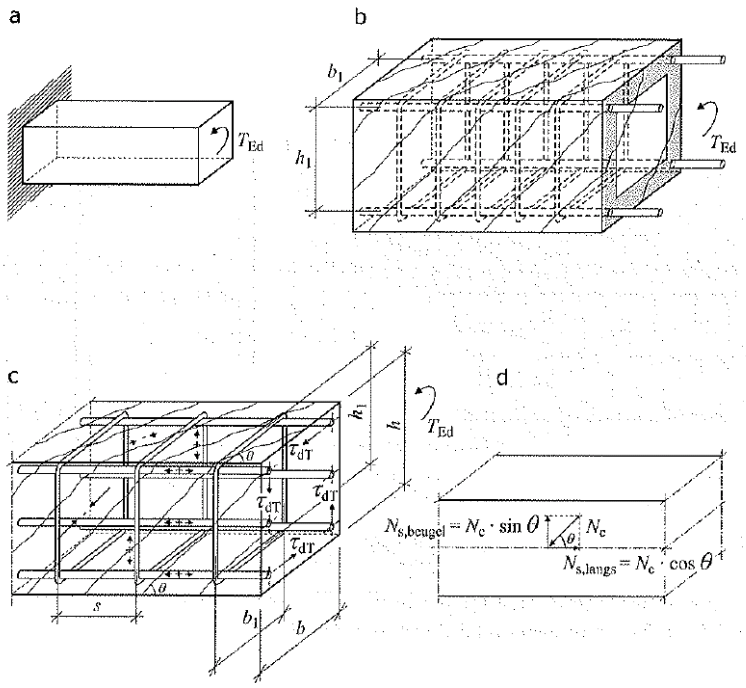

Figure 2-5 Three-dimensional truss model for torsion

2.3.3 Influence prestressing

The level of prestressing has a positive effect on the level that torsion cracks occur (Figure 2-6). The normal stresses can also be incorporated in the calculation of the principal stresses as shown in Figure 2-7. Consequently, the cracking direction will change.

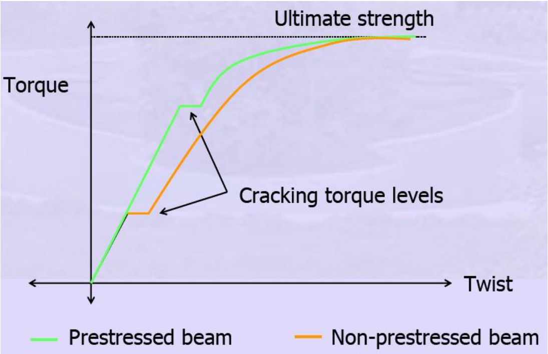

Figure 2-6 Schematized behaviour of concrete beam under torsion load

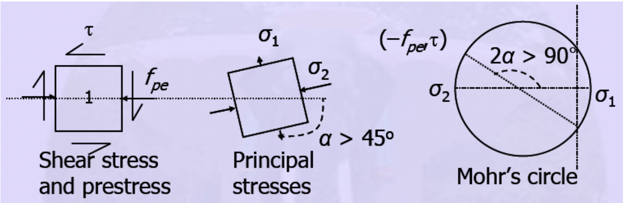

Figure 2-7 State of stresses in a prestressed beam

After cracking the crack width of a spiral crack is low. Thus the aggregate interlock is larger as compared to a non-prestressed beam under the same twisting moment. Zia and McGee showed that the contribution of the concrete to the ultimate torsional strength is much larger for prestressed than for non-prestressed beams.[5] They also present formulas to calculate the beneficial effect of the prestressing.

[5] Zia and McGee (march-april 1974), *Torsion design of prestressed concrete,* , PCI Journal, page 46 – 65

2.3.4 Interaction

2.3.4.1 Torsion and shear

For the interaction between torsion and shear a formula is presented in the NEN-EN 1992-1-1 and NEN-EN 1992-2 to sum up the effects. Both shear and torsion are calculated separately and combined in:

- Only minimum reinforcement:

$$\frac{T_{Ed}}{T_{Rd,c}} + \frac{V_{Ed}}{V_{Rd,c}} \leq 1{,}0$$

- Maximum capacity concrete:

$$\frac{T_{Ed}}{T_{Rd,max}} + \frac{V_{Ed}}{V_{Rd,max}} \leq 1{,}0$$

2.3.4.2 Torsion and bending

In the Eurocodes (mentioned in 2.3.4.1) no demands are set for the interaction between torsion and bending. However, literature is available , named Skew Bending Theory, which shall be briefly presented.[6]

Starting point of the theory is that torsion and bending moments can be combined to one resultant moment. This moment causes compression and tension in a planar surface inclined to the axis of the beam, see Figure 2-8.

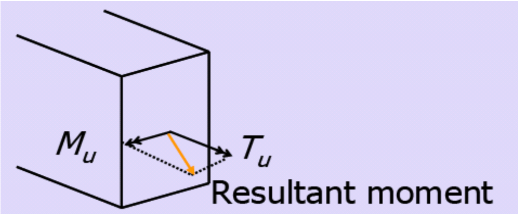

Figure 2-8 Torsional and bending moments combined

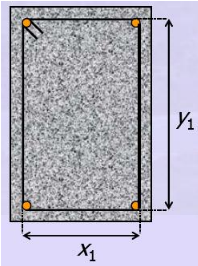

Figure 2-9 Dimensions of closed stirrup

The modes of failure are explained based on the relative magnitudes of the flexural moment (M_u) and torsional moment (T_u) in the ultimate limit state. For each mode an idealised pattern of failure is presented with the resultant compression (C_u) and tension forces (T_u).

[6] Rangan, B. V. and Hall, A. S. (March 1975), *Design of Prestressed Concrete Beams Subjected to Combined Bending, Shear and Torsion*, ACI Journal, American Concrete Institute, Vol. 72, No. 3, page 89 – 93

For design the following steps are important:

1. Calculate equivalent moment M_t from T_u:

$$M_t = T_u \cdot \sqrt{1 + \frac{2D}{b}}$$

2. For design of primary longitudinal reinforcement (bottom) equivalent moment M_{e1} is calculated (mode 1 failure, Figure 2-10):

$$M_{e1} = M_u + M_t$$

3. When $M_t > M_u$ (mode 2 failure, Figure 2-11)

$$M_{e3} = M_t \cdot \left(1 + \frac{x_1}{2e}\right)^2 \left(\frac{1 + \frac{2b}{D}}{1 + \frac{2D}{b}}\right) \; with\; e = \frac{T_u}{V_u}$$

4. When $M_t > M_u$ (mode 3 failure, Figure 2-12):

$$M_{e2} = M_t - M_u$$

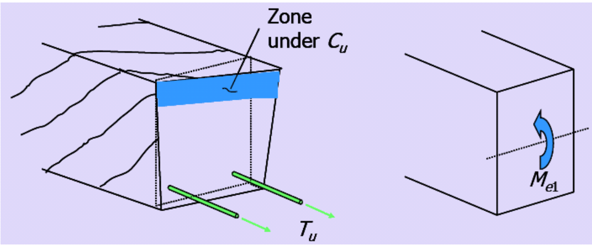

Figure 2-10 Mode 1 failure

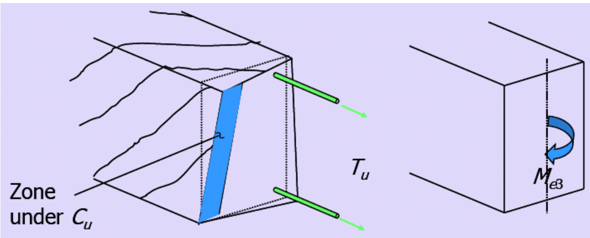

Figure 2-11 Mode 2 failure

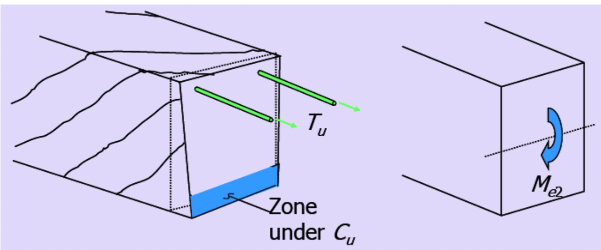

Figure 2-12 Mode 3 failure

3 Description of bridge

3.1 Geometry

The bridges that will be investigated are visualized in Figure 3-1, the axis for the models of the complete bridges are presented in the top view. A cross section is presented in Figure 3-2. The first ZIP is the interesting girder in the research, this girder is shaded grey in the top view.

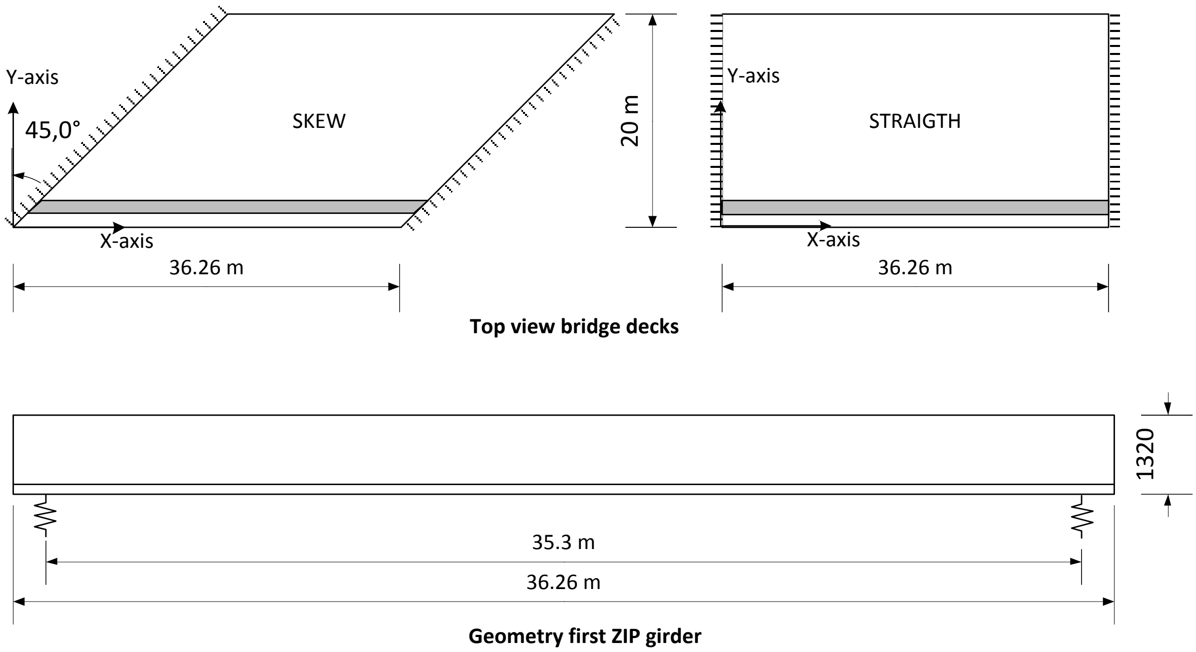

Figure 3-1 Geometry of bridges

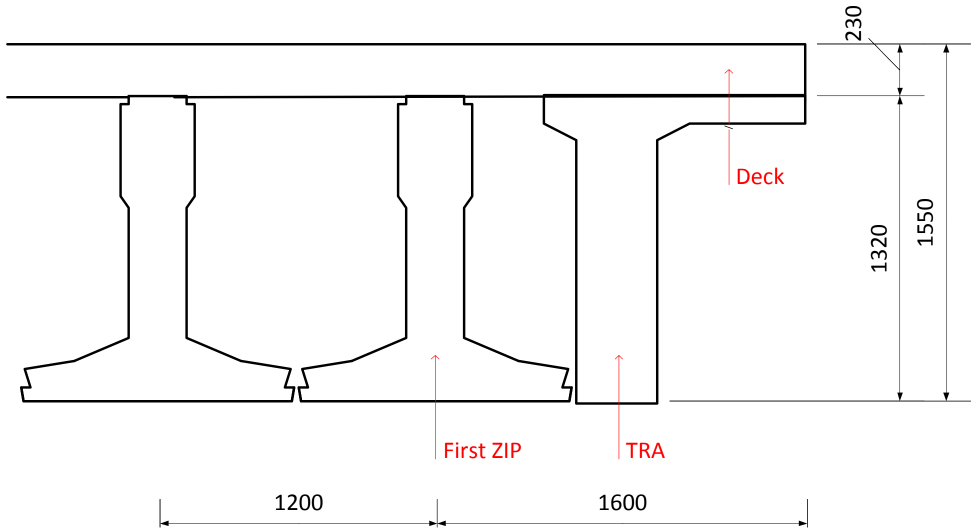

Figure 3-2 Cross-section edge of bridge (simplified height of deck)

3.2 Important properties

Girders:

Concrete quality:	C53/65
E-modulus:	38000 MPa
Poisson's ratio:	0.2

Deck:

Concrete quality:	C28/35
E-modulus:	16000 MPa (half of the stiffness in both directions)
Poisson's ratio:	0.2
Spring stiffness (rubber supports):	1130 MN/m (calculation presented in thesis Minalu[7])

In the calculation full torsional stiffness is used and half of the normal stiffness of the deck (in both directions). This is done because it is impossible to model the bridge else in ATENA. The girder will consequently take larger part of the torsional moment, this is conservative. Later in the project it was noted that for the different longitudinal and transversal bending stiffnesses in the deck a trick can be used using smeared reinforcement in the stiffest direction, this is not applied.

3.3 Construction stages

Important for the analysis is the fact that the bridge will be constructed in several stages:

A. The ZIP-girder is loaded by own weight and prestressing and the fresh poured concrete of the deck.
B. The fresh concrete is hardened and the ZIP-girders forms a system with the deck. This system bears the permanent and variable loads applied on the bridge deck.

3.4 Loads construction stage A

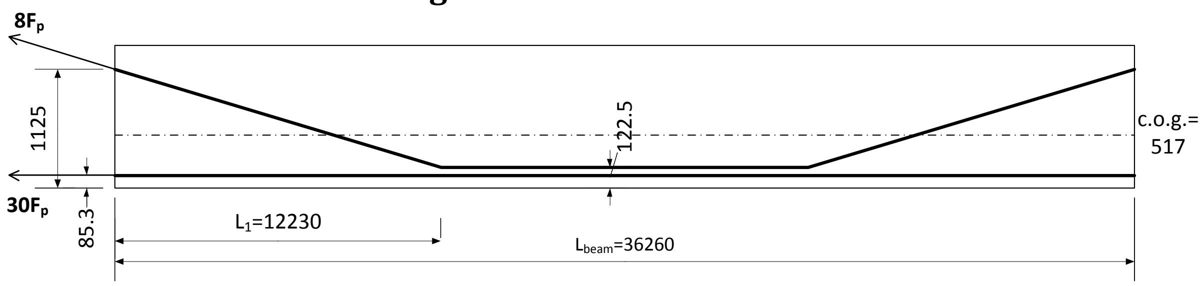

Figure 3-3 Configuration of prestressing strands

Prestressing force:	$161 < F_p < 187$ kN
Dead weight girder:	14.25 kN/m
Fresh poured concrete:	6.1 kN/m

3.5 Loads construction stage B

3.5.1 Permanent loads on deck

Edge load

- Handrail: 2.0 kN/m. Placed 0.17 m from the edge.
- Strip grazing: 0.4x25=10 kN/m^2, uniformly distributed on a width of 380 mm.
- Safety barrier: 1 kN/m. Placed at 0.973 m from edge.
- Footpath: 0.5x(0.215+0.23)x25=5.56 kN/m^2. Placed at 0.38 to 1.145 m from edge.

Asphalt

A layer of 140 mm asphalt is provided for the whole carriage way: 0.14x23=3.22 kN/m^2.
This is applied from 1400 mm to 18600 mm.

[7] Minalu, Kassuhun K. (2010), *Finite element modelling of skew slab-girder bridges*. Page 26.

3.5.2 Variable loads on deck; Load Case Spanbeton

The loads of Eurocode 1991-2 are applied to make a realistic calculation and comparison with the daily practice of calculating ZIP-systems. Spanbeton uses this combination in daily practice to get the governing combination for shear and torsion.

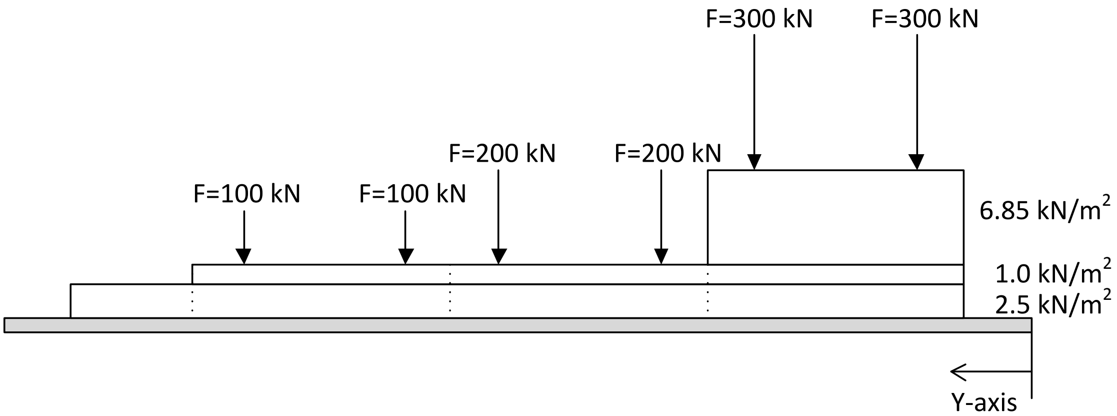

Figure 3-4 Lane loads on deck for the LC of Spanbeton

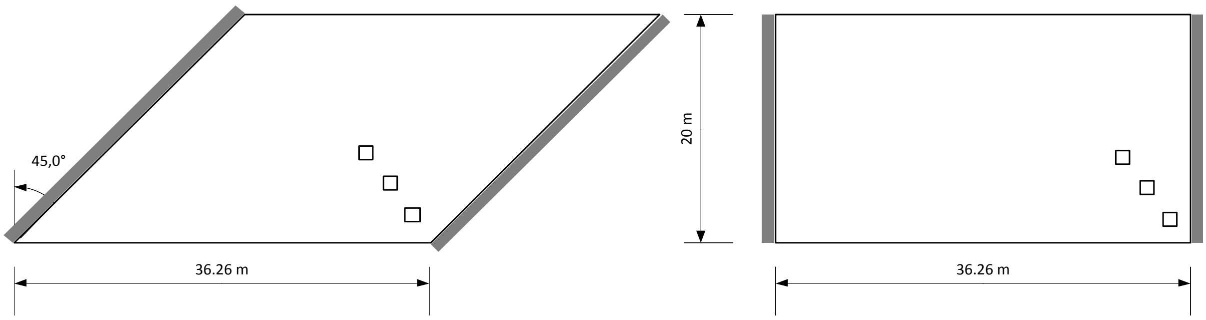

Figure 3-5 Top view of Spanbeton load configuration

UDL whole field with remaining area

UDL: 2.5 kN/m^2. Y = 1400-18600 mm from edge.

UDL whole field without remaining area (extra)

UDL: (1.4x2.5-2.5)=1.0 kN/m^2. Y = 1400-16400 mm from edge.

UDL slow lane (extra)

UDL: (10.35-3.5)=6.85 kN/m^2. Y = 1400-4400 mm from edge.

Axle loads

- Load system: Wheel load 0.5x300/0.4^2=937.5 kN/m^2. Centre of system Y = 2900 mm from edge.
  Longitudinal position 3000 mm from right edge (straight)
  Longitudinal position 6090 mm from right edge (skew)
- Load system: Wheel load 0.5x200/0.4^2=625 kN/m^2. Centre of system Y = 5900 mm from edge.
  Longitudinal position 7000 mm from right edge (straight)
  Longitudinal position 12390 mm from right edge (skew)
- Load system: Wheel load 0.5x100/0.4^2=312.5 kN/m^2. Centre of system Y = 8900 mm from edge.
  Longitudinal position 11000 mm from right edge (straight)
  Longitudinal position 18690 mm from right edge (skew)

3.5.3 Variable loads on deck; Load Case Minalu

Minalu investigated which load configuration, based on loads from Eurocode 1991-2, gives the largest torsional moments. That load is presented here.

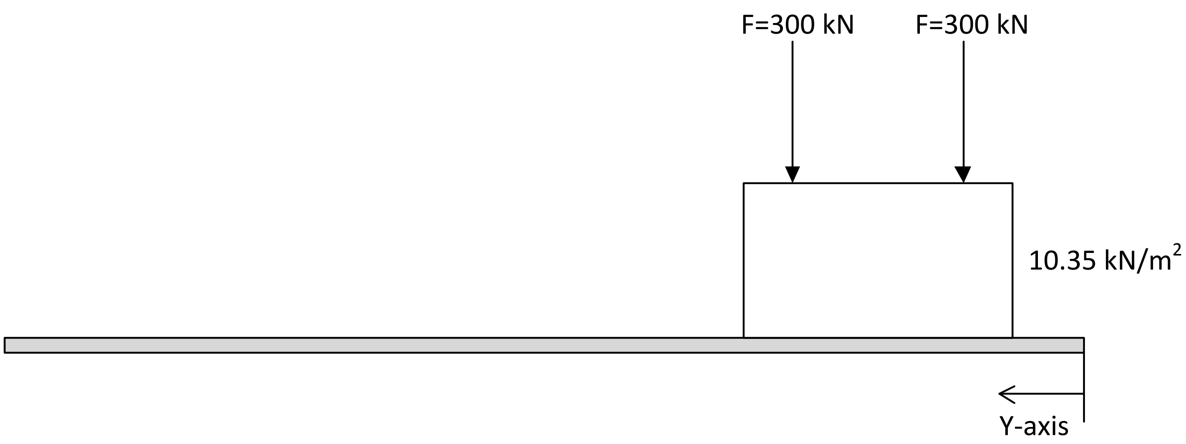

Figure 3-6 Lane loads on deck for the LC of Minalu

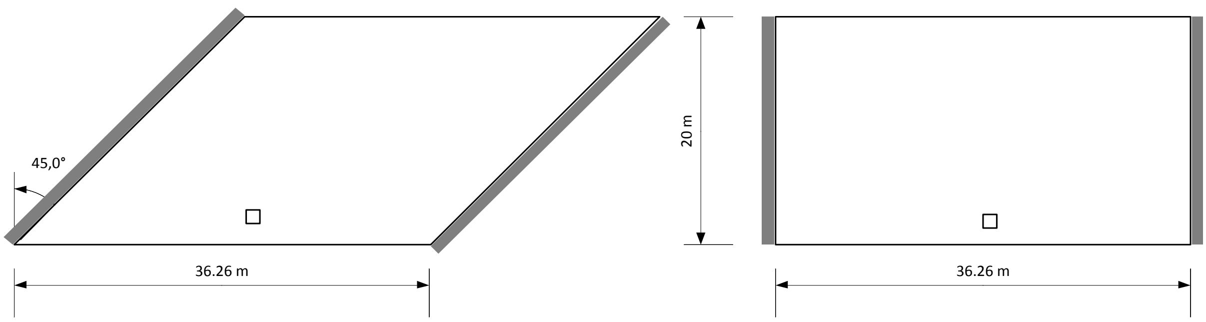

Figure 3-7 Top view of Minalu load configuration

UDL slow lane

UDL: 10.35 kN/m^2. Y = 1400-4400 mm from edge.

Axle loads

Load system: Wheel load 0.5x300/0.4^2=937.5 kN/m^2. Centre of system Y = 2900 mm from edge.

Longitudinal position 18130 mm from right edge (straight)

Longitudinal position 18130 mm from right edge (skew)

3.6 Load combinations

Three load combinations are interesting:

1. Construction stage A: Dead weight and prestressing
2. Construction stage A: Dead weight, prestressing and weight fresh poured concrete
3. Construction stage B: Dead weight, prestressing, weight fresh poured concrete, permanent load on deck.
4. Construction stage B: Dead weight, prestressing, weight fresh poured concrete, permanent and variable load Spanbeton on deck.
5. Construction stage B: Dead weight, prestressing, weight fresh poured concrete, permanent and variable load Minalu on deck.

3.7 Load factors

Serviceability Limit State (SLS)

- All loads: γ=1.0

Ultimate Limit State (ULS)

- All loads (except prestressing): γ=1.35
- Prestressing load: γ=0.9

3.8 Standard Spanbeton calculation

The bridges are calculated using the standard procedure of Spanbeton. Doing this calculation provides insight in the main issues making a calculation of a ZIP bridge system. Because it was intended to do a whole physically non-linear analysis all reinforcement is calculated. The reason to use the Spanbeton procedure is to be able to make a comparison with the reinforcement that would result from their standard procedure.

Minalu investigated a load model which results in the largest torsional moment[8]. To check if this will really give differences a comparison is made between a calculation using the Spanbeton configuration and the configuration of Minalu (Appendix B). Only for the TRA-girder the load configuration of Minalu gives a higher amount of shear reinforcement, but due to the governing fatigue calculation no problems will occur. For the ZIP-girders the Spanbeton load configuration is sufficient. A explanation for this is that the load configuration of Minalu results in higher torsional moments than the load configuration of Spanbeton, but those moments are accompanied by lower shear forces than found with the load configuration of Spanbeton.

[8] Minalu, Kassuhun K. (2010), *Finite element modelling of skew slab-girder bridges.* Page 33.

4 A physical non-linear model of the bridge

4.1 Introduction

The first idea ‘a physically non-linear model of the complete bridge’ is investigated. Both compressive membrane action (CMA) and torsion can be analysed. Cervenka Consulting believed that it was possible to do this job and gave a lot of help during the process. At the end it appeared to be impossible due to a lot of problems and due to lack of time. The occurring problems are briefly described.

The main reason to make a physical non-linear model is that the effect of cracking on the load distribution in the bridge is visible. When a girder in a skew bridge cracks due to torsion the redistribution over the other beams is be visible.

4.2 Bug in the program

In the first week a bug was discovered in the F.E. program. The program has the possibility to copy macro-elements which saves a lot of time. In one run also the applied loads, supports and springs can be copied. The found bug result in: “when the macro-elements were copied including the springs an error occurred and the total file was unusable”. This occurred when the first finite element model was nearly finished.

4.3 Behaviour of individual girders

Dobromil Pryl, employee of Cervenka Consulting advised to model the bridge using as many shell elements as possible to have good accuracy with minimal degrees of freedom. For the end diaphragm beam tetra elements could be used. Using this advice the individual girders where analysed to investigate their behaviour. Furthermore it was found that the CEB-FIB bond model for the prestressing strands as modelled in ATENA will not give correct results, the Bigaj model works better. Applying the prestressing force results in cracks at the end of the girders, as expected.

Unexpected is cracking in in the top of the TRA-girders. Some refinements and other choices of elements types did not help. These cracking is not relevant but increases the calculation time, because the number of iterations increases. This phenomena is not further investigated.

4.4 Construction stages

For linear-elastic calculations the stresses can be simply added to each other. In practice a ‘distribution calculation’ will be made for the deck loads (using an orthotropic plate model, construction stage B). The results of that calculation are input for a ‘detail calculation’ in which the effects of the prestressing, dead weight and weight of the fresh poured concrete of deck (construction stage A) also are considered. When a physically non-linear material behaviour is used it is impossible to sum up the stresses because the principle of superposition is only applicable for linear elastic calculations.

The stresses of construction stage A can be applied by loading the girders separately. After that the deck must be present to bear the permanent and variable loads on the deck. It is possible to simulate this in ATENA by using the option ‘construction stages’. However, there are limits to this option. First, applying this possibility of the program makes it more difficult to find the sources of errors. Secondly, the optimum is to have large shell-elements for the deck and some finer volume-elements for the girders. The program connects these elements by master-slave relations. Only the larger elements can be the master-element. It would be clear what happens when in the first stage only the girders are active. In that case the master-elements are not available and the program will not run. There is a dummy solution available to avoid this problem: for the deck elements a variable material stiffness can be used. In construction stage A the stiffness of the deck is set very low, in construction stage B the stiffness is adapted to the normal stiffness.

4.5 Eccentricity of TRA

The prestressing of the ZIP-girders will not give horizontal deformations (in theory). For the TRA-girder some horizontal deformation is permitted, limited by L/1000. It is very difficult to design a strand configuration that will give zero horizontal deformation, and indeed some deformation occurred. In the next stage 'pouring fresh concrete of deck' some enlargement of the horizontal deformation was visible which is not happening in practice. Perhaps the connected deck reinforcement will restrain this deformation.

When the deck is modelled with a variable stiffness (low in construction stage A and normal in construction stage B) the deck with low stiffness gives disturbances in the stress distribution of the ZIP-girders close to the edge. This is due to the different height of the centre of gravity of ZIP- and TRA-girders. This will of course occur in the stage when the deck is hardened, but not in the stage that the girders are individually prestressed. For this reason a construction stage for only the edge part of the deck was considered to avoid this problem. That idea appeared to work, but of course makes it more difficult and complex because both solutions (construction stages and variable stiffness of deck) are applied then.

4.6 Convergence and calculation time

One of the largest problems appeared to be the calculation time. Running the model linear-elastic takes already 5-10 hours using the DCG solver on a modern desktop computer. In that model no construction stages and reinforcement bars are included. For linear elastic calculations the convergence is very good, two iterations are normally needed to reach the solution. For a non-linear analysis more iterations and load steps are needed, especially when the post-cracking stage is analysed.

At the moment ATENA do not use the capacity of the modern computers with quad-core processors and 64 bit techniques. Cervenka Consulting is improving that. Due to interaction between modelling and the long time it takes to run a trial calculation no complete calculation is finished. The use of ATENA Console can speed up the calculation significantly for some problems. This is tested for the smaller models and helps indeed.

4.7 Future

The current linear elastic bridge model can be built and analysed conveniently. The non-linear analysis cannot be performed on this model because the computer memory and hard disk capacity are insufficient. Therefore, the single girder model has been built which has far less elements (Chapter 5). Nearly all of the development time has been spend on creating a good mesh and compatible loading. None of this would have been necessary if the linear elastic model of the bridge could have been nonlinearly analysed.

In paragraph 5.6.1 it is shown that the model of the complete bridge would have sufficient accuracy if each linear elastic element is replaced by approximately 18 quadratic elements. The linear elastic elements have 8 nodes each while the quadratic elements have 20 nodes each. Therefore, a nonlinear model of the bridge needs 18 x 20/8 = 54 as many nodes as the current bridge model. The structural stiffness matrix needs 54 x 54 times as much data. However, a smart solver can optimize the matrix band width to perhaps 10 times larger than the current band width. Therefore the structural stiffness matrix needs 54 x 10 = 540 times as much data.

In the future a personal computer will have more capacity. Moore's law states that computer capacity doubles each two years. In 18 years there will be 9 improvements steps of 2 years. Computers will have 2^6 = 512 times as much capacity as nowadays, which is sufficient for the physical non-linear model of the bridge.

4.8 Conclusion

All the mentioned difficulties together made the assignment to make a physical non-linear model of the bridge too complicated. Developing a 3D finite element model requires substantial training and experience, especially when physically non-linear behaviour is included. Due to all occurring side-effects the scope of the research is not clear anymore.

The bottleneck doing this large calculation is the required calculation time and the needed memory. A rough estimation is that within 18 years it is possible to do physical non-linear calculations for complete bridges.

5 Alternative modelling of torsion

5.1 Introduction

To reduce complexity a simplified procedure is developed to simulate the occurring torsion in the first ZIP-girder. This procedure contains the following steps:

1. Make a linear elastic (LE) finite element model of the bridge;
2. Analyse the occurring deformations of the first ZIP-girder;
3. Make a physical non-linear (PNL) model of one ZIP girder;
4. Apply the determined calculations on that model.

Is it valid to simulate the torsion in this way? The relation between stiffness and occurring torsion is neglected now (full torsional stiffness is used in the linear elastic model of the bridge), is that acceptable? For SLS and ULS the answer is different:

- SLS-stage. In this stage no cracking due to bending or shear will occur. For torsion effects this must be investigated, but also these cracks are not expected. In this phase the deformations of the linear elastic model of the bridge will be correct.
- ULS-stage. It is expected that in this stage cracking, sure due to bending, will occur. In that case the linear elastic model of the bridge do not predict the deformations correctly.

In the following paragraphs some important notes about the used models will be made. A detailed description is available in appendix E.

5.2 Make a linear elastic finite element model of the bridge

A linear elastic model of the bridge will be made with end diaphragm beams. Also a model without end diaphragm beams is analysed (in a later stage of research), only to analyse the differences in rotations and to be able to compare with the orthotropic plate model (in which the end diaphragm beam is neglected).

The model must describe the deformations correctly. Accurate deformations are important because they will be applied on the small model of one ZIP-girder. In appendix E a comparison is made between some different meshed girders. The girder meshed as presented in Figure 5-1 has a good balance between calculation time and accuracy. So linear elements are used in the model.

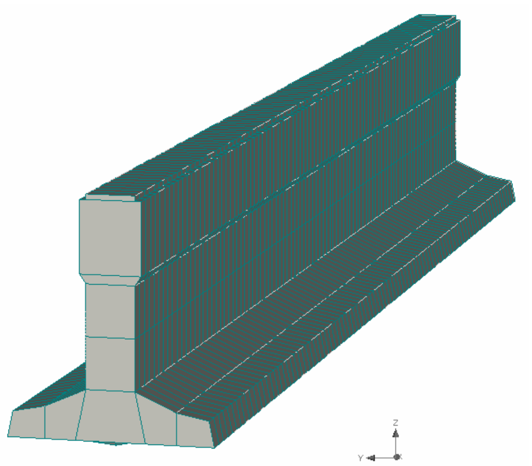

Figure 5-1 Model ZIP-girder for the linear elastic model of the bridge

The model presented in Figure 5-2 and Figure 5-3 is used to determine the deformations in the bridge. The model consists of the following layers:

1. Loading shell, needed to apply the loading on the bridge. Made of ATENA 3D shell elements (4 layers are used).
2. The deck. Made of quadratic brick elements with size 400x400 mm.
3. Girders with end diaphragm beams. The model for the ZIP-girders is already shown in Figure 5-1. The end diaphragm beams consists of tetra-elements.
4. This model is vertically supported by springs. To avoid rigid body movement the model is supported at the top of the first ZIP girder as indicated in Figure 5-3.

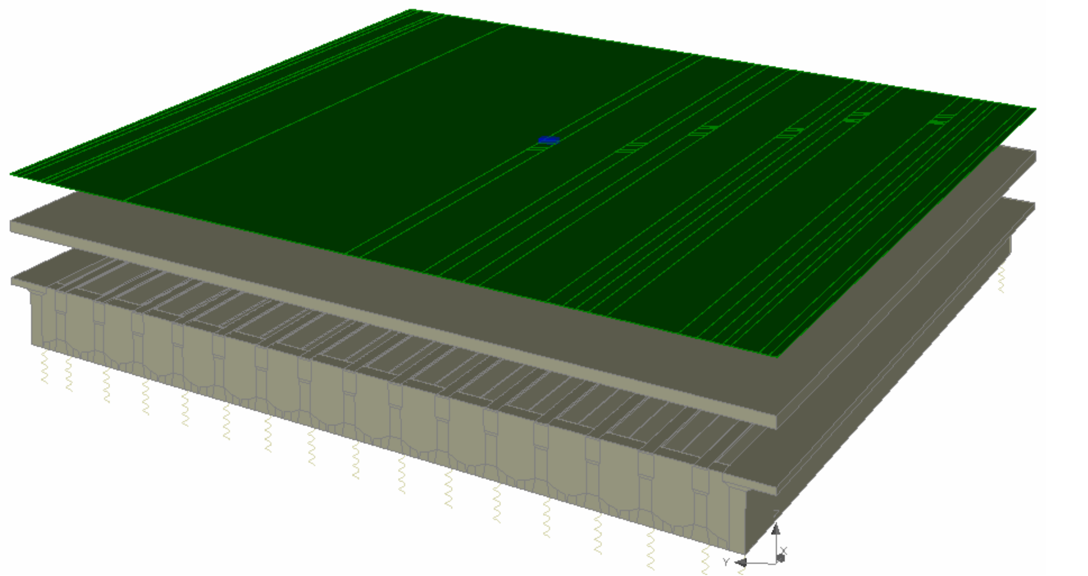

Figure 5-2 Linear elastic model of the bridge

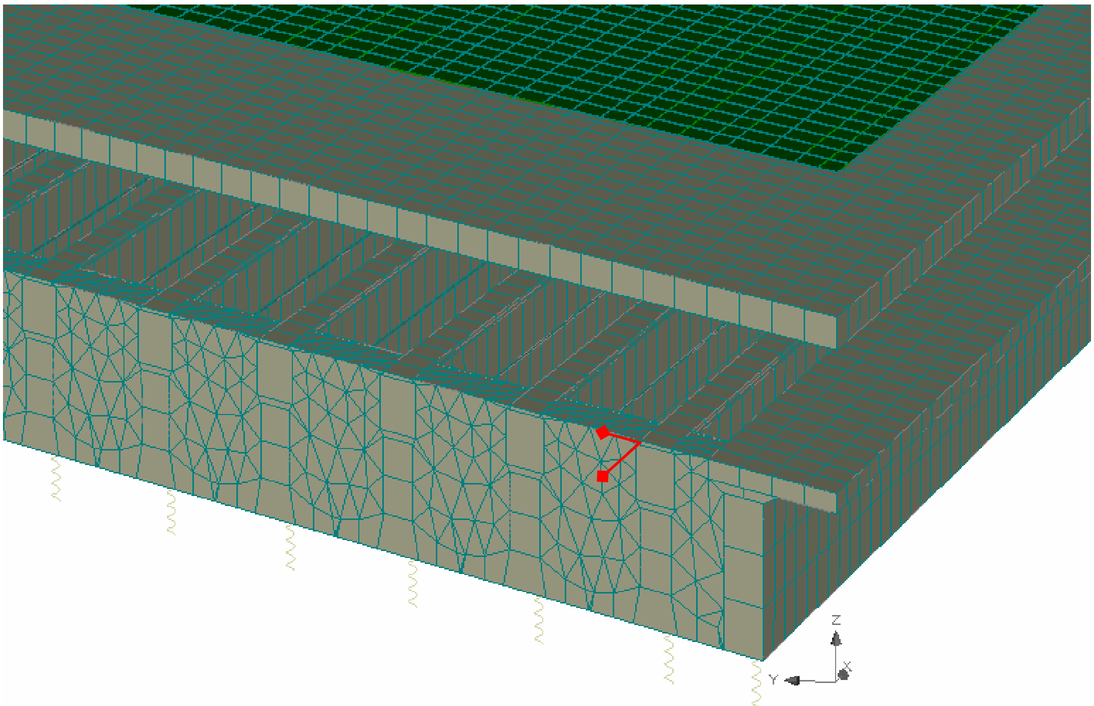

Figure 5-3 Finite element mesh for the LE model of the bridge (horizontal supports indicated in red)

Remarks:

1. During making the model a bug was found (in ATENA). Applying shell-elements for the deck gives strange results, no equilibrium in all directions was found, also the distribution of support reactions seems to be incorrect. Based on some experiments with different models it was found out that applying quadratic volume elements for the deck gives reasonable results. Furthermore an equilibrium calculation is made.
2. The thickness of the deck is not constant at the edge of the bridge between the first ZIP and TRA girders (Figure 3-2). But this gives difficulties in the finite element model. Chosen is to take a constant thickness for the whole deck of 230 mm.

5.3 Analysis of the deformations of first ZIP girder in skew bridge

The deformations of the LE model must be applied on the small PNL model. For that reason first the deformations are investigated. The procedure to get the results from ATENA is presented in appendix F. The orthotropic model, presented in paragraph 9.2, is used to compare the deformations with.

In the linear elastic model of the bridge two load steps are calculated (construction stage B):

1. Permanent loads on deck, with or without end diaphragm beam.
2. Permanent and variable loads on deck, with or without end diaphragm beam. This is done for the load case of Spanbeton and Minalu.

The found data for the first ZIP girder is split up in different components (Figure 5-4) and will be analysed in the next paragraphs:

1. Transverse deflection of top of girder, dY (top)
2. Average vertical deflection of top of girder (representing shear force), dZ average
3. Rotations, ddZ or dY (top) and dY (bottom)

Important is that all deformations are plotted along the length as defined in Figure 5-4.

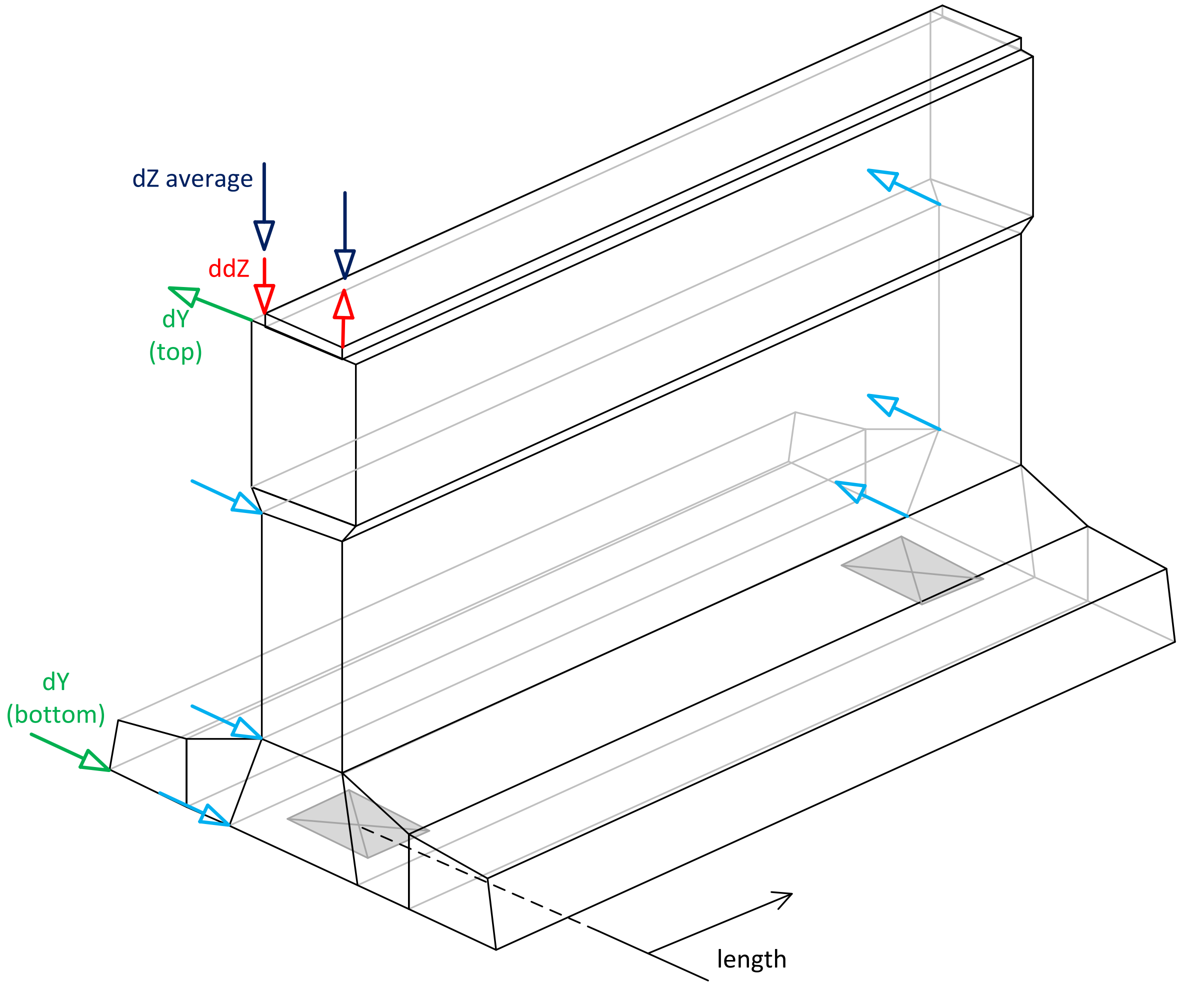

Figure 5-4 Schematized deformations of the girder

5.3.1 Transverse deformation; dY (top)

The distribution of the transverse deformations, dY (top), along the length are presented in Figure 5-5 and Figure 5-6. In both figures the deformations due to load step 1 (permanent load) are identical because only the variable load differs.

In Figure 5-5 and Figure 5-6 some things are remarkable:

- The end diaphragm beam gives a kind of clamping effect causing negative deformations in the zone length = 30 – 36 meter
- The deformations are larger when the end diaphragm beam are neglected
- The shape of the deformations is not changing

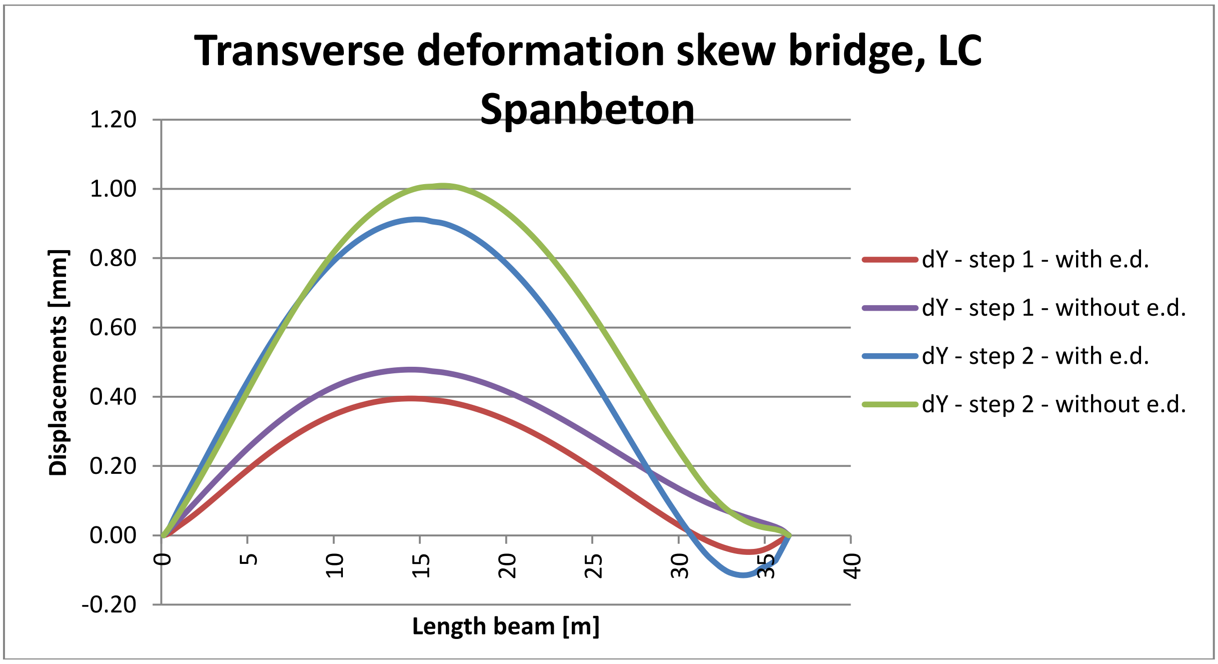

Figure 5-5 Transverse deformation skew bridge, load case Spanbeton

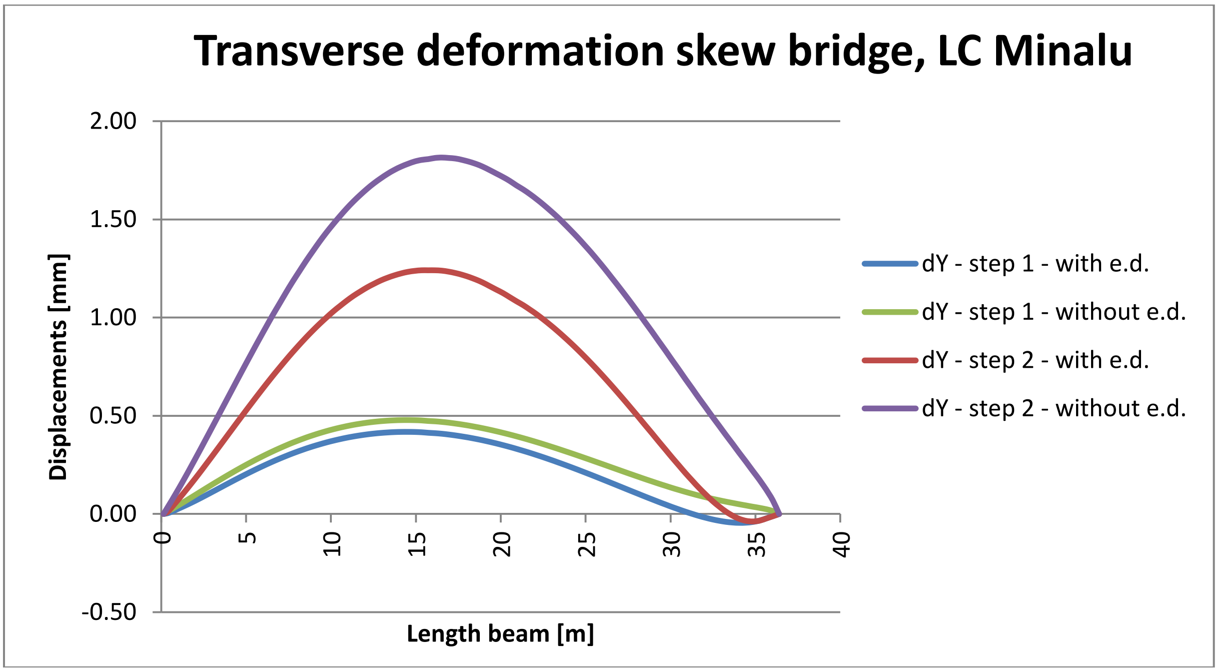

Figure 5-6 Transverse deformation skew bridge, load case Minalu

5.3.2 Average vertical deflection; dZ average

The average vertical deflection represents the bending and shear deformation. The average is taken from the deformations, Figure 5-7.

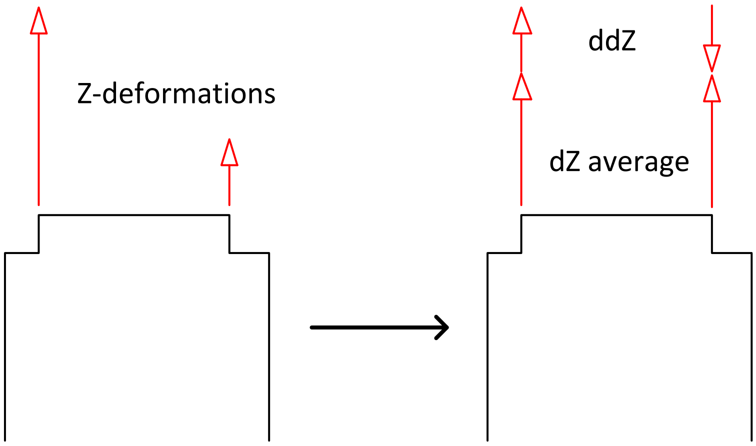

Figure 5-7 Splitting up the Z-deformations

In this paragraph the dZ average deformations are presented, Figure 5-8 and Figure 5-9. Some comments:

- For the first step the deformations are the same
- The end diaphragm beam has a beneficial effect on the deflection.

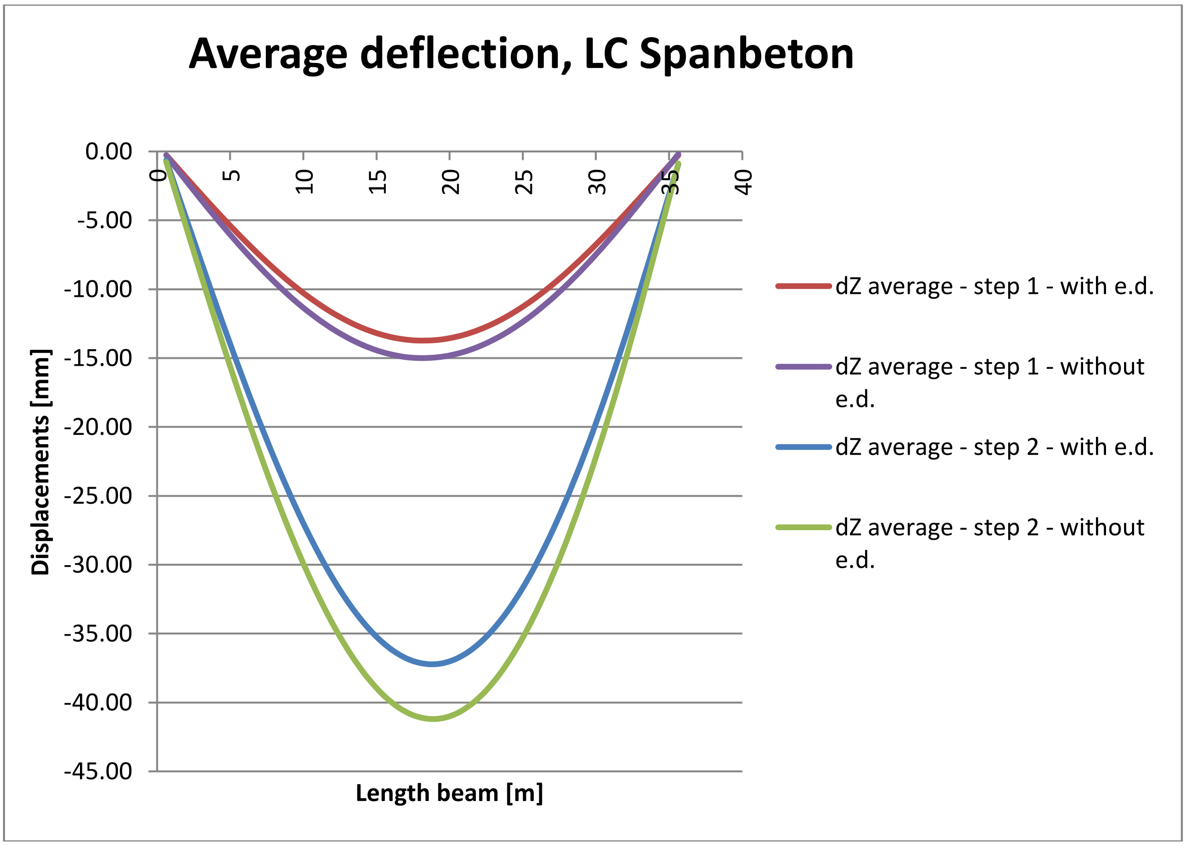

Figure 5-8 Average deflection of beam, load case Spanbeton

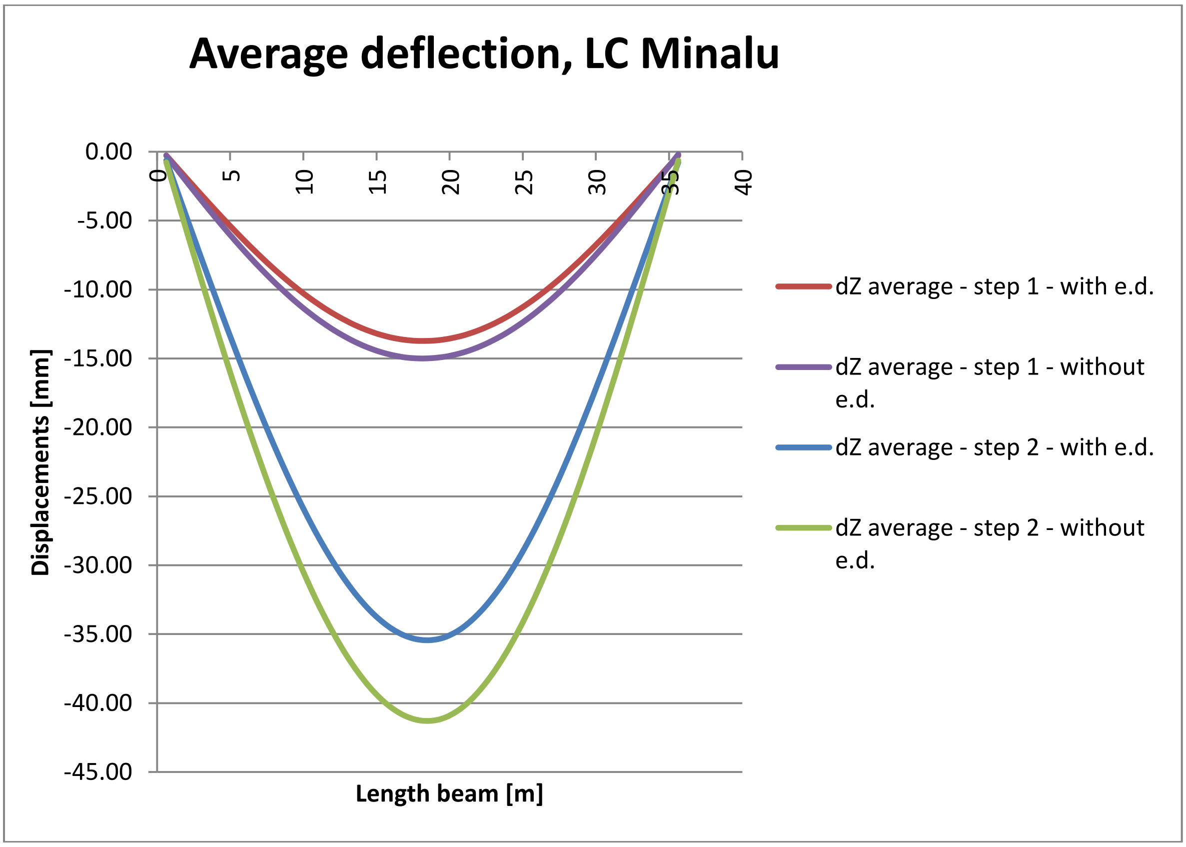

Figure 5-9 Average deflection skew bridge, load case Minalu

The orthotropic plate model gives similar deformations, presented in Figure 5-10, Figure 5-11 and Figure 5-12. It is visible that the deformations for load step 1 and 2 for both load cases are corresponding quite good. From this is concluded that the deformations in the ATENA model are reliable.

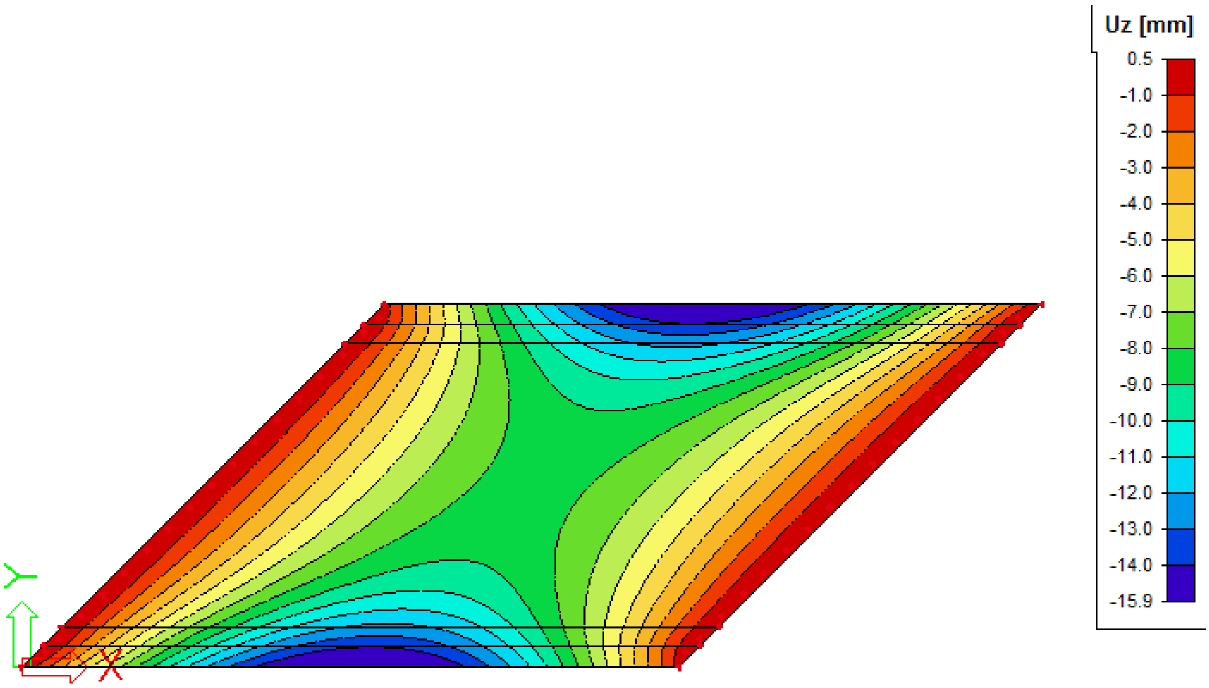

Figure 5-10 Deflection due to permanent load (step 1) calculated with Scia Engineer

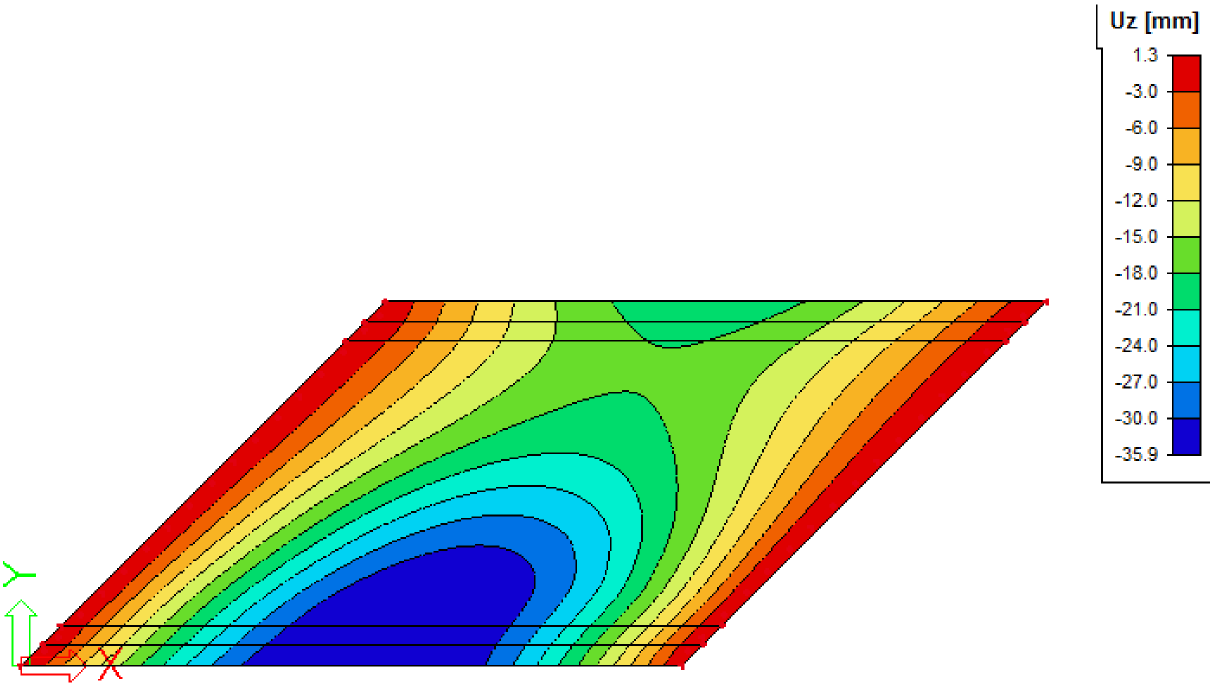

Figure 5-11 Deflection due to permanent load and variable load of Spanbeton (step 2) calculated with Scia Engineer

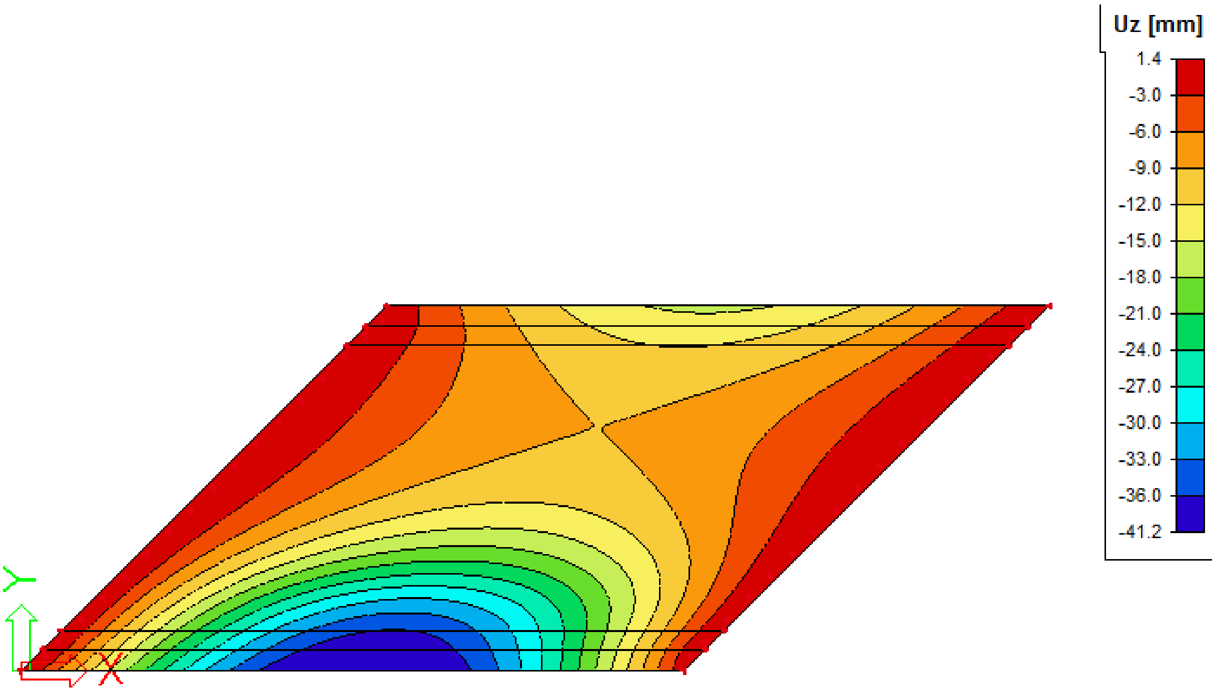

Figure 5-12 Deflection due to permanent load and variable load of Minalu (step 2) calculated with Scia Engineer

5.3.3 Rotations

The rotations of the beam need to be calculated for two directions as illustrated in Figure 5-13.

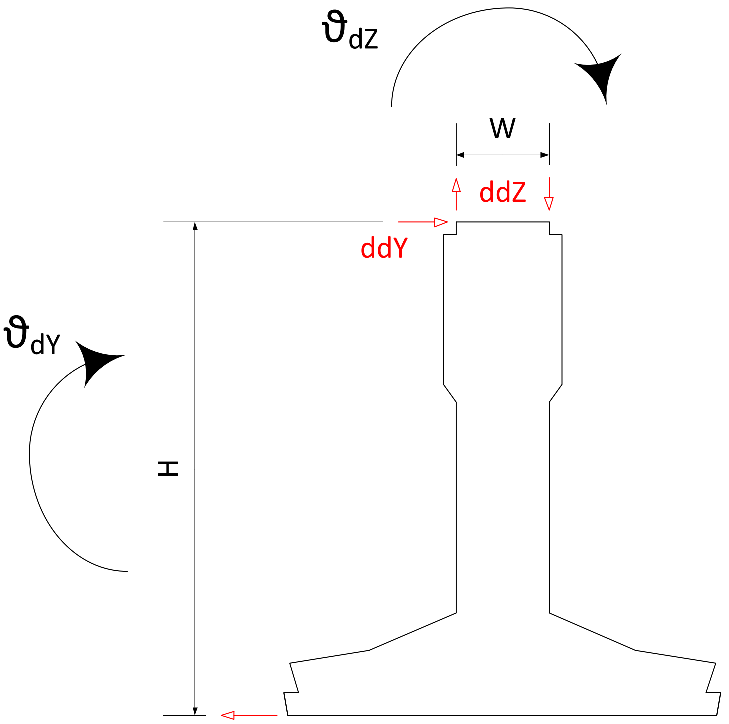

Figure 5-13 Calculation of rotation of beam

The used formulae are:

$$\vartheta_{dY} = \frac{ddY}{H}$$
$$\vartheta_{dZ} = \frac{ddZ}{W}$$

In Figure 5-14 and Figure 5-15 the rotations are plotted and it can be observed that:

- Again the clamping effect of the end diaphragm beam is visible.
- Neglecting the end diaphragm beam gives larger rotations.

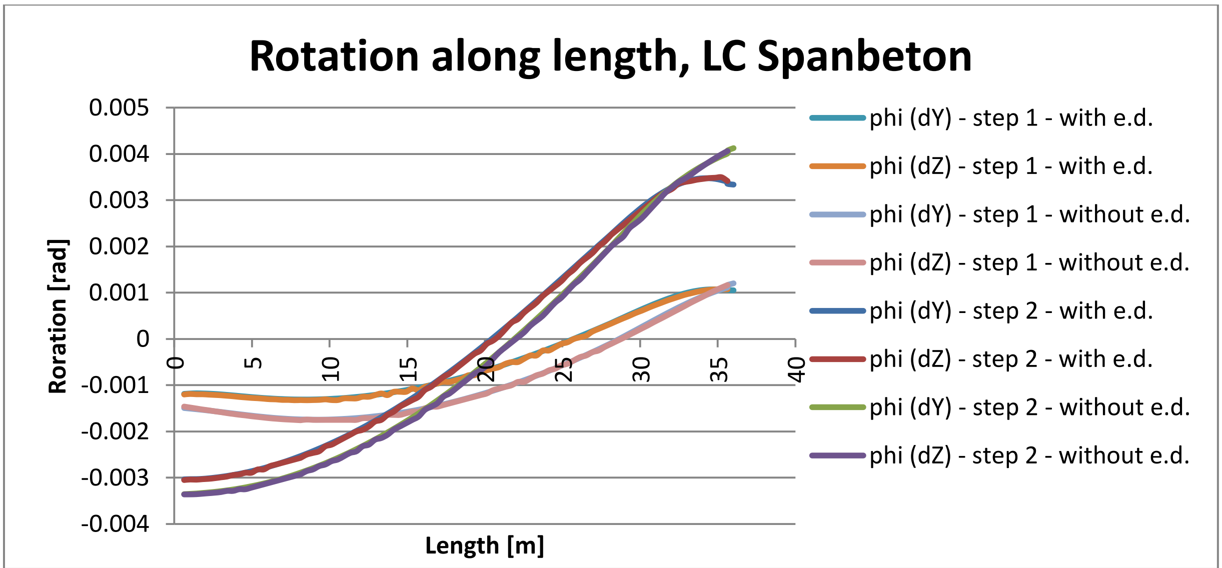

Figure 5-14 Rotation along length for skew bridge, LC Spanbeton

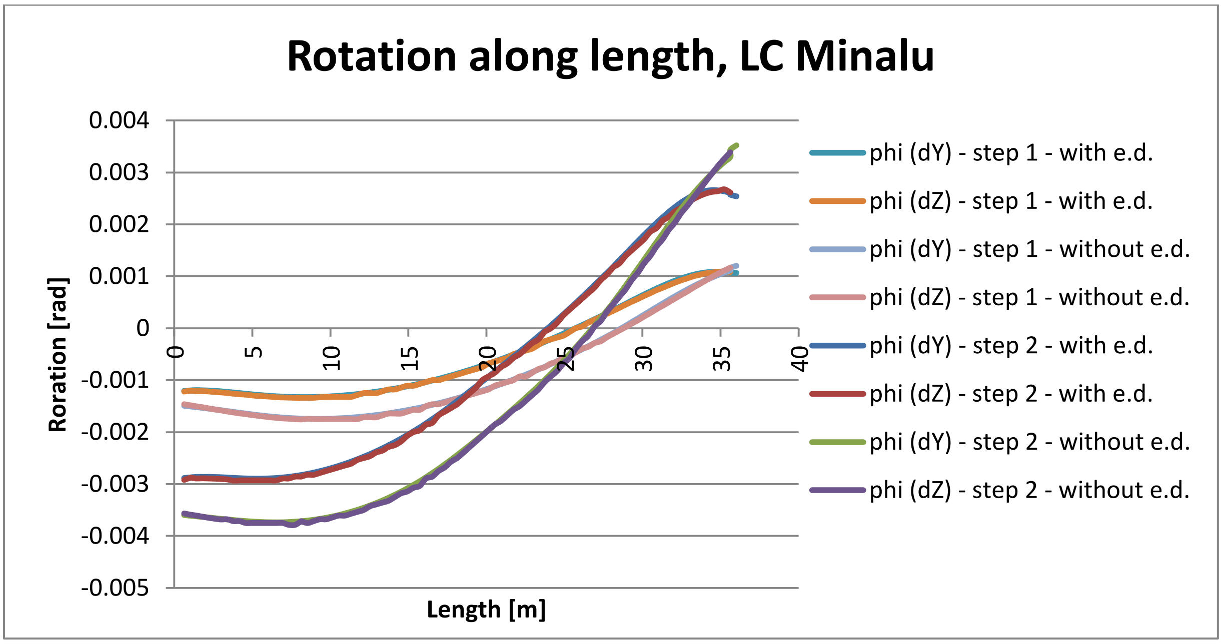

Figure 5-15 Rotation along length for skew bridge, LC Minalu

The Scia 2D-model gives similar rotations, presented in Figure 5-10, Figure 5-11 and Figure 5-12. It is visible that the deformations are corresponding the best for the load case of Minalu. From this is concluded that the rotations are reliable.

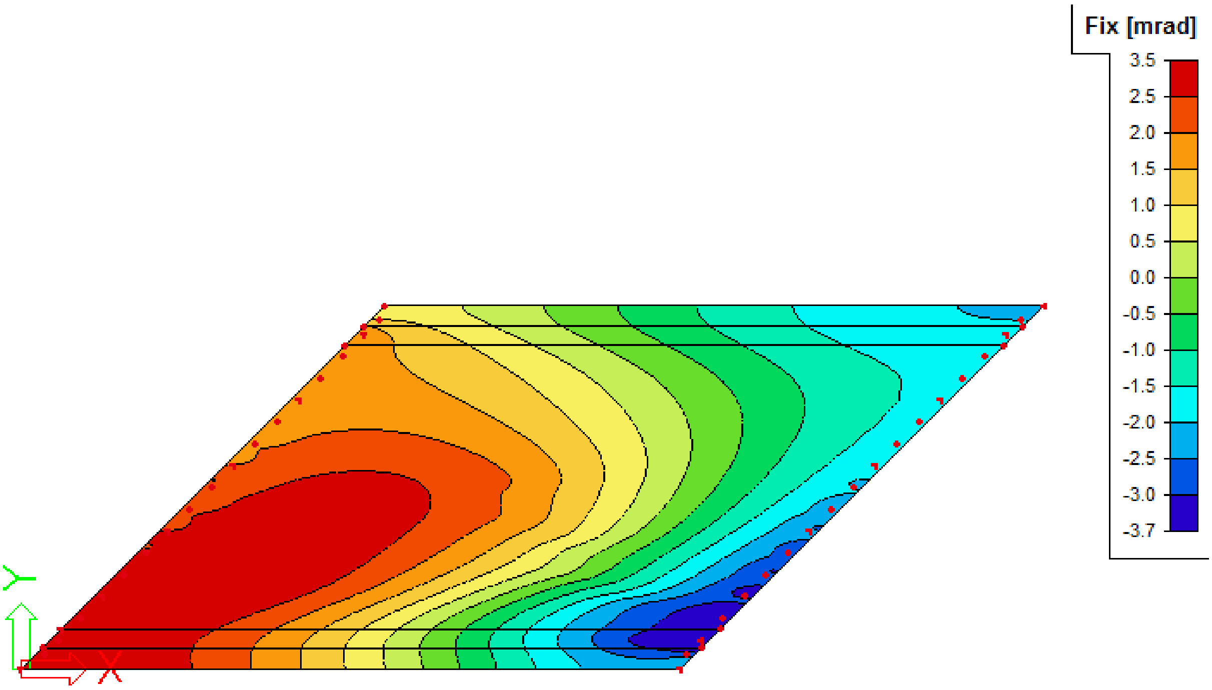

Figure 5-16 Rotations in bridge due to permanent load and variable load of Spanbeton calculated with Scia Engineer

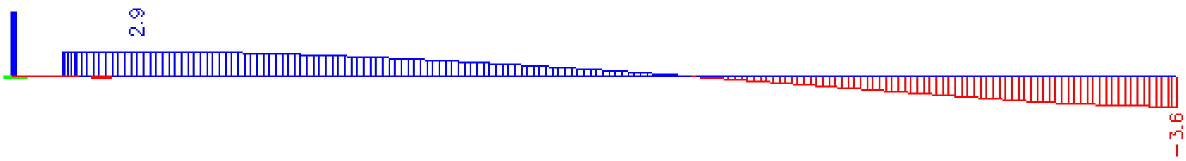

Figure 5-17 Rotations in first ZIP girder due to permanent load and variable load of Spanbeton calculated with Scia Engineer

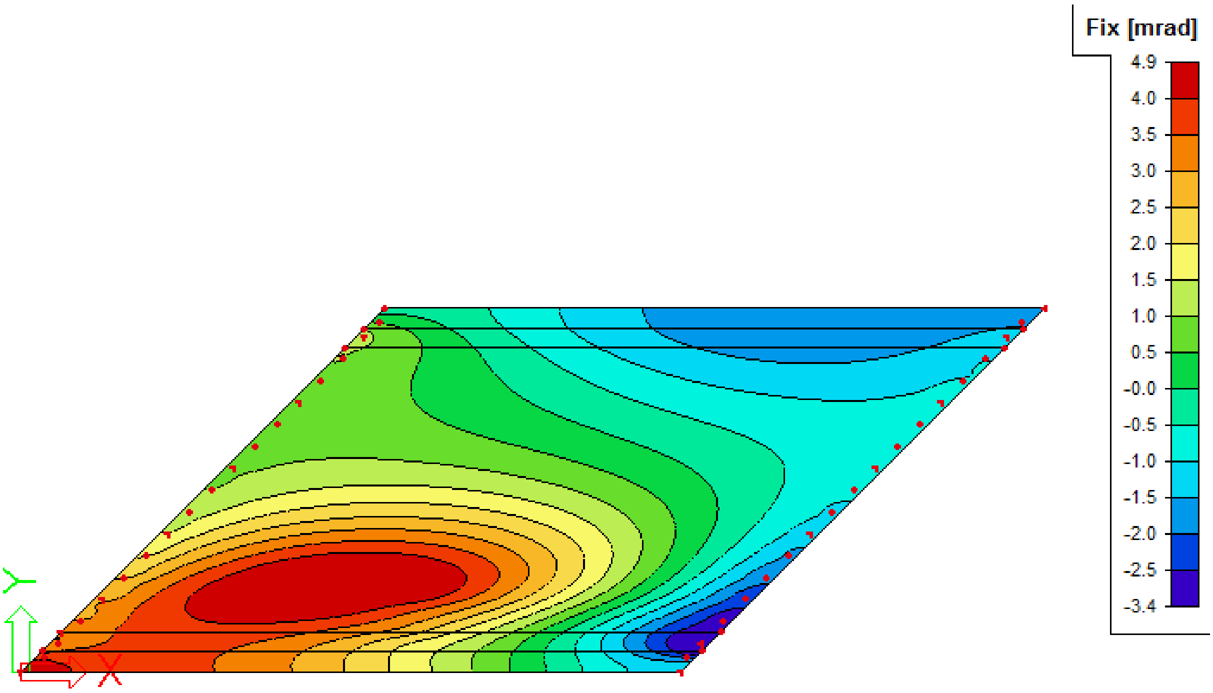

Figure 5-18 Rotations in bridge due to permanent load and variable load of Minalu calculated with Scia Engineer

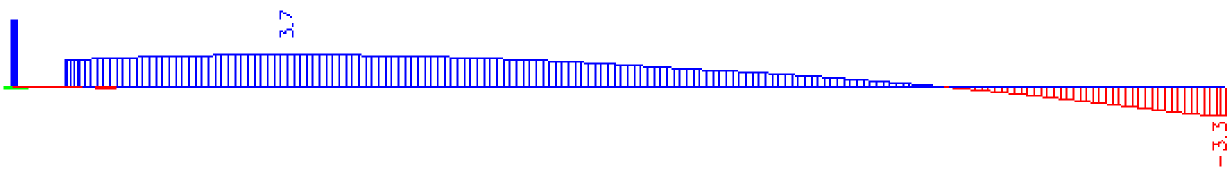

Figure 5-19 Rotations in first ZIP girder due to permanent load and variable load of Minalu calculated with Scia Engineer

5.4 Analysis of the deformations of first ZIP girder in straight bridge

It appeared that the torsion in a straight bridge is much lower than for a skew bridge (paragraph 2.2.2). For that reason only for the load case of Spanbeton the deformations of a straight bridge are investigated and presented briefly.

5.4.1 Transverse deformation; dY (top)

The occurring transverse deformations are very small, five times lower than occurring for the skew bridge, Figure 5-20.

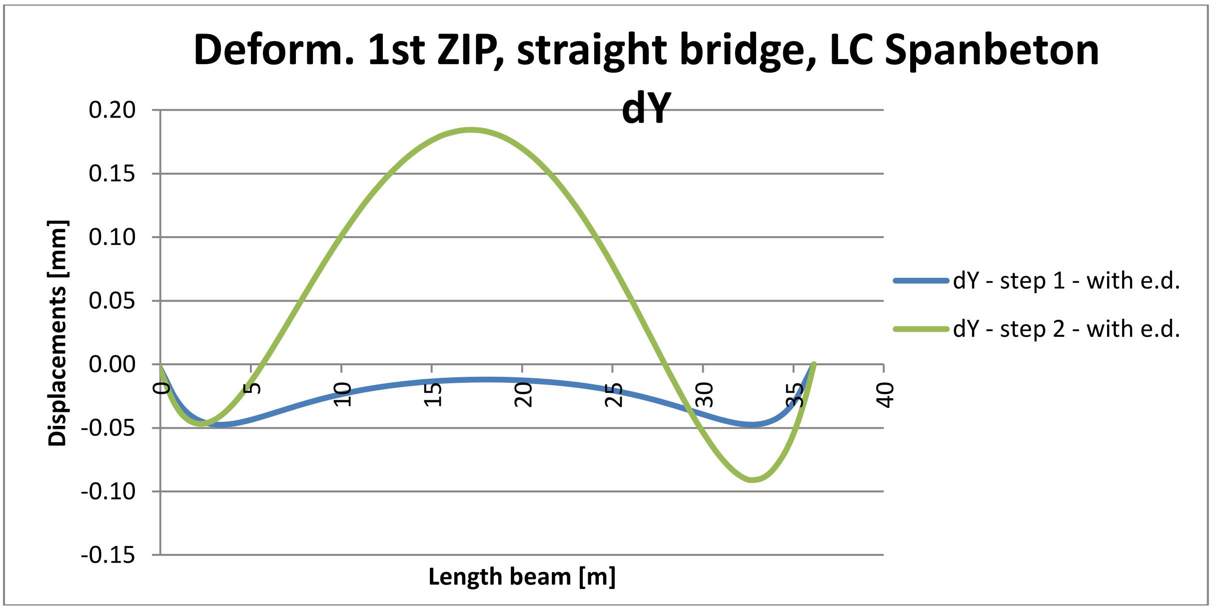

Figure 5-20 Transverse deformation straight bridge, load case Spanbeton

5.4.2 Average vertical deflection; dZ average

The deflection of the beam is larger for the straight bridge than for the skew bridge. This is because more load is carried by bending in a straight bridge, Figure 5-21.

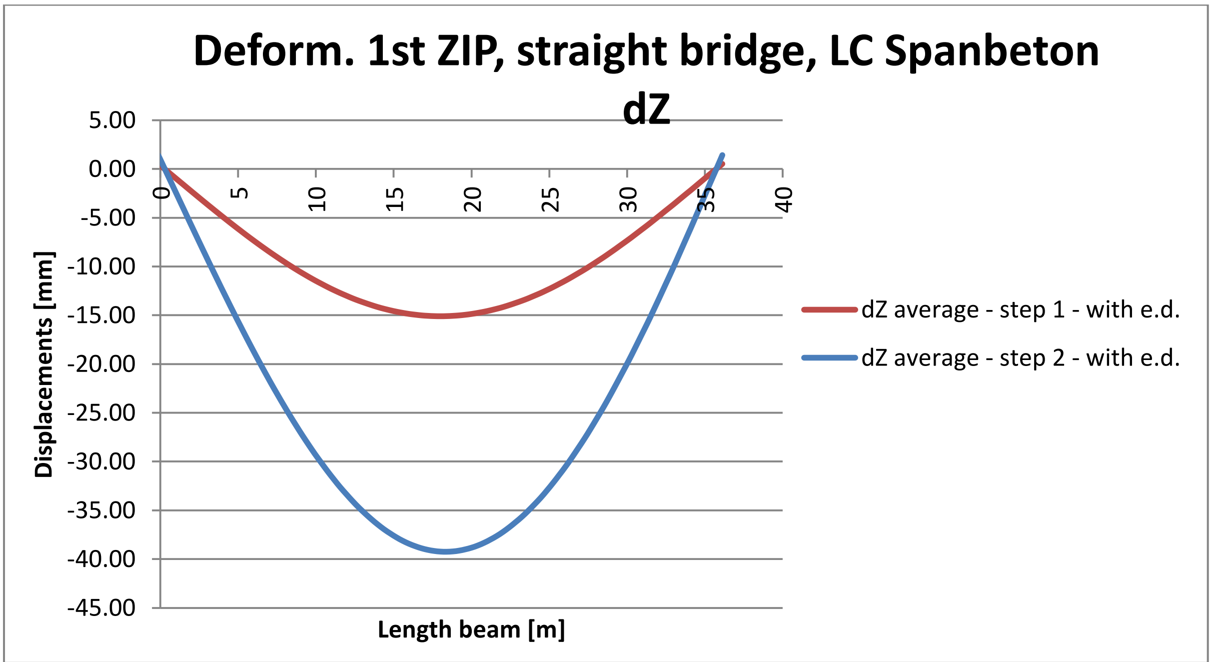

Figure 5-21 Average deflection straight bridge, load case Spanbeton

5.4.3 Rotations

Interesting is that for the observed load case only the permanent load gives the largest rotations, the variable load reduces this, Figure 5-22.

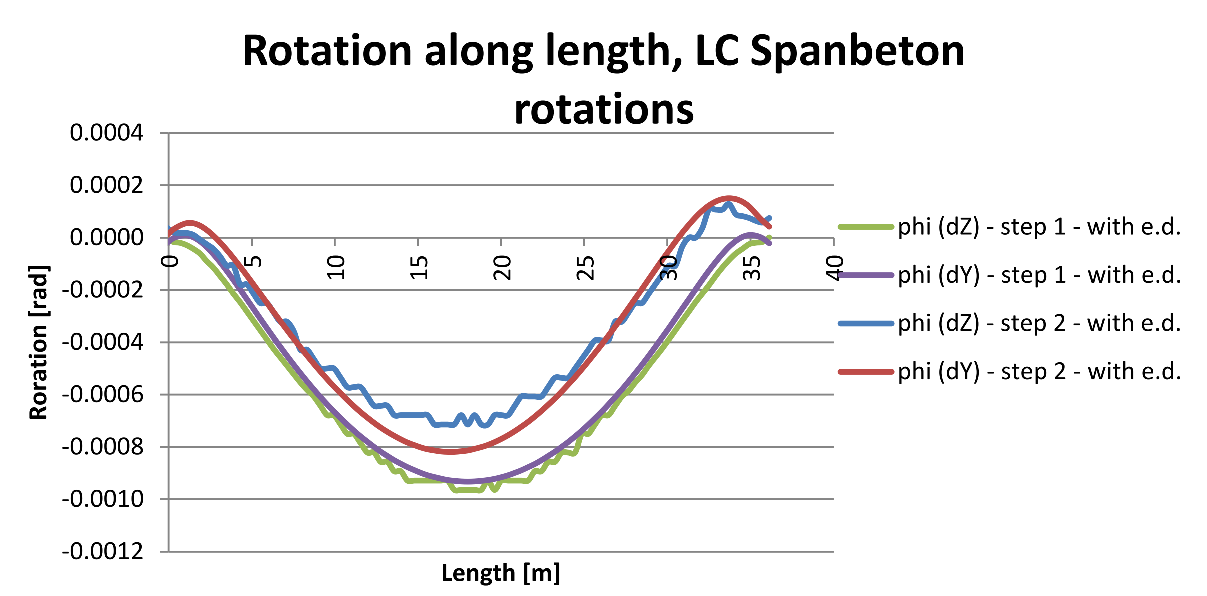

Figure 5-22 Rotation along length for straight bridge, LC Spanbeton

A comparison of the rotations occurring in a skew and straight bridge is illustrative for the behaviour of the bridges, Figure 5-23. When in the first ZIP girder of the skew bridge no torsion cracks appear this will sure not happen in the straight bridge. So first the skew bridge will be investigated. Depending on the results it may be necessary to investigate the straight bridge further.

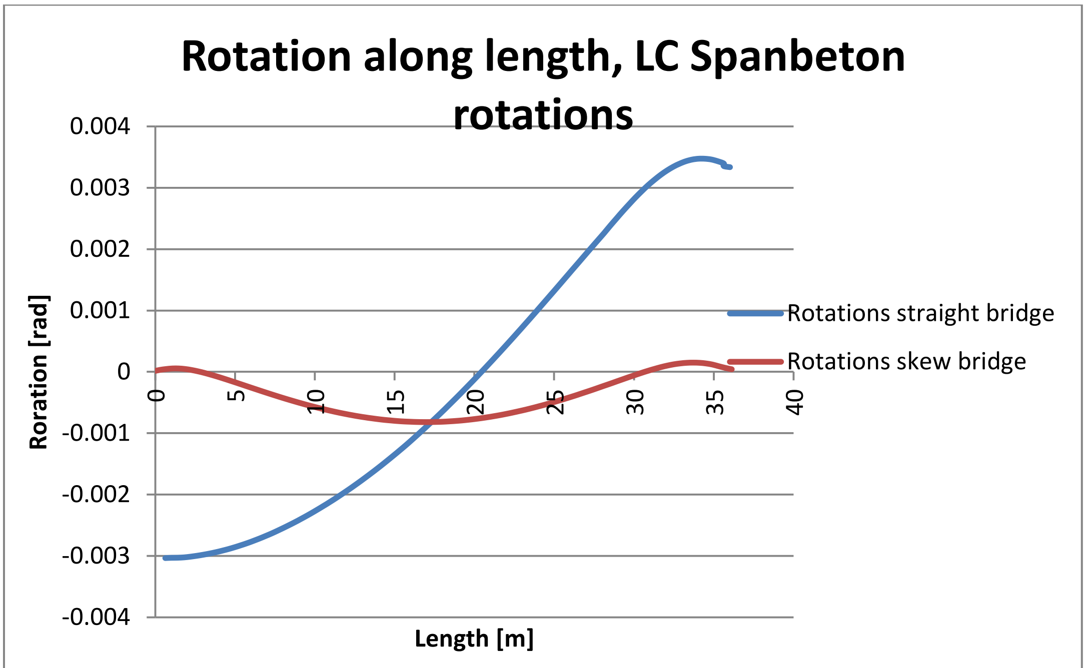

Figure 5-23 Comparison rotations in a fully loaded skew and straight bridge for LC Spanbeton

5.5 Applying loads on the PNL model of one ZIP girder

The deformations from the previous analysis have been investigated. Important is that they should be applied in a correct way on the small model.

The load is applied, using the following steps, the figures are presented below:

1. Dead weight and prestressing. Figure 5-25.
2. Fresh concrete deck. It is assumed that the girder in this phase is supported along the top edge by the reinforcement. Figure 5-25. The eccentricity of this loading is not incorporated.
3. Average deflection. Figure 5-26.
4. Rotations and transverse deflection. Figure 5-27.

The loads 3 and 4 are applied alternately because they are occurring simultaneously.

Loading 4 is the most complicated one. The deformations are correctly applied on the loading plate. But due to the low stiffness of the loading plate the transverse deformations are not applied correctly on the girder, there is some deviation, this is visualized in Figure 5-24. The rotations, the most important deformations, are still correct.

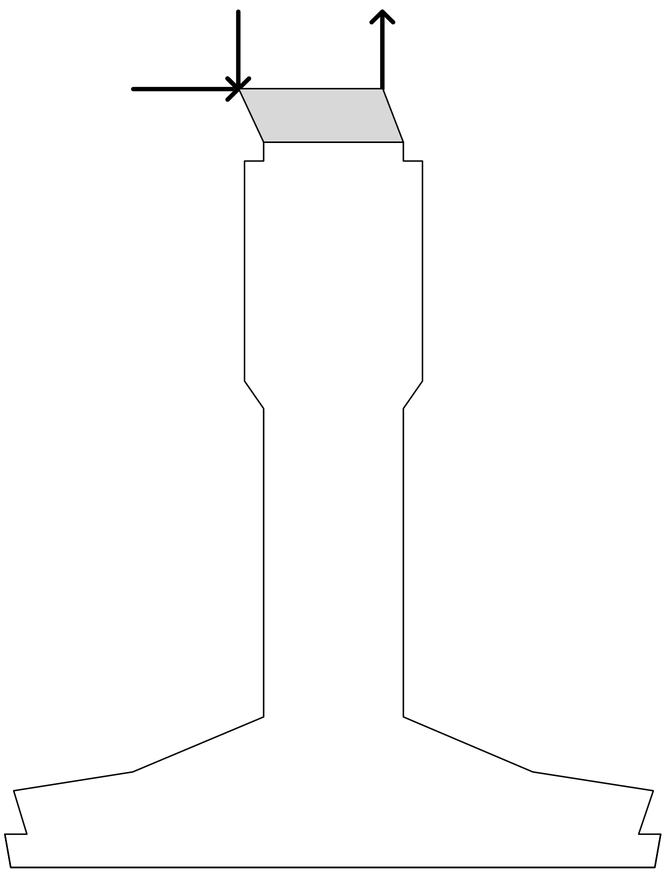

Figure 5-24 Difference in transverse deformation

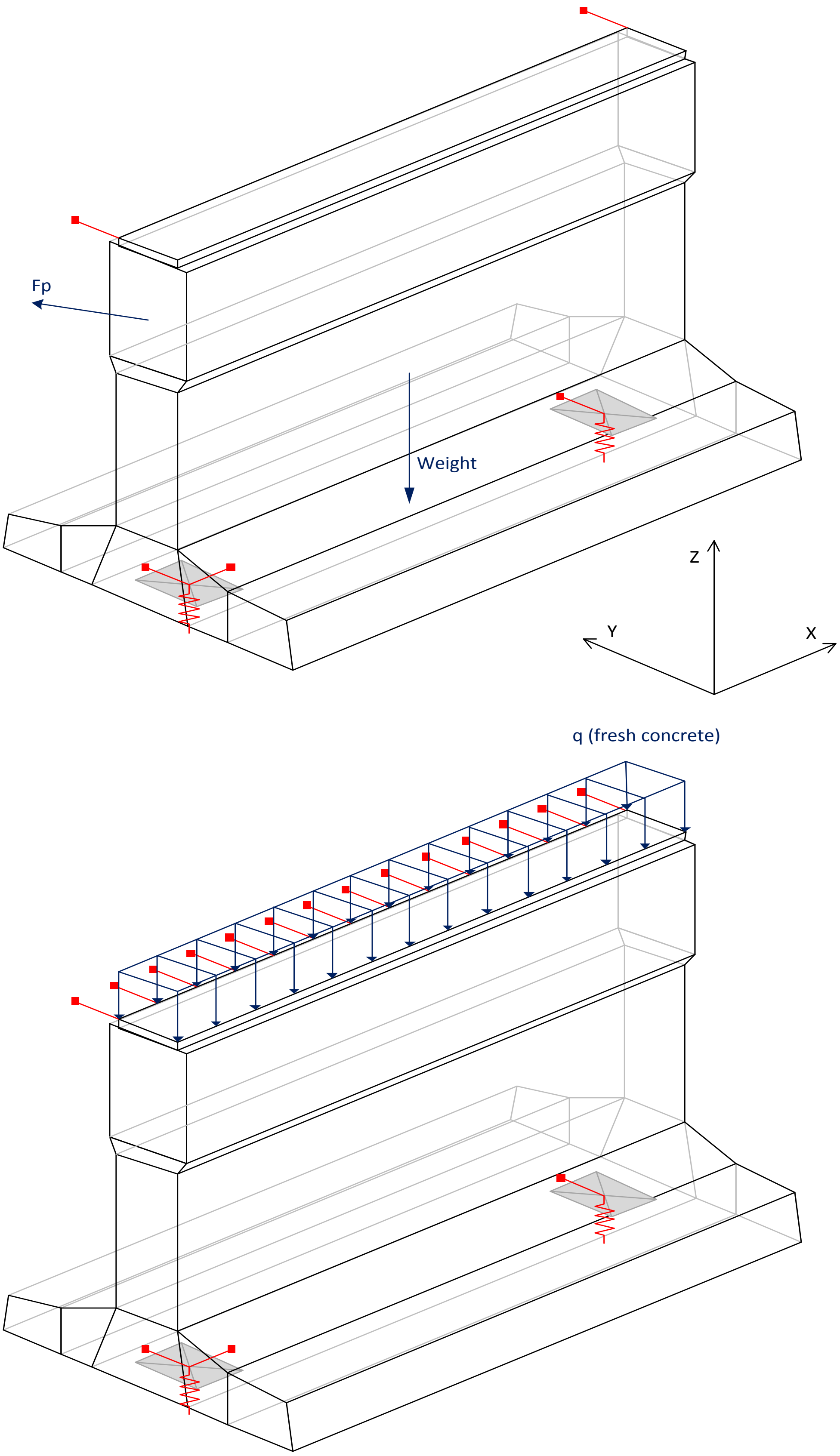

Figure 5-25 Dead weight, prestressing and fresh poured concrete (loads and boundary conditions)

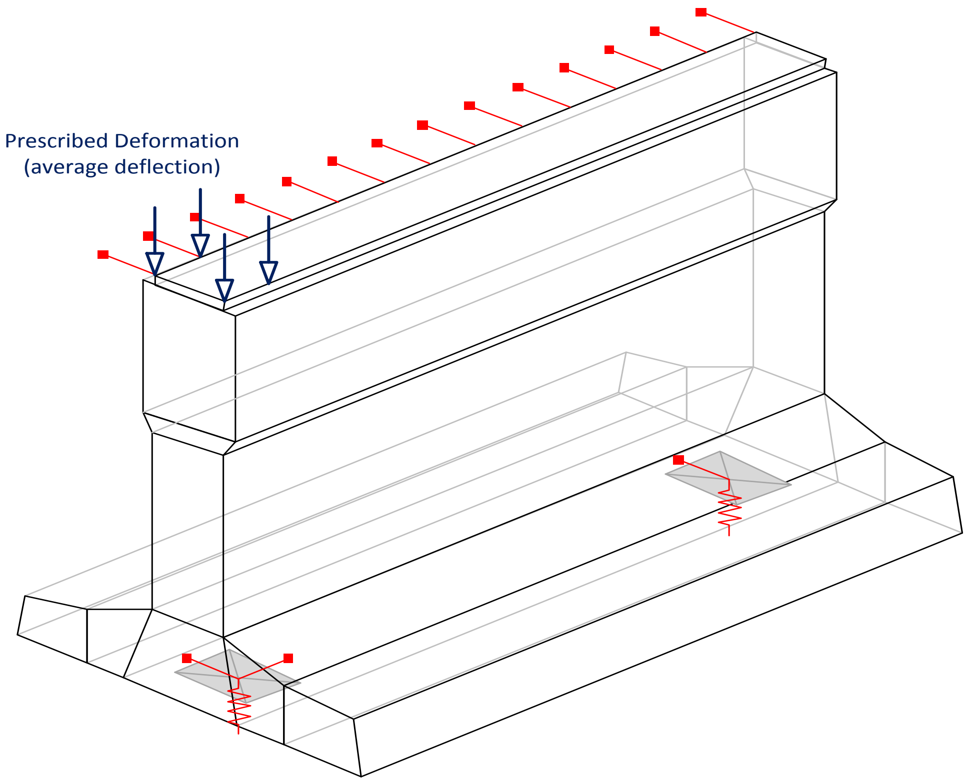

Figure 5-26 Average deflection (prescribed deformations and boundary conditions)

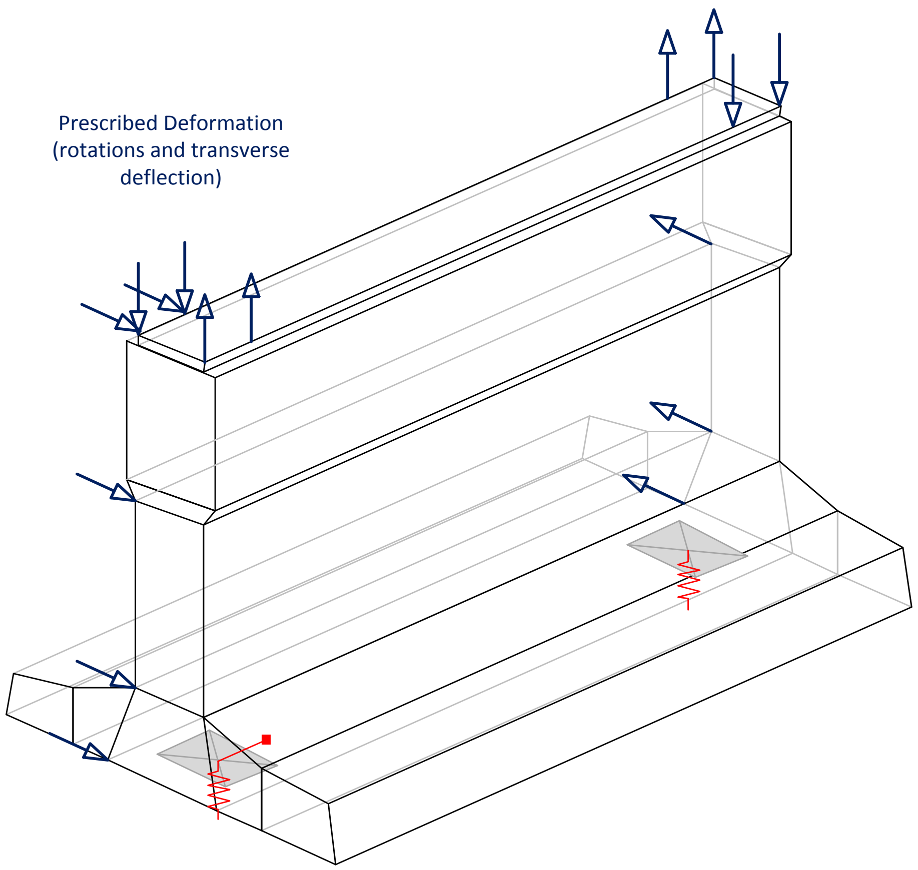

Figure 5-27 Transverse deflection and rotations (prescribed deformations and boundary conditions)

5.6 A physical non-linear model of one ZIP girder

The physical non-linear model of one girder is described in this paragraph. Also the occurring phenomena are presented and explained. In this model the end diaphragm is included.

5.6.1 Torsion stresses in finite elements

It is important that the finite elements can visualize correctly the shear stresses due to torsion. Minalu used coarse elements and integrated stresses to obtain the torsional moments in the girder which gave accurate results.[9] For his research this was sufficient, but for the current model the real occurring torsional stresses in the web are important.

The torsion behaviour is simulated using the rotations of the load case of Spanbeton (paragraph 5.3.3). Linear elastic material properties are used. No prestressing is applied. The maximum torsion is expected at the location 26-27 meter, see Figure 9-9. The occurring torsional moment is 68 kNm. At that location a refinement of the mesh is made (Figure 5-28). The expected shear stress can be calculated using the knowledge from the program ShapeBuilder, paragraph 6.1. The model was carried out in ULS, so a factor of 1.35 must be applied.

$$\tau = 1.35 \cdot \frac{68}{100} \cdot 2 = 1.84\ {}^{N}/_{mm^2}$$

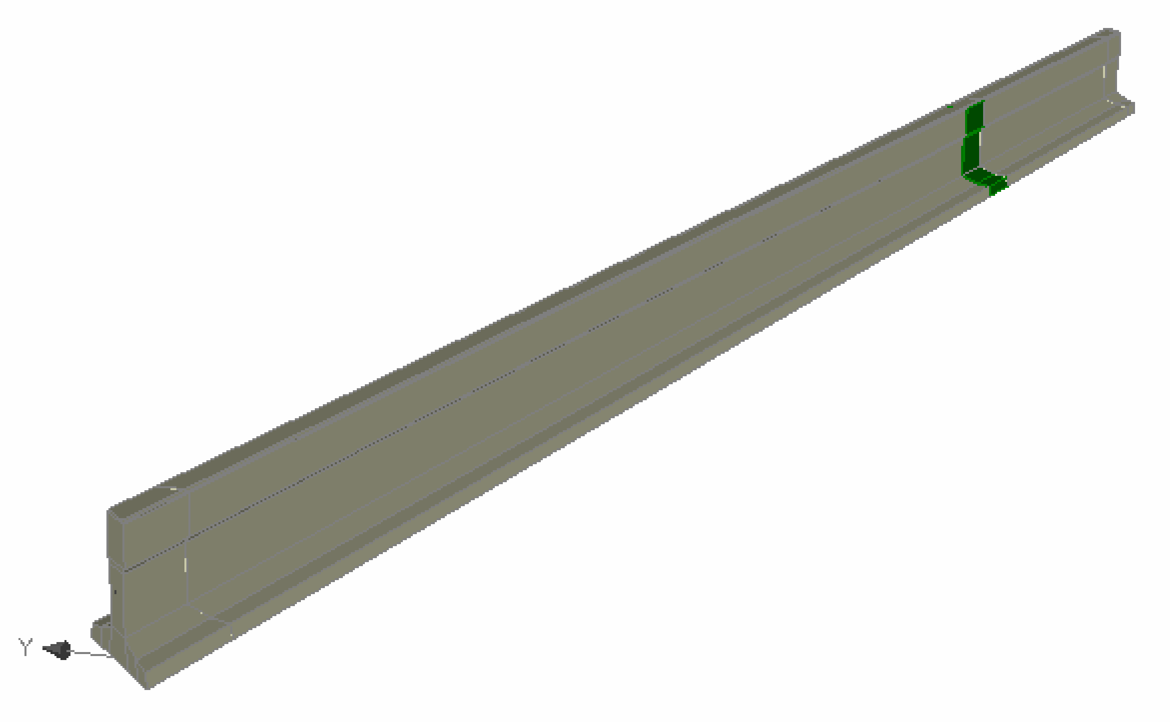

Figure 5-28 Local refinement in ZIP-girder

Five different finite element types or sizes are compared:

1. Coarse linear elements, size 0.2 m
2. Fine linear elements, size 0.04 m
3. Coarse quadratic elements, size 0.2 m
4. Fine quadratic elements, size 0.1 m
5. More refined quadratic elements, size 0.05 m

[9] Minalu, Kassuhun K. (2010), *Finite element modelling of skew slab-girder bridges.* Page 89.

The shear stresses are measured along the surface of the ZIP girders as indicated in Figure 5-29. In the same figure the shear stresses for the five considered cases are presented.

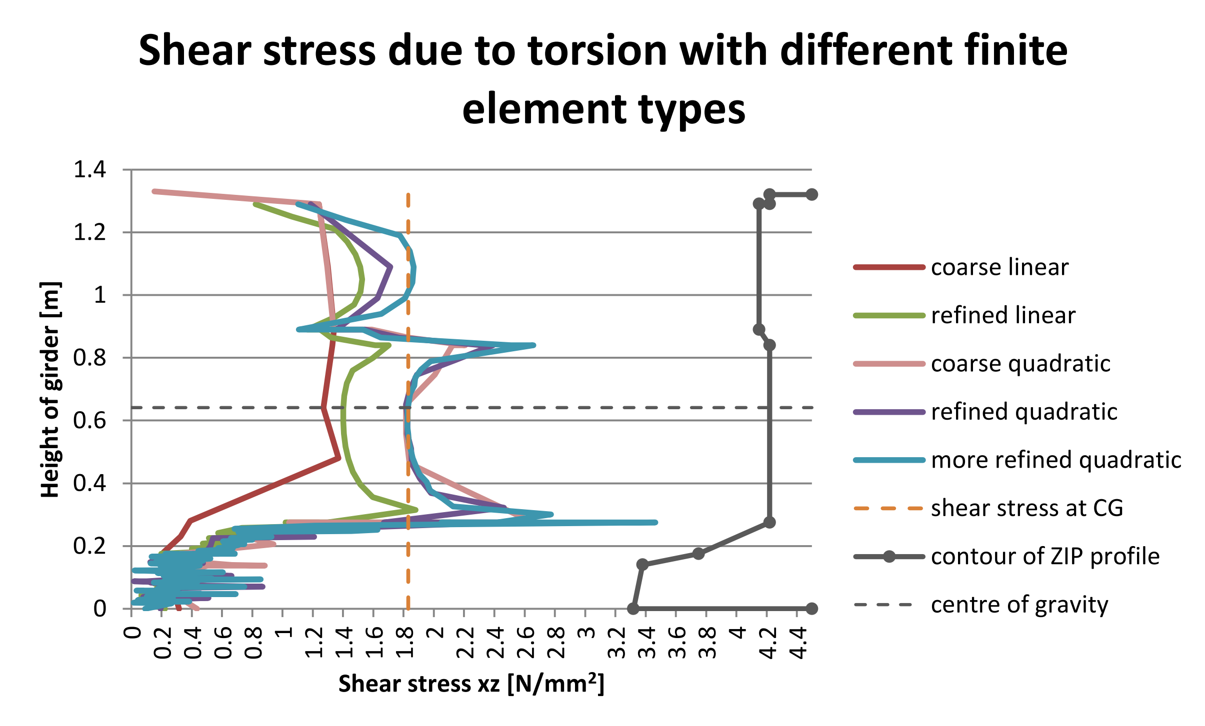

Figure 5-29 Comparison of shear stress due to torsion along perimeter of ZIP girder

The shear stress occurring at the height of the centre of gravity is dependent on the choice of finite element type, see Table 5-1. Especially quadratic elements can visualize shear stresses due to torsion accurately.

Case	Shear stress at centre of gravity
Course linear elements	1.28
Fine linear elements	1.40
Coarse quadratic elements	1.82
Fine quadratic elements	1.83
More refined quadratic elements	1.83

Table 5-1 Comparison shear stresses at centre of gravity

It is visible that quadratic elements calculates the shear stresses due to torsion correctly. The peak stresses are also visible in the analysis of the cross-section made with ShapeBuilder (Figure 6-1). A mesh refinement causes larger peak stresses. These are very local effects and are neglectable.

The coarse and fine quadratic elements shall be used for further analysis. The first chosen mesh is presented in Figure 5-30. Basically this is a mesh using coarse linear elements. Locally the beam can be refined in the important region at the end of the girder. In Figure 5-31 the refinement of the end of the girder is visible using fine quadratic elements, also the coarse quadratic elements can be used to refine this part of the girder. The top part of the girder is roughly meshed to be compatible with the loading plate on top of the girder. This way of modelling causes minimal modelling cracking (not real occurring cracks).

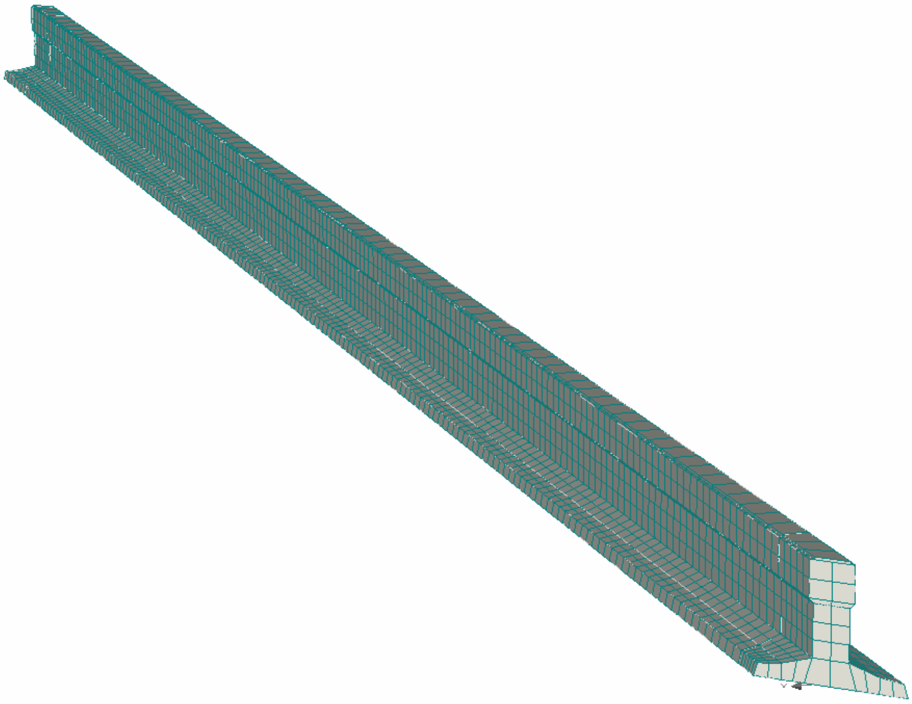

Figure 5-30 Coarse mesh for ZIP-girder in physical non-linear model, size 0.2 m

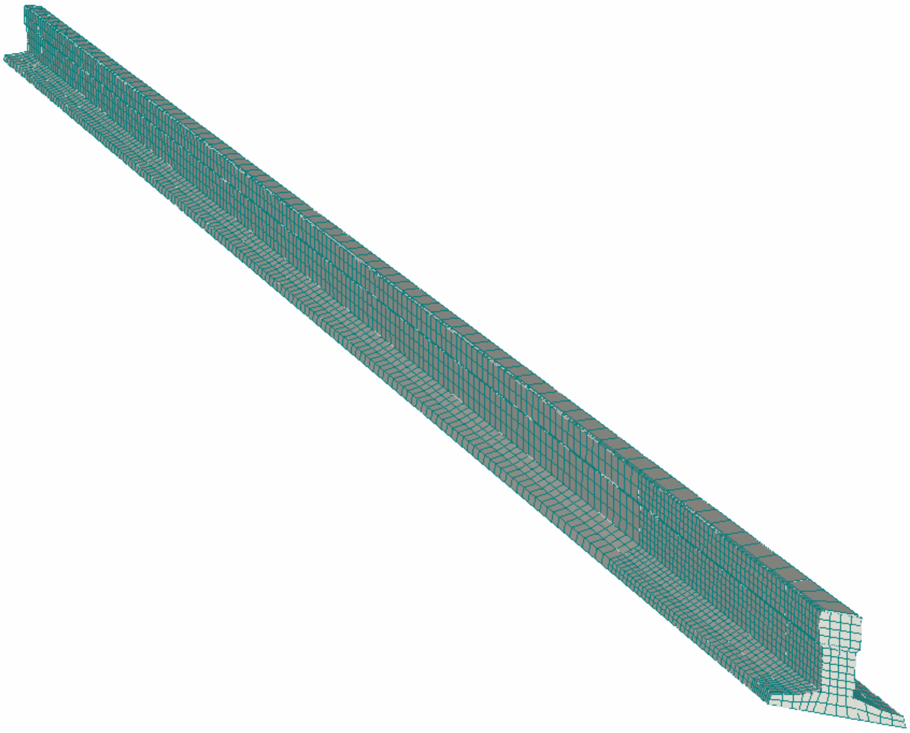

Figure 5-31 Mesh for ZIP-girder in physical non-linear model partially refined with quadratic elements, size 0.1 m

5.6.2 Material properties

The design material properties are used to model the bridge. For detailed information about the used materials, see appendix E.

5.6.3 Prestressing and reinforcement

The strands are positioned using the standard detailing rules of Spanbeton. The Bigaj bond model is used to model the bond between the prestressing cables and the concrete. Only in the ends of the girders the reinforcement stirrups are applied, also the reinforcement bars above the bend in the prestressing cables are modelled. See Figure 5-32 for an impression. For detailed information about the used materials, see appendix E.

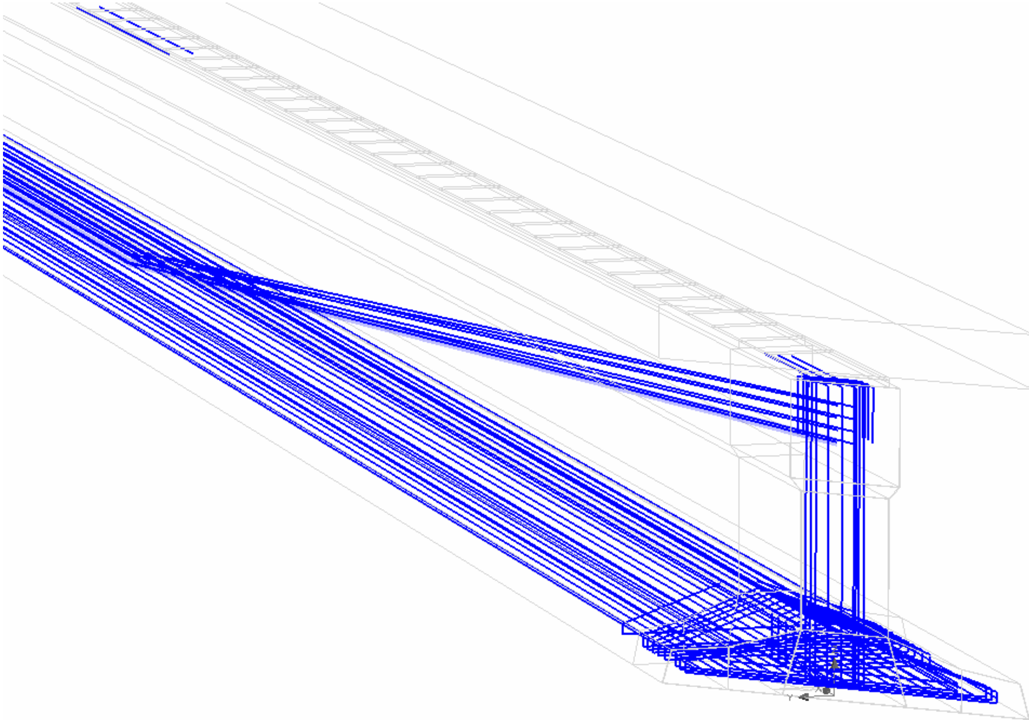

Figure 5-32 Prestressing cables and reinforcement in physical non-linear model of ZIP girder

Note: the Bigaj bond model is used to model the bond between the prestressing cables and the concrete. For that reason not the theoretical normal stresses are found but an approximation.

5.6.4 Connection with deck

The deformations occurring at the connection between the girder and deck are modelled using a loading plate. The loading plate is presented in Figure 5-33. The stiffness used is 10.000 MPa, and the plate thickness is 10 mm. This low values are chosen to avoid a substantial shift of the centre of gravity.

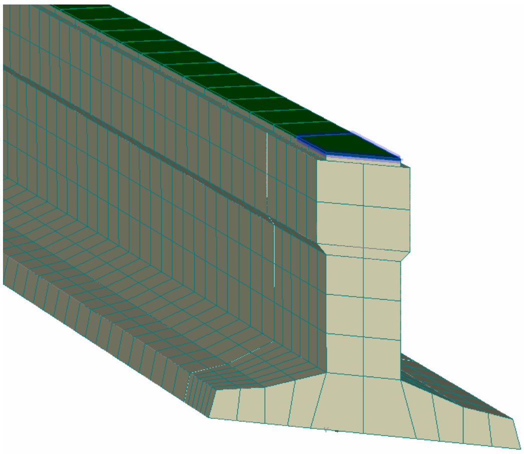

Figure 5-33 Top loading plate

5.6.5 Concrete deck

The first models did not have a deck on top of it. Only the determined Y- and Z-deformations are applied on the top of a ZIP girder, but the corresponding X-deformations are not correct in that case, due to a lower position of the centre of gravity. It can be analysed that, due to a lower level of the centre of gravity, at the top the longitudinal deformations will be too large and at the bottom the longitudinal deformations will be too small. For that reason on top of the loading plate a ‘dummy deck’ is applied to compensate this, as visualized in Figure 5-34. The stiffness of the deck is used to calibrate the deformations in the PNL-model to the deformations in the LE-model of the complete bridge.

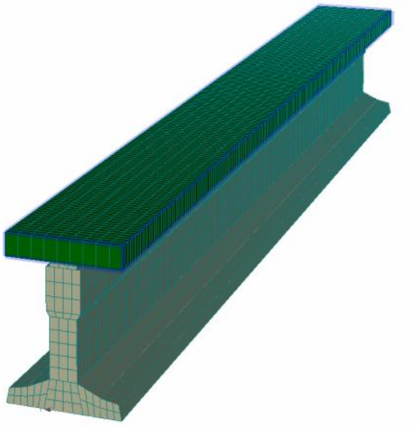

Figure 5-34 Dummy-deck in physical non-linear model

The required stiffness for the ‘dummy deck’ is determined using a model with coarse linear elements. In Figure 5-35 the reference longitudinal deformation due to load step 2, dX2 reference (following from the LE model of the bridge), is plotted for the bottom of the girder. It would be optimal to reach that deformation. Also the occurring deformation when no dummy deck is applied in the PNL-model, dX2 without dummy deck, is plotted. A large difference is visible.

First the stiffness as used in the LE-model of the bridge (16000 MPa) is applied, but this did not give a correct deformation. Chosen is for a ‘trial-and-error’ method to determine the stiffness which gives the correct X-deformations. A stiffness of 30000 MPa gives good results. In the figure this process is visible. An explanation for this high stiffness could be that in the total bridge system a larger width carries the normal force.

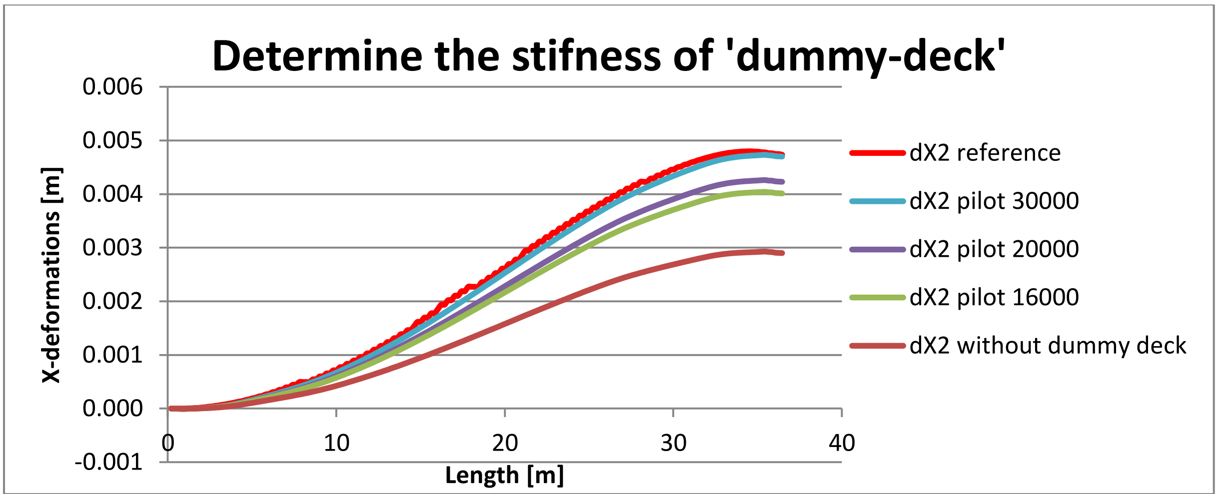

Figure 5-35 Deformations in bottom of girder

5.6.6 End diaphragm beam

5.6.6.1 Description of model

In the detail PNL model the end diaphragm beams must be simulated. It is very complicated to include all the effects of this beam.

Two models are investigated:

1. A loading plate on the ends of the girders, made of steel (Figure 5-36). In the indicated nodes (Figure 5-27) deformations are applied. With this method the 'clamping effect' of the beam is neglected. The loading plate is made of steel, the plate thickness is 10 mm. Only transversal prescribed deformations are applied.
2. A more advanced model which simulates the 'clamping effect' of the end diaphragm beam. This model is presented in Figure 5-37. Steel plates with a minimal thickness of 30 mm are applied. Only transversal prescribed deformations are applied.

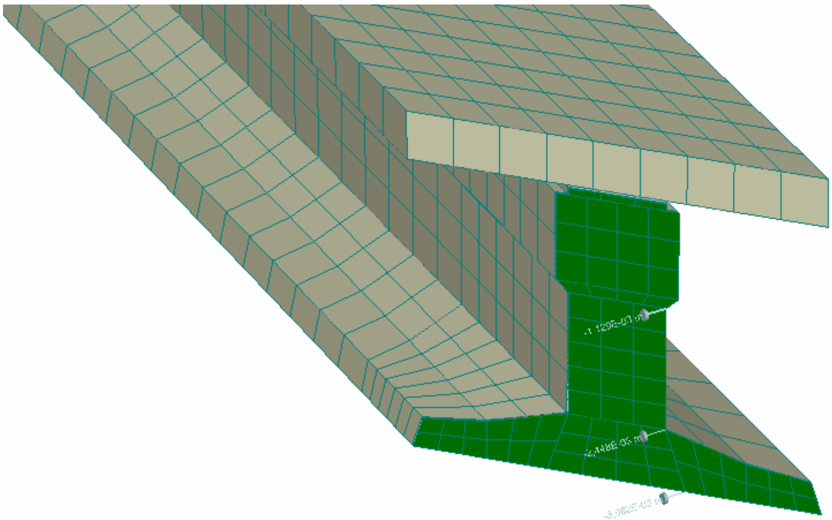

Figure 5-36 End load plate

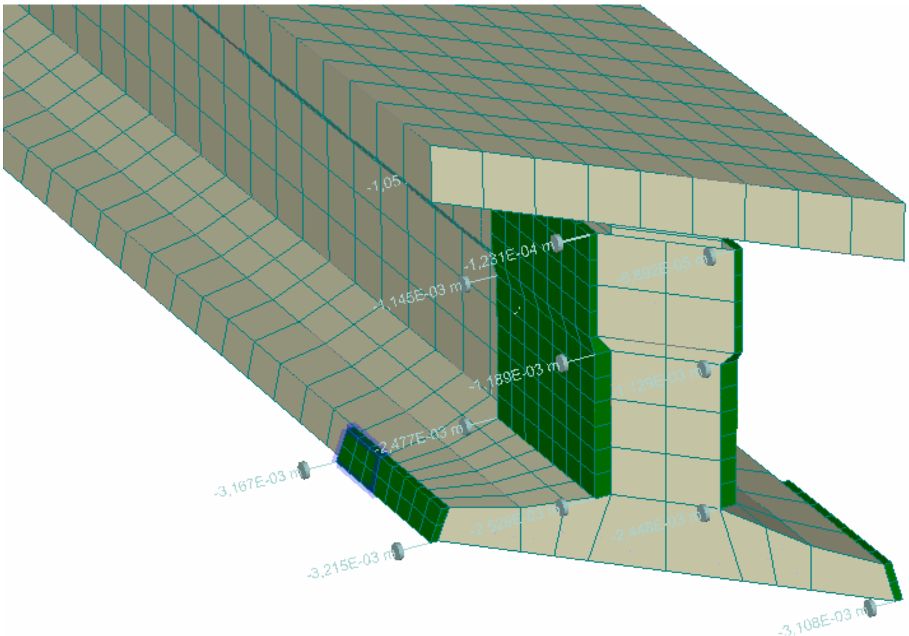

Figure 5-37 More advanced end loading plates

5.6.6.2 Comparison of models

A model of the ZIP-girder refined with coarse quadratic elements is used to analyse the deformations for the different models for the end diaphragm beam. The deformations in X- and Z-direction do not change when a different model for the end diaphragm beam is used, Figure 5-39 and Figure 5-40.

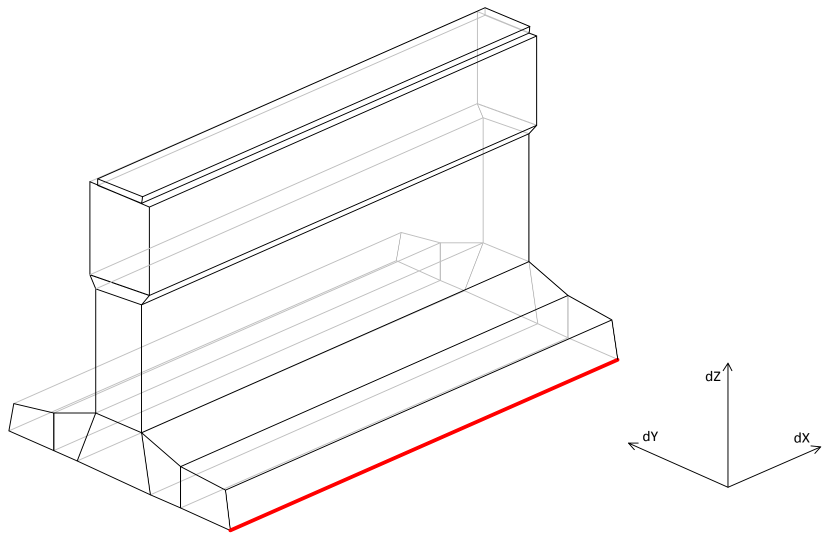

Figure 5-38 Check of deformations in the edge indicated with red

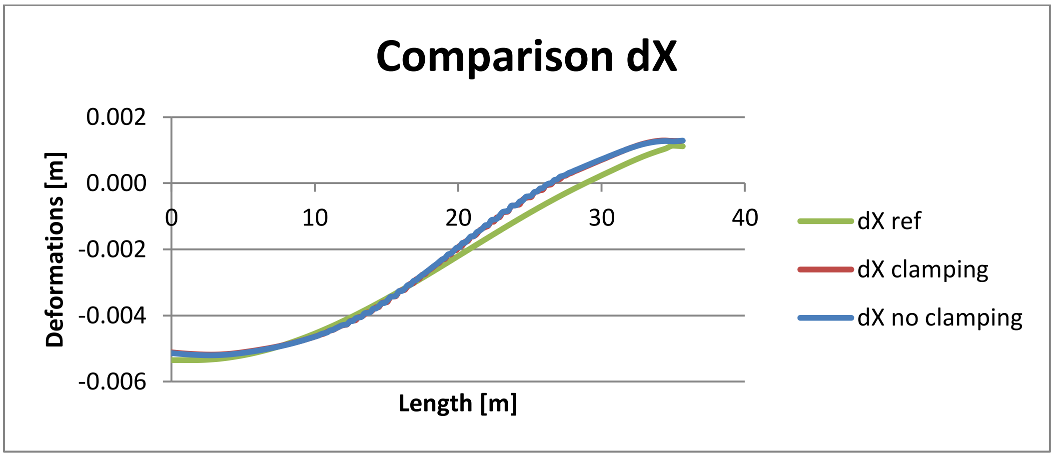

Figure 5-39 Comparison longitudinal deformation, dX

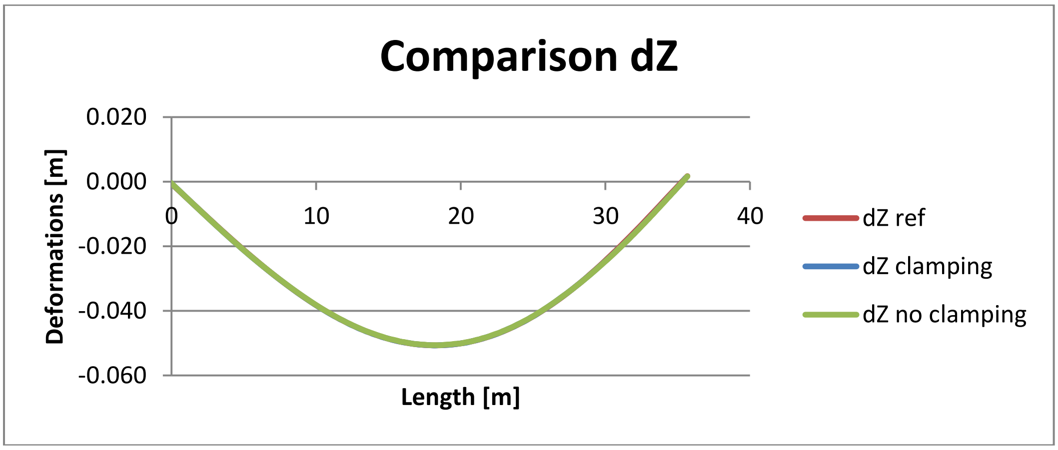

Figure 5-40 Comparison deflection, dZ

The deformation in Y-direction is changing. In Figure 5-41 the deformations are presented. It is visible that in the acute corner the different models do not influence the deformations a lot, at the obtuse corner however a substantial difference is found. The influence of this deviation shall be investigated later.

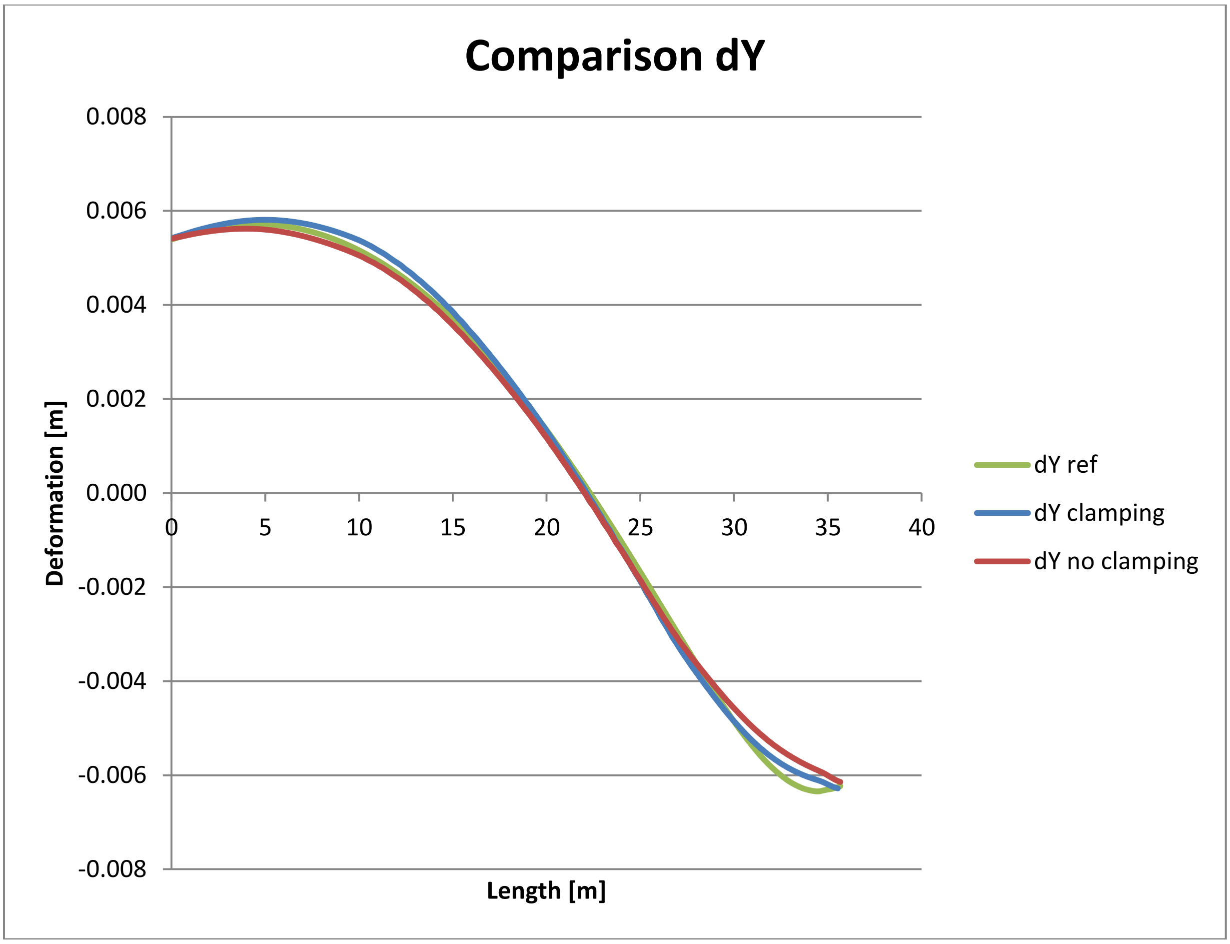

Figure 5-41 Comparison transverse deformation, dY

From the comparison of the two models to simulate the end diaphragm beam follows that including the ‘clamping effect’ gives better results. That model, Figure 5-37, shall be used in the PNL model for one ZIP girder.

5.7 Results skew bridge for load case Spanbeton

Only the results for the model loaded with the load case of Spanbeton are presented, the load case of Minalu leads to similar results. The models are carried out in ultimate limit state (ULS).

Models carried out:

I. PNL model, locally refined with coarse quadratic elements
II. PNL model, locally refined with fine quadratic elements

5.7.1 PNL model, locally refined with coarse quadratic elements

5.7.1.1 Check deformations

Is already presented in Figure 5-39, Figure 5-40 and Figure 5-41 for the model 'with clamping'. The deformations are reasonable. Note the difference in transverse deformation.

5.7.1.2 Stresses

Sections are made at x=33.08 m to visualize the stresses because at that location maximal stresses occur.

Shear stresses at x=33.08 meter. Shear stress (Figure 5-42):

- Total: 3.30 N/mm^2
- Shear force: 2.73 N/mm^2
- Torsion moment: 0.58 N/mm^2

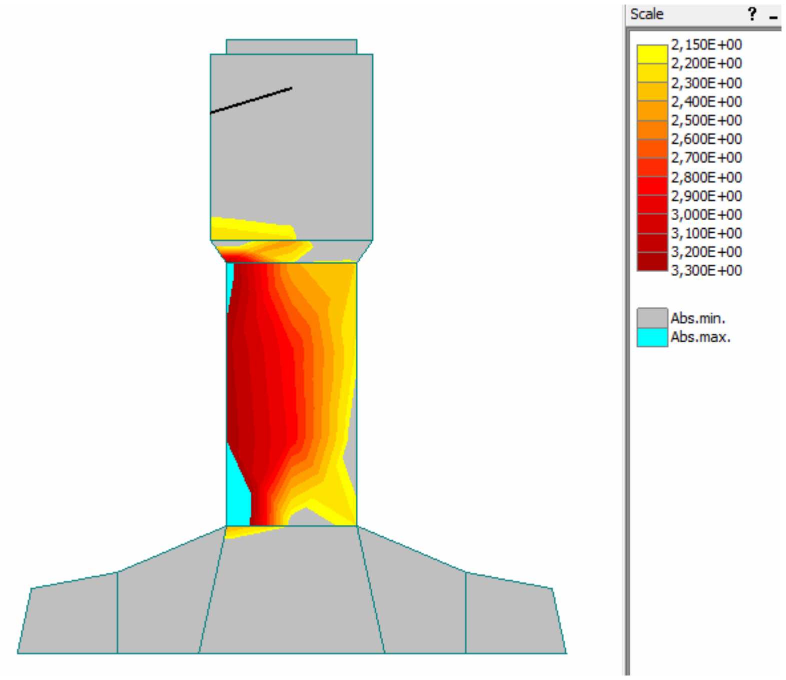

Figure 5-42 Shear stresses in PNL model I

When the principal stresses are studied they are higher than expected. The principal stresses that occur are presented in Figure 5-43. It appeared that vertical stresses occur.

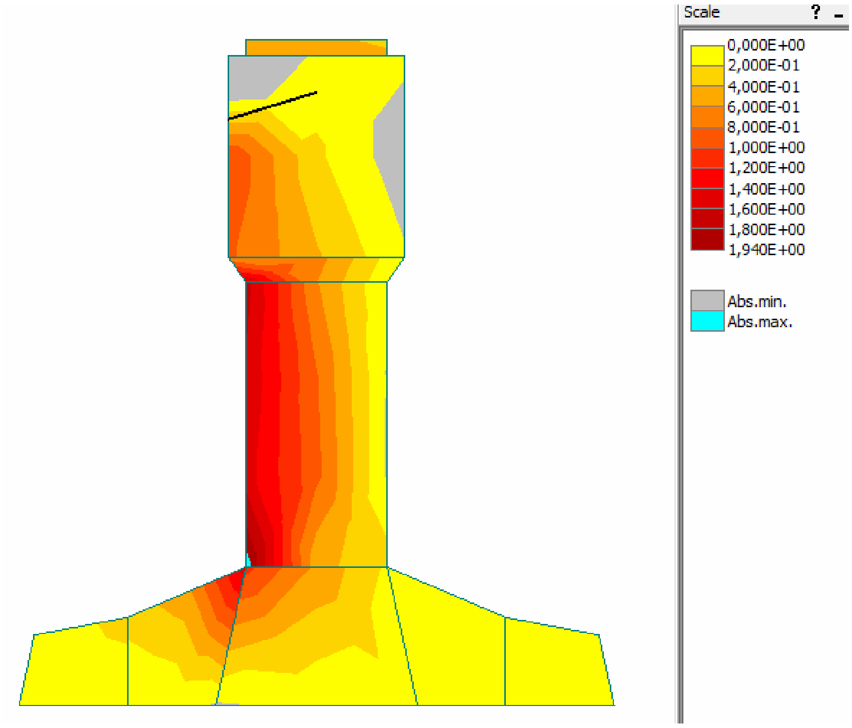

Figure 5-43 Principal stresses in PNL model I

The occurring vertical stresses that occur are presented in Figure 5-44.

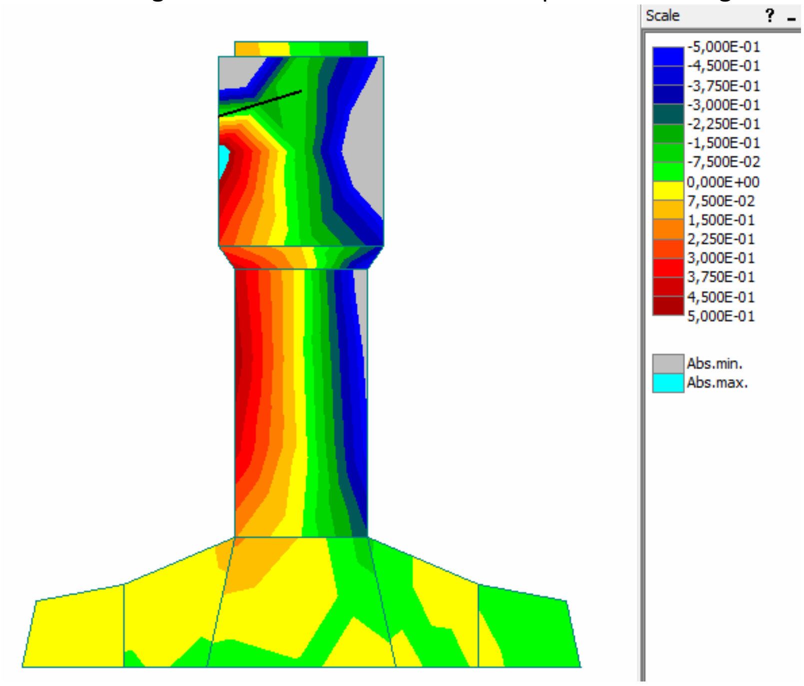

Figure 5-44 Vertical normal stresses in PNL model I

5.7.1.3 Cracking

Due to introduction of the prestressing force in the concrete in the ends of the girders cracks occur. Spanbeton uses standard reinforcement in that area to control the crack widths. In all the following models this cracks are visible but not further investigated.

The skew bridge of 45° is modelled with a sharp end (see presented figures). In practice this corner is not made because it will be simply damaged during handling the girder. Cracking, and all kind of other effects, in the region of this sharp corner are for that reason of no interest.

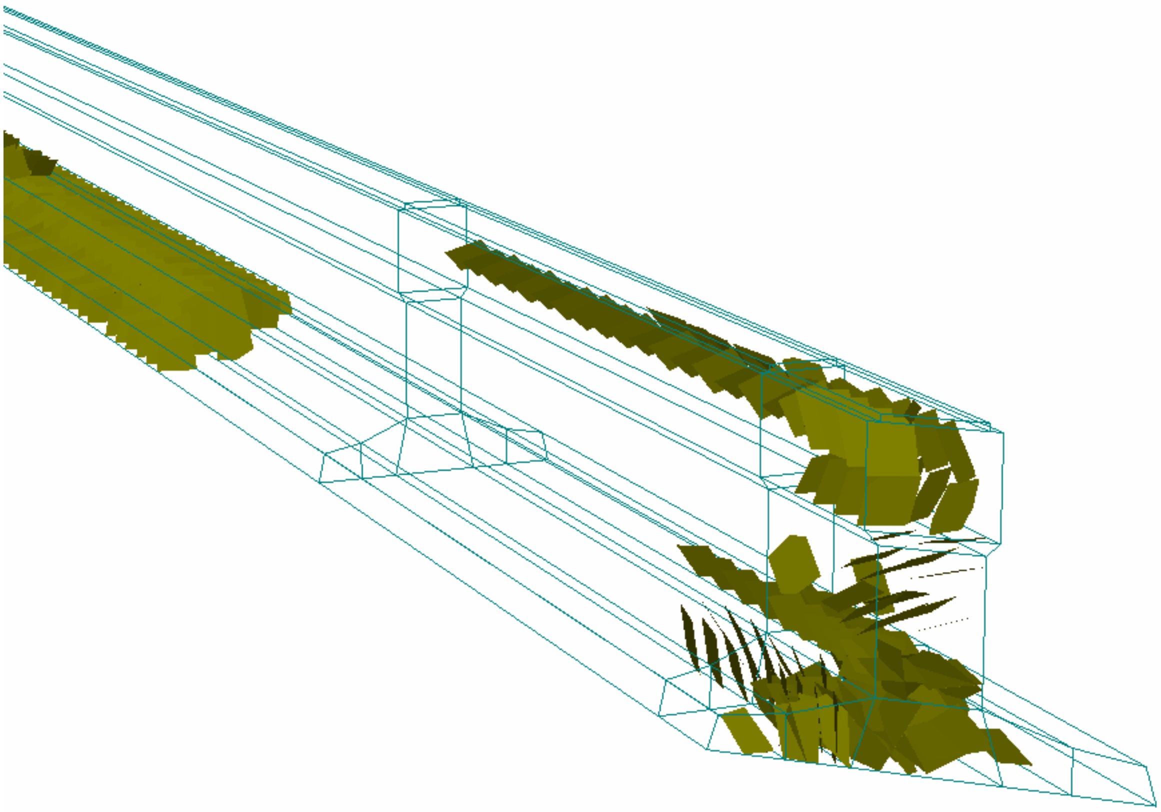

Figure 5-45 Occurring cracks in PNL model I

Remarkable are the cracks occurring in the top of the girder, the maximum crack width is $1.76 \cdot 10^{-4}$ m. In the same zone no flexural cracks are visible. So an uncracked zone appears in which principal stresses can be checked.

5.7.2 PNL model, locally refined with fine quadratic elements

This model is carried out to be sure that a mesh refinement does not influence the results.

5.7.2.1 Check deformations

The deformations can be checked as presented before, yet visualized in Figure 5-46. Only the transverse deformation is presented, it is already noted that this deformation deviates from the reference deformation. The deviation is more severe for 'the refinement with fine quadratic elements' compared with 'the refinement with coarse quadratic elements'.

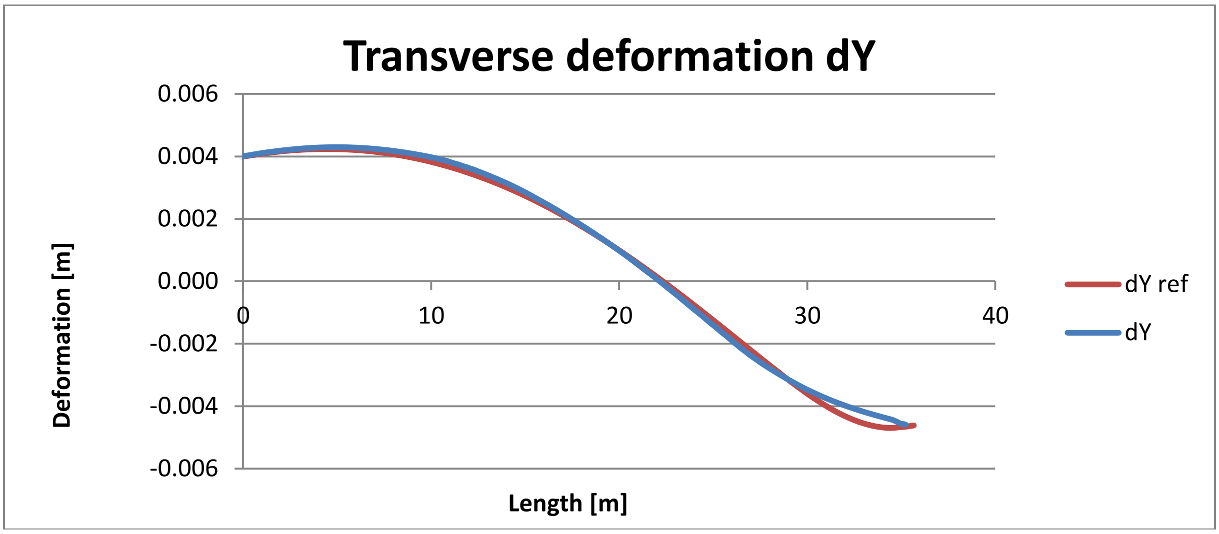

Figure 5-46 Transverse deformation, dY

5.7.2.2 Stresses

The shear stress at x=33.08 meter consists of the following parts:

- Total: 3.00 N/mm^2
- Shear force: 2.28 N/mm^2
- Torsion moment: 0.73 N/mm^2

The shear stresses are presented in Figure 5-47.

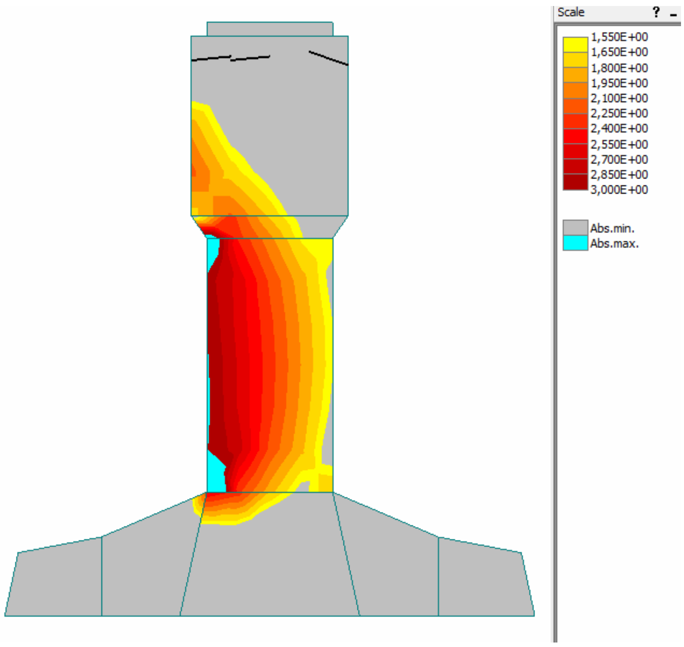

Figure 5-47 Shear stresses in PNL model II

The principal stresses are presented in Figure 5-48.

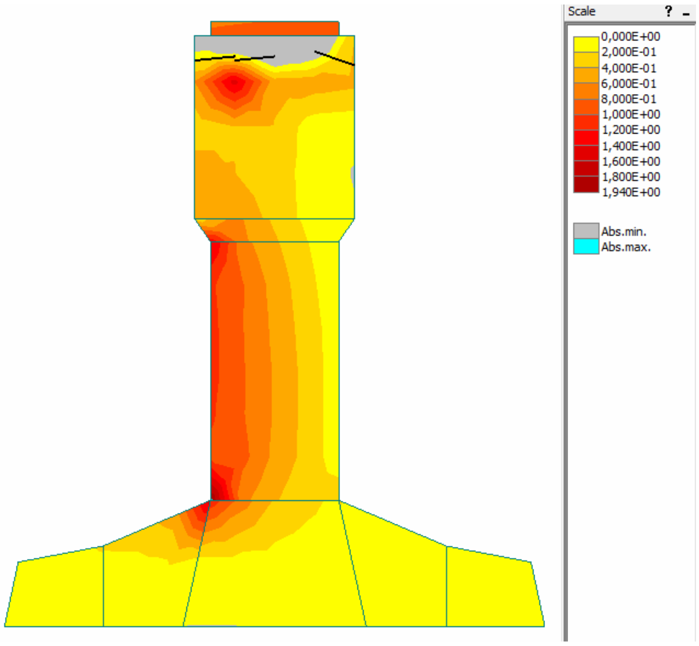

Figure 5-48 Principal stresses in PNL model II

The vertical normal stresses are presented in Figure 5-49.

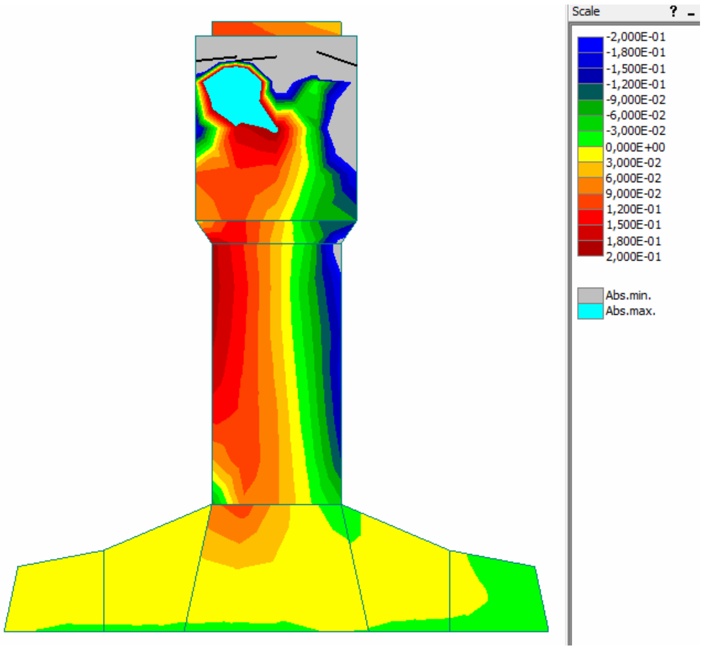

Figure 5-49 Vertical normal stresses in PNL model II

5.7.2.3 Cracking

In the top of the girder cracks with a magnitude of 0.5 mm occur. In relation with the deviating transverse deformations: the applied deformations on top of the girder are not connected with the transverse deformations at the bottom of the girder because the connection is broken. The cracks at the bottom of the web are very small and neglectable (0.002 mm). Also here no flexural cracks are visible.

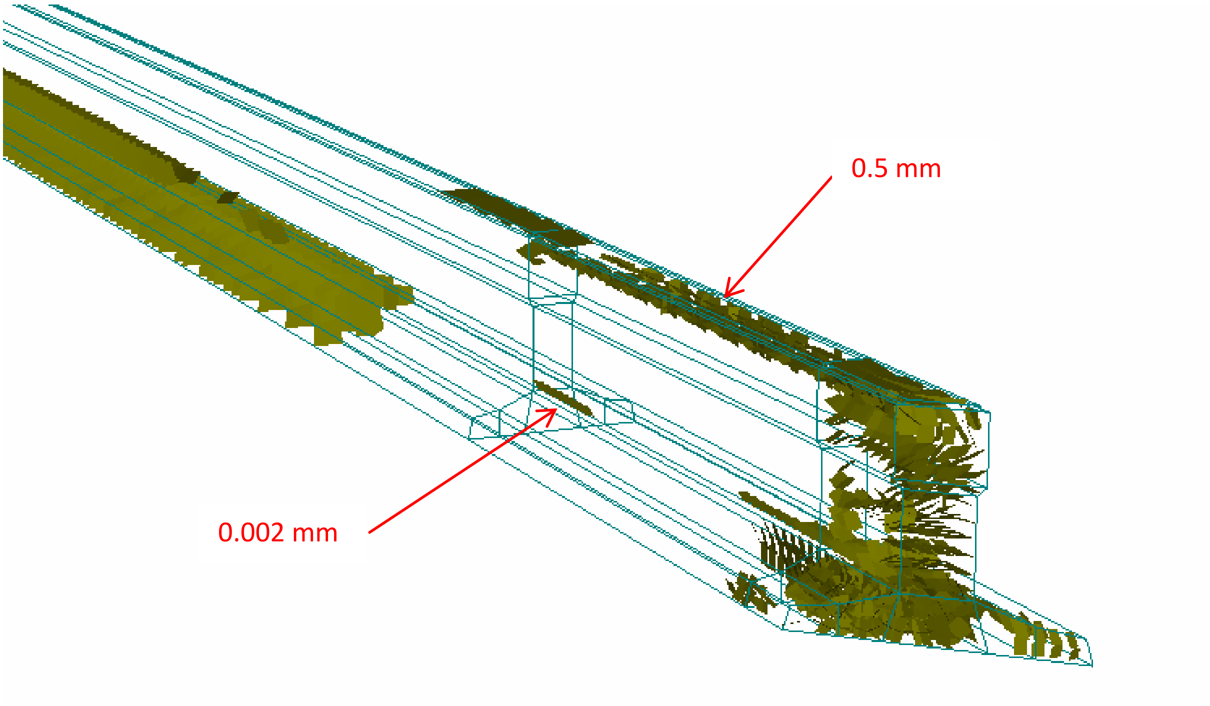

Figure 5-50 Occurring cracks in PNL model II

5.7.3 Comparison observations

The cracking in both models occurs at the same locations. Cracks due to prestressing and flexural cracks are visible. Also cracking in the top is present in both models, this cannot be explained physically. It is visible that beside this cracking in a large zone of the girder no cracking occurs.

The total shear stresses in both models are comparable, the ratio between the part due to shear force and due to torsion changes.

It is visible that this models contains some unexpected phenomena as the mentioned cracking and the changing ratio between shear stresses due to shear force and torsion. Also a vertical tension stress is measured which influences the principal stress. Finally the transverse deformations are not totally correct. This will be investigated further.

5.8 Analysis of unexpected phenomena

The observed phenomena mentioned in paragraph 5.7.3 can be explained. Important is the deviating transverse deformation. This deviation causes vertical tensile stress, but also a deviation in the applied rotations, and consequently a deviation in the applied torsion moments.

5.8.1 Vertical normal stress

5.8.1.1 Introduction

In the models carried out vertical stresses are observed, are these stresses really occurring? The vertical stresses occurring in the model refined with coarse quadratic elements (model I) can be plotted, Figure 5-51.

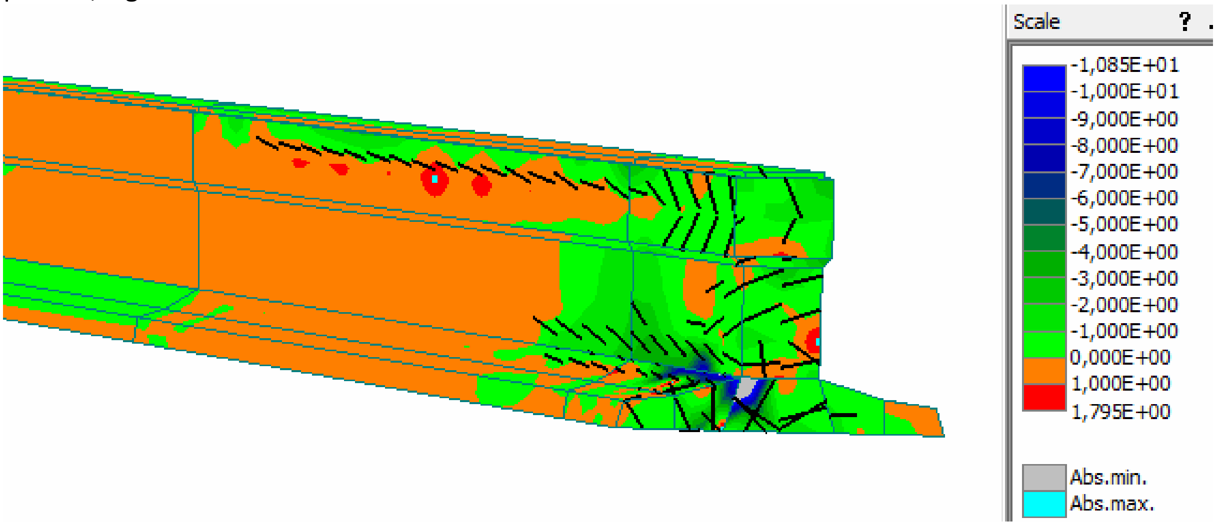

Figure 5-51 Vertical stresses in end of ZIP-girder in PNL model I

When the vertical stresses are analysed in the linear elastic model of the bridge (presented in paragraph 5.2) the following stress distribution is visible, presented in Figure 5-52. This are stresses at the height of the centre of gravity. Only a stress of 0.1 N/mm^2 is found in SLS, this means about 0.14 N/mm^2 in ULS. That is much smaller than the stresses occurring in the physical non-linear model where the stresses are about 1-2 N/mm^2. So it is expected that the observed high vertical stresses are not correct.

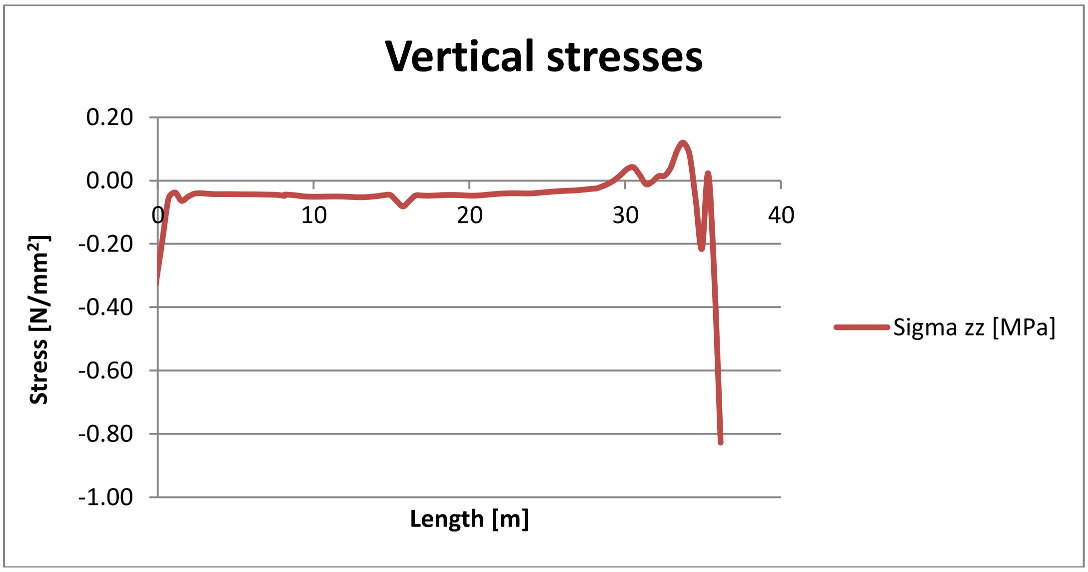

Figure 5-52 Vertical stresses occurring in the linear elastic model of the bridge in SLS at the height of the centre of gravity

5.8.1.2 Compatibility problem

The explanation for the occurring vertical stresses is that the small deviation of the transverse deformation causes a compatibility problem. The difference in transverse deformation in the cracked zone is enlarged from Figure 5-41 and presented in Figure 5-53. It was expected that including the 'clamping effect' of the end diaphragm beam would reduce the difference more.

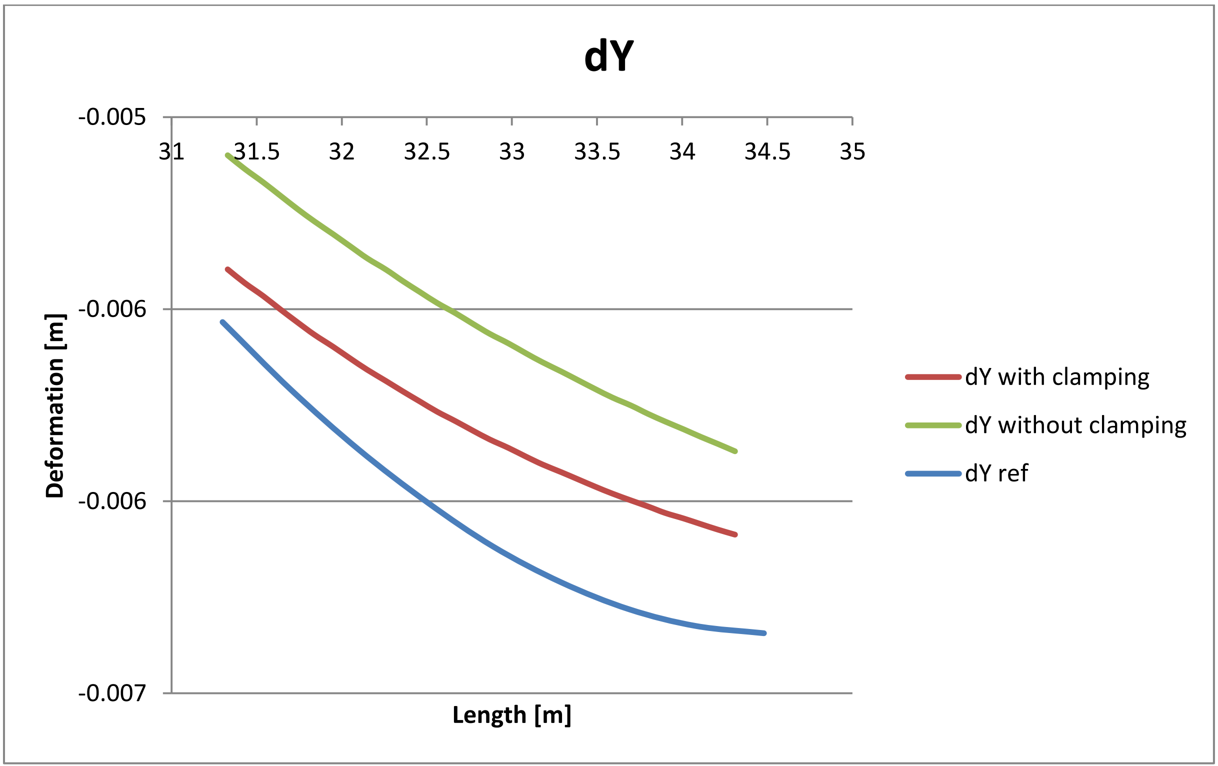

Figure 5-53 Difference in transverse deformation for different models of the end diaphragm beam in ULS

The rotation of the beam was calculated two times in paragraph 5.3.3 when the rotations from the linear elastic model of the bridge were analysed. The two calculations correspond well for that model. The relevant figure is shown again in Figure 5-54.

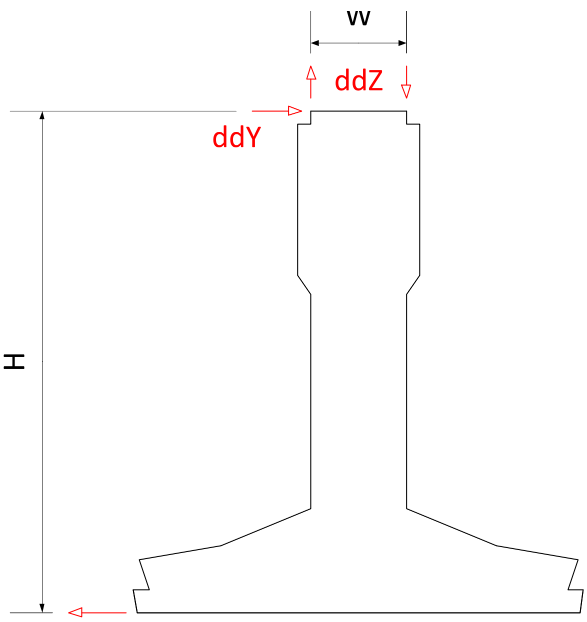

Figure 5-54 Determination of rotations

The deviation in transverse deformation influences the calculation of the rotations. This can be explained with formulae. The used formulae in paragraph 5.3.3 are:

$$\vartheta_{dY} = \frac{ddY}{H}$$
$$\vartheta_{dZ} = \frac{ddZ}{W}$$

When ddY is too small: $\vartheta_{dY} < \vartheta_{dZ}$. This causes vertical stresses.

5.8.1.3 Estimate of stresses

An estimation of the occurring stresses can be made. At 33.3 m a difference of 0.29 mm is found.

The difference in rotation at that location is:

$$\vartheta_{dY} = \frac{0.29 \cdot 10^{-3}}{1.32} = 2.17 \cdot 10^{-4}\ [rad]$$

This leads to an compatibility difference of $2.17 \cdot 10^{-4}$ x 0.28 = $0.61 \cdot 10^{-5}$ m for ddZ. The applied ddZ deformation is $4.35 \cdot 10^{-4}$ m, the deviation is 13%!

The deformations are applied with 400 mm distance on the top of the girder. It is assumed that this is the depth in which the difference in deformation is taken. An estimation of the stress can be made as follows:

$$\varepsilon = \frac{ddZ}{d} = \frac{0.61 \cdot 10^{-5}}{0.4} = 1.525 \cdot 10^{-5}\ [-]$$
$$\sigma = \varepsilon \cdot E = 1.525 \cdot 10^{-5} \cdot 38000 = 0.6\ {}^{N}/_{mm^2}$$

5.8.1.4 Experiment with ATENA

A simple model (length 4 meters) is carried out in ATENA to analyse the occurring vertical tension stresses. The loads and boundary conditions are applied as visualized in Figure 5-55. The found deviation of deformation ($0.61 \cdot 10^{-5}$ m) is applied on all the nodes along the top of the girder.

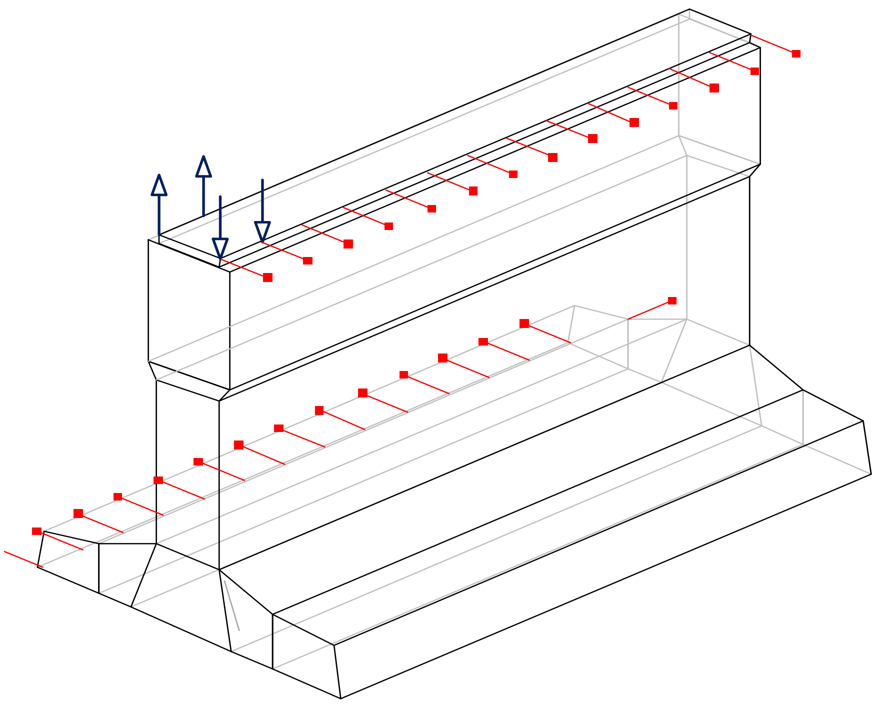

Figure 5-55 Model to simulate imposed deformation

The occurring stresses for the coarse and refined quadratic model are shown in Figure 5-56 and Figure 5-57. Visible is that the local applied deformations causes local peak stresses. Another observation is that in the model with refined quadratic elements the vertical stresses in the web are more localized.

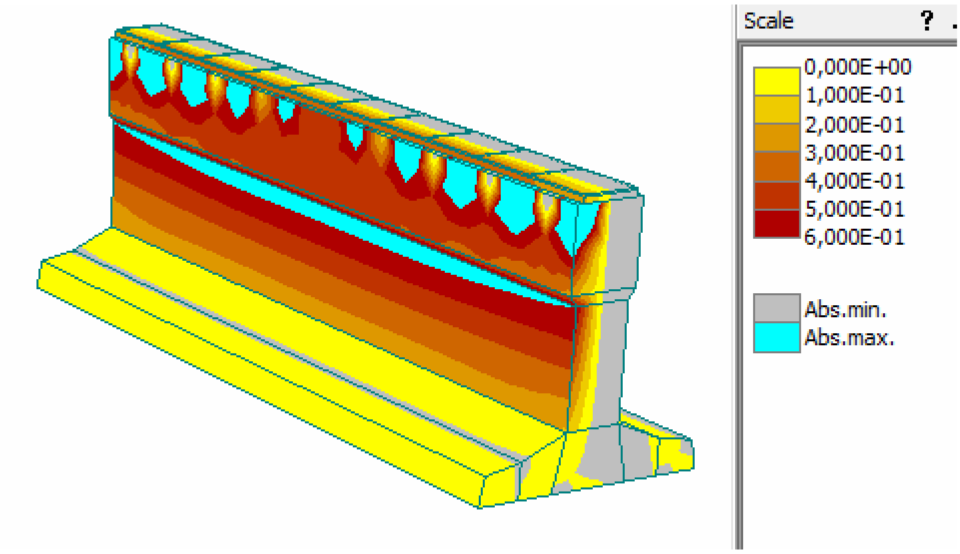

Figure 5-56 Model with coarse quadratic elements, peak stress 1.924, no cracks occur

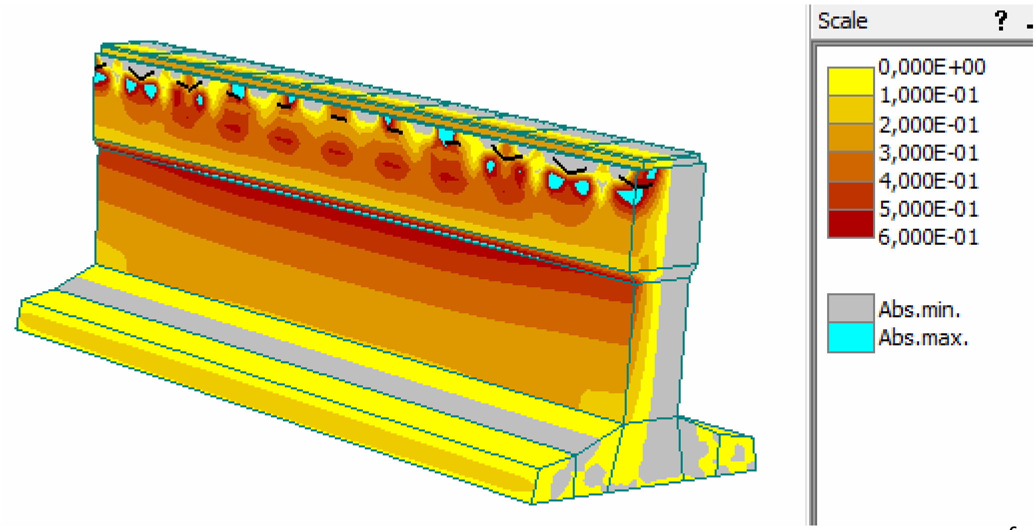

Figure 5-57 Model with refined quadratic elements, peak stress 1.911, cracks of about $5 \cdot 10^{-6}$ m occur

5.8.1.5 Conclusion

From the hand calculation and the experiments with ATENA the relation between the deviating transverse deformations and the vertical stresses is sufficiently proven.

5.8.2 Deviation in applied torsional moments

The torsion moments are applied on the model by prescribed deformations, which represent rotations. When the rotations are deviating this load is also not applied correct anymore. With the knowledge of paragraph 9.3.2 the deviation can be determined.

The calculation of the deviation for model II (refined with fine quadratic elements) is presented. The rotations can be calculated using the function presented in Figure 5-58.

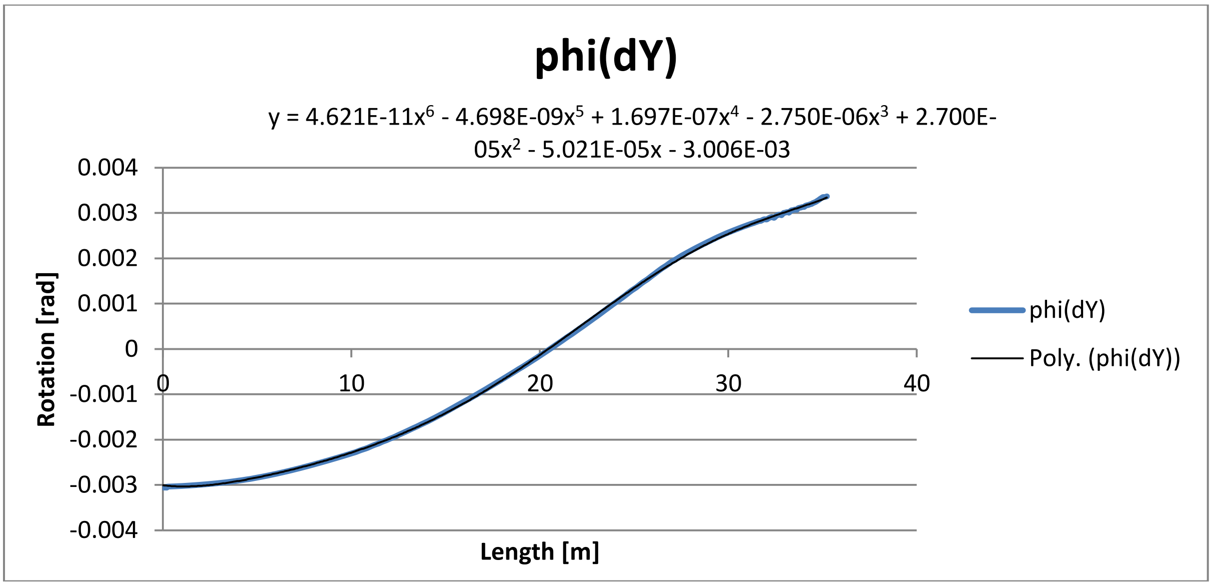

Figure 5-58 Rotation for model I

Using the function of the rotation the torsional moments can be determined, presented in Figure 5-59. The occurring torsional moments can be compared with the torsional moments that should occur, the following curves are plotted:

- Blue: Reference torsional moment (Figure 9-9).
- Green: Torsional moments that occur.
- Red: A substantial difference.

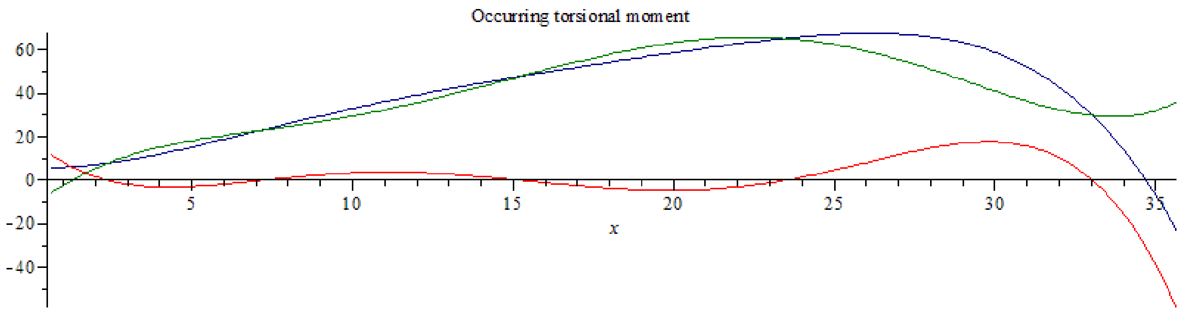

Figure 5-59 Deviations in torsional moments for model I

It is visible that in this model the occurring torsional moments deviates a lot from the intended load due to the deviation in transverse deformation.

5.9 Conclusion

A small deviation in transverse deformation has influence on the stresses and cracking in the model. Firstly the deviation causes vertical stresses. In the analytical calculation of the principal stresses it was assumed that no vertical stresses occur. In the finite element model however these stresses are present and disturb the calculation of the principal stresses. Secondly the deviation influences the applied torsional moments.

Despite the observed deviations in the models an uncracked zone is visible. This zone will be further analysed. This will be done by more detailed analyses of the occurring stresses in that region.

6 Shear stresses due to torsion in cross-section of ZIP girder

It is important to understand the distribution of shear stresses due to torsion in a ZIP girder. In daily practice hand calculations are used to distribute the torsion over the different parts of a cross-section. Calculating correctly the shear stresses needs more attention.

The occurring stresses at the height of the centre of gravity due to a torsional moment of 100 kNm is calculated using different methods.

6.1 Method 1: Calculation of shear stresses with a finite element program

The program ShapeBuilder is used to determine the occurring shear stresses due to a torsional moment of 100 kNm. A shear stress of 2 N/mm^2 occurs at the height of the centre of gravity. This stress is determined by placing the cursor in the interesting point, the program gives than the stress at that location as output.

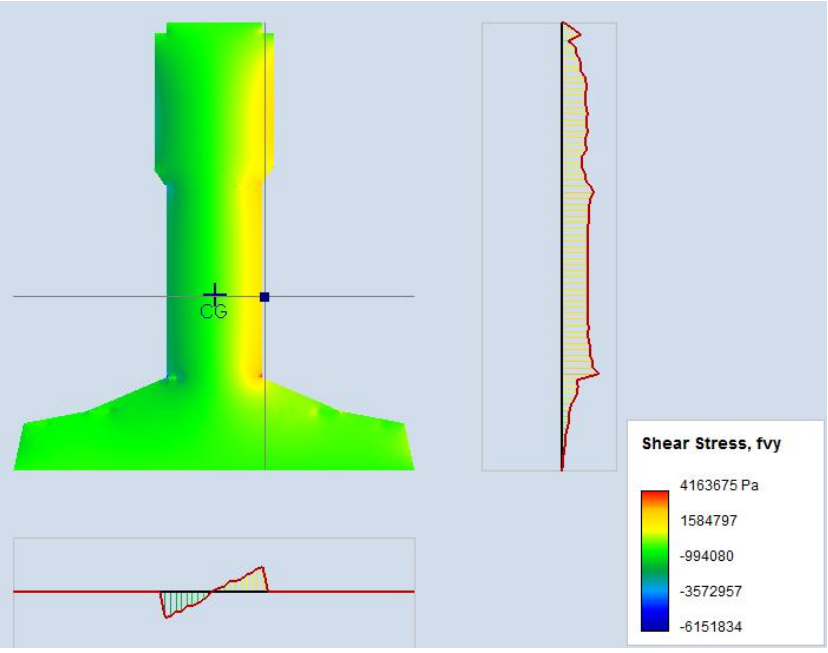

Figure 6-1 Shear stresses due to torsion calculated with ShapeBuilder

Also the program Scia Engineer can be used to analyse the stresses (Figure 6-2), a mesh size of 3 mm is used. In this program the value in a particular point cannot be determined.

The stresses presented in Scia Engineer are too low. The shear stress can be calculated by multiplying the values by a factor 1000·M_T. The value of M_T is 100 kNm. It is visible that at the height of the centre of gravity the stress than is between 1.44 N/mm^2 and 2.01 N/mm^2. This corresponds well with the results found with the program ShapeBuilder.

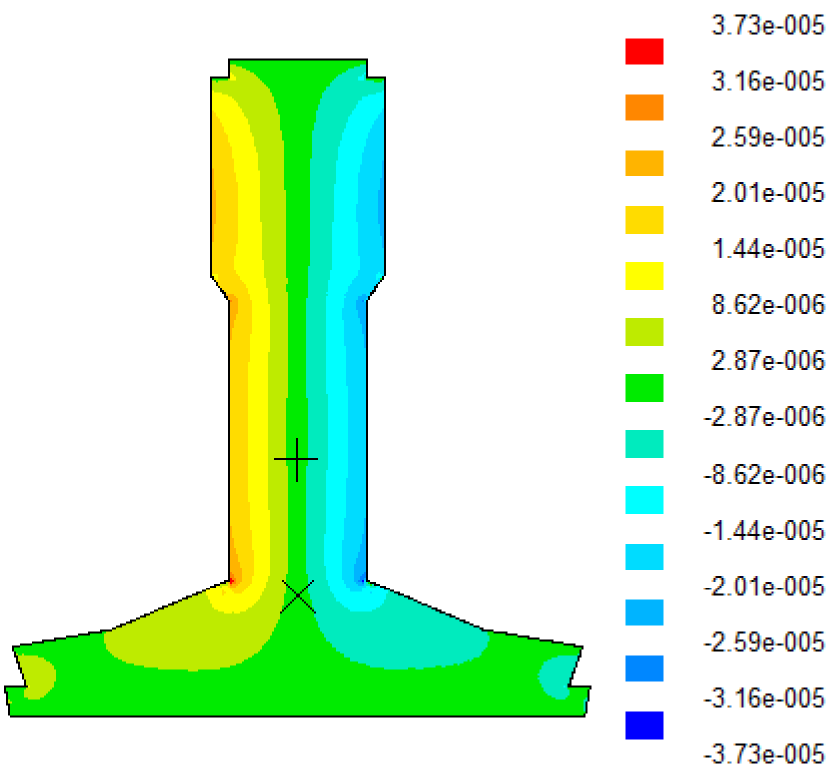

Figure 6-2 Shear stresses due to torsion calculated with Scia Engineer

6.2 Method 2: Estimation of torsion stresses by hand

Some different possible cases are studied to see the influence of the chosen simplification on the results.

Case 1

The girder can be split up in some parts as visualized in Figure 6-3.

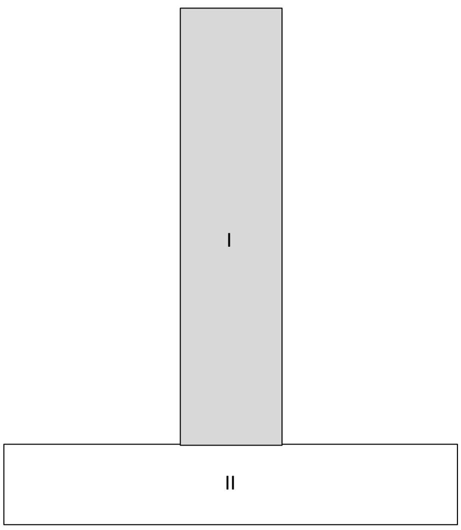

Figure 6-3 Model of first ZIP with deck to distribute torsion moments for case 1

The general formula for torsional stiffness is (can be derived from Table 2-2):

$$I_w = C_{I_w} \cdot b \cdot h^3$$

Applying the formula on the parts of the girder gives:
Part I:

$$\frac{b}{h} = \frac{1127}{280} = 4.03$$
$$I_{w,I} = 0.281 \cdot 1127 \cdot 280^3 = 6.95 \cdot 10^9 \; mm^4$$

Part II:

$$\frac{b}{h} = \frac{1180}{193} = 6.11$$
$$I_{w,II} = 0.297 \cdot 1180 \cdot 193^3 = 2.52 \cdot 10^9 \; mm^4$$

Part of torsion carried by the web of the ZIP-girder (shaded area in Figure 6-4):

$$\frac{I_{w,I}}{I_{w,total}} = \frac{6.95 \cdot 10^9}{6.95 \cdot 10^9 + 2.52 \cdot 10^9} = 0.73 \; [-]$$

A torsional moment of 73 kNm with $C_\tau = 0.288$ will give a shear stress of:

$$\tau = \frac{M_T}{C_\tau \cdot b \cdot h^2} = \frac{0.73 \cdot 100 \cdot 10^6}{0.288 \cdot 1127 \cdot 280^2} = 2.87 \; {}^{N}/_{mm^2}$$

Case 2

The girder can be split up in some other parts as visualized in Figure 6-4.

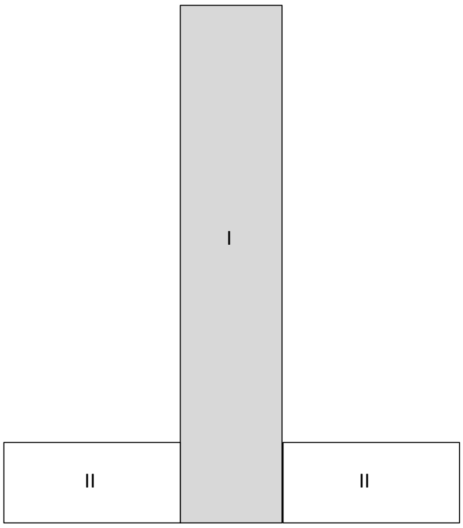

Figure 6-4 Model of first ZIP with deck to distribute torsion moments for case 2

The general formula for torsional stiffness is (can be derived from Table 2-2):

$$I_w = C_{I_w} \cdot b \cdot h^3$$

Applying the formula on the parts of the girder gives:
Part I:

$$\frac{b}{h} = \frac{1320}{280} = 4.71$$
$$I_{w,I} = 0.289 \cdot 1320 \cdot 280^3 = 8.37 \cdot 10^9 \; mm^4$$

Part II:

$$\frac{b}{h} = \frac{450}{193} = 2.33$$
$$I_{w,II} = 0.243 \cdot 450 \cdot 193^3 = 7.86 \cdot 10^8 \; mm^4$$

Part of torsion carried by the web of the ZIP-girder (shaded area in Figure 6-4):

$$\frac{I_{w,I}}{I_{w,total}} = \frac{8.37 \cdot 10^9}{8.37 \cdot 10^9 + 2 \cdot 7.86 \cdot 10^8} = 0.84 \; [-]$$

A torsional moment of 84 kNm with $C_\tau = 0.289$ will give a shear stress of:

$$\tau = \frac{M_T}{C_\tau \cdot b \cdot h^2} = \frac{0.84 \cdot 100 \cdot 10^6}{0.289 \cdot 1320 \cdot 280^2} = 2.81 \; {}^{N}/_{mm^2}$$

6.3 Comparison methods

The different methods give deviating results. The hand calculations roughly give 40% higher results than the FEM calculations. A comparison is presented in Table 6-1.

Method	Type	Shear stress τ	Ratio M_T/τ
Method 1	FEM	2.00 N/mm²	50
Method 2, case 1	Hand calculation	2.87 N/mm²	34.8
Method 2, case 2	Hand calculation	2.81 N/mm²	35.6

Table 6-1 Comparison different methods

When the simplified cross-section is analysed with Scia Engineer a shear stress distribution is found as presented in Figure 6-5. The stresses are between 2.41 and 2.85 N/mm². That corresponds quite well with the made hand calculations.

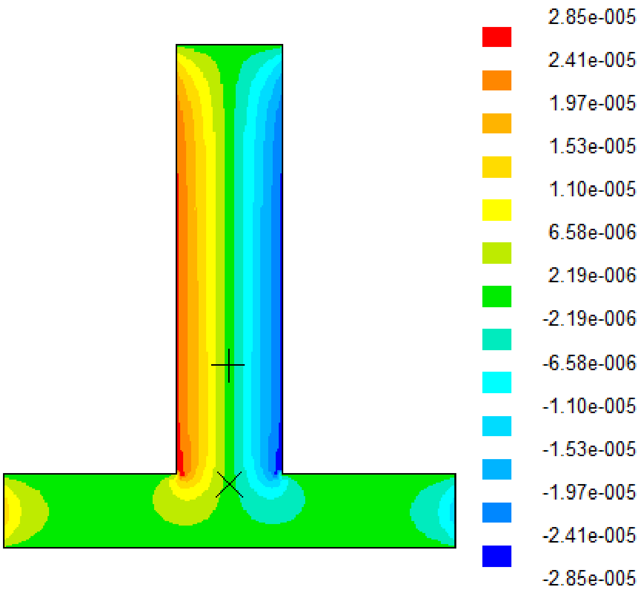

Figure 6-5 Shear stress in simplified cross-section calculated with Scia Engineer

The reason that there is a difference between the results of the two presented methods is that the phi-distributions are not the same. The phi-distribution for the simplified cross-section of the hand calculation is presented in Figure 6-6. In Figure 6-7 the distribution for the real cross-section is presented.

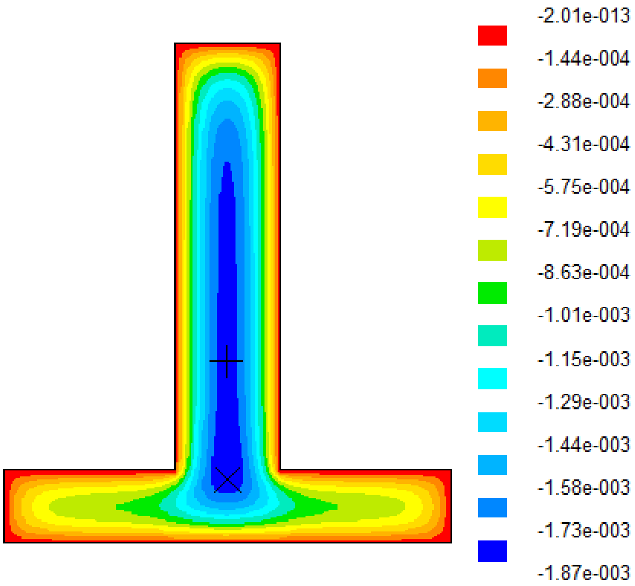

Figure 6-6 Phi distribution in simplified cross-section for hand calculation calculated with Scia Engineer

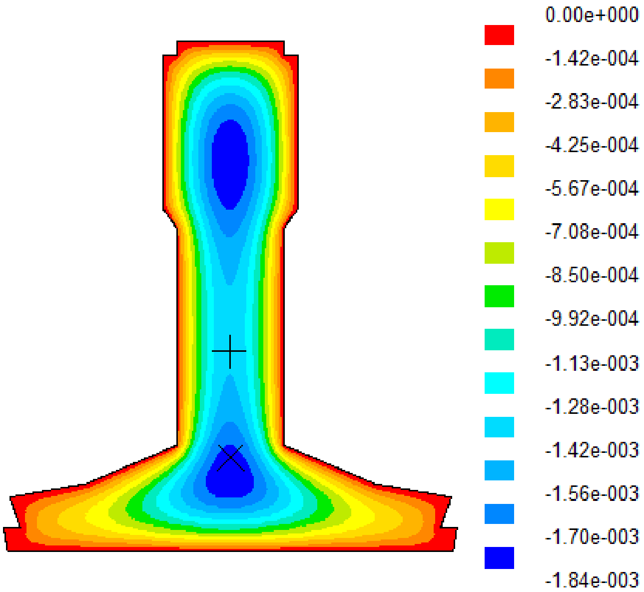

Figure 6-7 Phi-distribution in correct cross-section in FEM calculated with Scia Engineer

When Figure 6-6 and Figure 6-7 are compared follows that the thicker part of the web and the flange attracts shear stress away from the region around the centre of gravity. So using method 2 will be very conservative. The results of method 1 are used for the analytical calculations in this report.

Note: The influence of the deck on the phi-distribution is not presented. A quick check pointed out that this influence is neglectable.

7 Analytical Analysis

7.1 Procedure

To have insight in the behaviour of the girder a hand calculation (as far as possible) is made. When no hand calculation is possible a finite element model is used.

The analytical calculation is only carried out in the ultimate limit state (ULS). This is done because the physical non-linear finite element model of the girder is also carried out in ULS. In that limit state no cracking is expected.

The occurring forces in construction stage A and B are investigated and evaluated in chapter 8 and 9. From this forces the normal and shear stresses can be calculated, presented in chapter 10. Finally the principal stresses will be checked, also presented in chapter 10

7.2 Governing point

For maximal shear stress the severest combination of shear stresses due to shear force and torsional moment is occurring at the centre of gravity. Chosen is the point indicated with a red square in Figure 7-1. This is the centre of gravity of the girder and deck together (h=641 mm). The occurring shear stresses in this point are plotted along the length of the beam in the next chapters. For normal force the top and bottom of the girder are interesting to determine if there is an zone in the girder without flexural cracking. It is assumed that there are no vertical stresses in the girder.

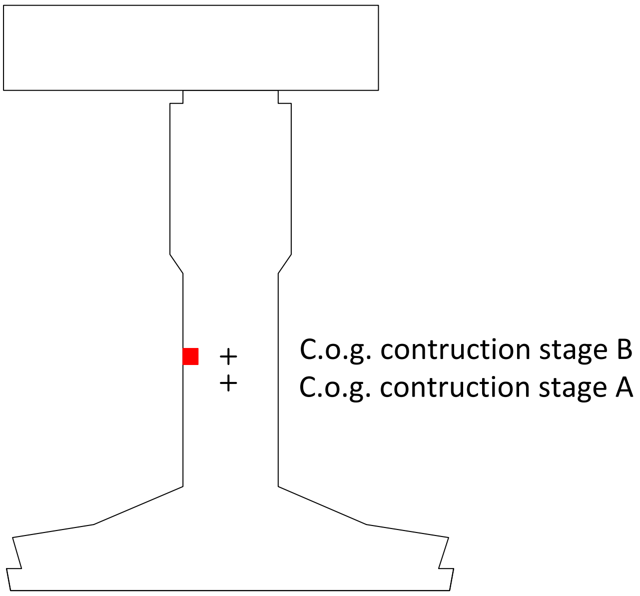

Figure 7-1 Cross-section, indication of governing point for check of principal stress

7.3 Tensile strength of concrete

A boundary tensile strength is necessary to be able to determine if cracks occur. The available design tension strength for concrete C53/65:

- Mean: 4.16 N/mm^2
- Characteristic: 2.91 N/mm^2
- Design: 1.94 N/mm^2

The capacity can be higher when the flexural tensile strength is used, this capacity is not used in this report.

7.4 Determination of stresses

The following formulae are used to calculate the normal and shear stresses:

- For normal stresses the formula: $\sigma_N = \frac{N_x}{A}$
- For shear stresses the formula: $\tau_V = \frac{V_x \cdot S^{(a)}}{I_{xx} \cdot b^{(a)}}$
- For torsion a finite element model is used. This is presented in chapter 6.

This different stresses are combined to principal stresses using the following formulae:

$$\sigma_1 = \frac{\sigma_{xx} + \sigma_{yy}}{2} + \sqrt{\left(\frac{\sigma_{xx} - \sigma_{yy}}{2}\right)^2 + \sigma_{xy}{}^2}$$

$$\sigma_2 = \frac{\sigma_{xx} + \sigma_{yy}}{2} - \sqrt{\left(\frac{\sigma_{xx} - \sigma_{yy}}{2}\right)^2 + \sigma_{xy}{}^2}$$

It is very conservative to check the stress in one outer fibre to the design strength. The shear stresses due to torsion are maximal at that point but decrease quickly to lower values. Pure elastically thinking, the distributions as presented in Figure 7-2 must be used. When plasticity is allowed, the distribution will change to the distribution as presented in Figure 7-3.

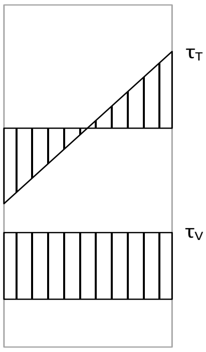

Figure 7-2 Shear stresses due to torsion moment and shear force, elastic distribution

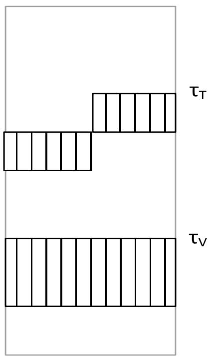

Figure 7-3 Shear stresses due to torsion moment en shear force, plastic distribution

The following to checks are done:

1. Check of principal using the shear stress distribution from Figure 7-2. The stress limit for this check is the mean tensile strength. The name for the check is 'principal stress elastic'.
2. Check of principal using the shear stress distribution from Figure 7-3Figure 7-2. The stress limit for this check is the design tensile strength. The name for the check is 'principal stress plastic'.

8 Analysis of ‘Construction stage A’

In construction stage A the prestressing force and dead weight are applied. After that the fresh concrete deck is poured and totally supported by the girder. The stresses are calculated at the centre of gravity of the girder.

8.1 Stresses due to prestressing

The prestressing causes normal force, shear force and bending moments in the girder. The bond length of the cables has influence in the first part of the girder. The bond length can be determined following the Eurocode 1992-1-1, a safe assumption is a length of 1.5 meter, appendix C.

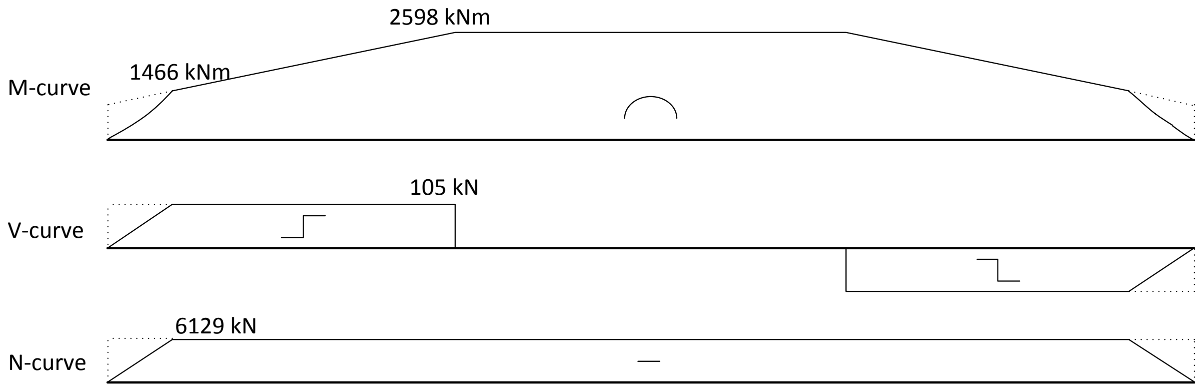

Figure 8-1 Force distributions due to prestressing (for F_p = 161.4 kN in SLS)

The derivation of the force distributions is presented in appendix D.

The stresses due to the occurring shear and normal forces are calculated at the end of the bond length (this stresses develop linear over the bond length, this is the maximum), in ULS:

$$\tau_{V,prestressing} = \frac{V_x \cdot S^{(a)}}{I_{xx} \cdot b^{(a)}} = 0.9 \cdot \frac{-105 \cdot 1000 \cdot 1.072 \cdot 10^8}{1.016 \cdot 10^{11} \cdot 280} = 0.356\ \frac{N}{mm^2}$$

$$\sigma_N = 0.9 \cdot \frac{-6129 \cdot 1000}{A} = 0.9 \cdot \frac{-6129 \cdot 1000}{5.685 \cdot 10^5} = -9.70\ \frac{N}{mm^2}$$

8.2 Stresses due to dead weight and fresh poured concrete deck

The weight of the girder and the weight of the fresh poured concrete gives an extra moment. For simplicity the moments are assumed zero above the supports. In reality there is a very small negative moment from the cantilevering part of the beam.

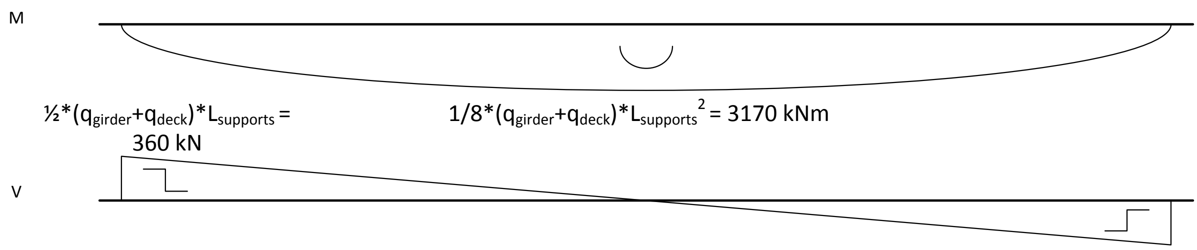

Figure 8-2 Force distributions for dead weight and fresh poured concrete deck in SLS

The stresses due to dead weight and fresh poured concrete are calculated at the supports (that is the maximum shear force), in ULS:

$$\tau_{V,dead\ weight} = -\frac{V_x \cdot S^{(a)}}{I_{xx} \cdot b^{(a)}} = 1.35 \cdot \frac{-360 \cdot 1000 \cdot 1.072 \cdot 10^8}{1.016 \cdot 10^{11} \cdot 280} = -1.832\ \frac{N}{mm^2}$$

9 Analysis of 'Construction stage B'

9.1 Introduction

The force distribution for construction stage B is calculated using finite element models. The forces are considered in half of the beam (indicated in Figure 9-1).

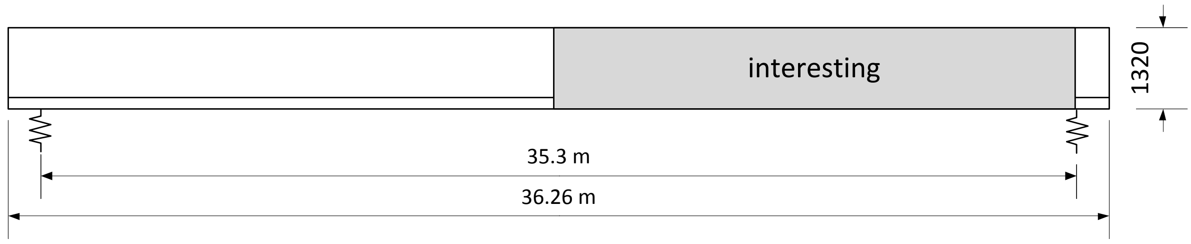

Figure 9-1 Geometry of girder

In the following paragraphs the force distribution is calculated using finite elements models:

1. Orthotropic plate model (2D) without end diaphragm beams, Scia Engineer.
2. Volume element model (3D) without end diaphragm beams, ATENA 3D.
3. Volume element model (3D) with end diaphragm beams, ATENA 3D.

The load case of Spanbeton and Minalu are investigated both.

9.2 Orthotropic plate model of bridge

9.2.1 Parameters model

The bridge is modelled as an orthotropic plate. The function of Scia Engineer to calculate cross-section properties is used, the results are presented in Table 9-1. This properties are used to calculate the stiffness parameters for the orthotropic plate, presented in Table 9-2.

Property	ZIP	First ZIP	TRA	Unity
Width b	1.2	1.023	1.177	m
Effective shear area A_z	0.36989	0.27404	0.36209	m^2
Bending stiffness I_y	0.18260	0.16680	0.14740	m^4
Torsional stiffness I_t	0.015809	0.015669	0.022319	m^4
Centre of gravity (with/without deck)	517/673	517/641	798/888	mm

Table 9-1 Cross-section properties

Formula	ZIP	First ZIP	TRA	Unity
$D_{11} = \frac{E_x \cdot I_x}{b}$	5782	6196	4759	MNm
$D_{22} = \frac{E_y \cdot t^3}{12 \cdot (1 - \nu^2)}$	16.9	16.9	16.9	MNm
$D_{12} = \nu \cdot \frac{E_y \cdot t^3}{12 \cdot (1 - \nu^2)}$	3.4	3.4	3.4	MNm
$D_{33} = \frac{1}{4} \cdot \left(\frac{G_x \cdot I_t}{b} + \frac{G_y \cdot t^3}{6} \right)$	56	64	79	MNm
$D_{44} = \frac{G_x \cdot A_z}{b}$	4880	4241	4871	MN/m
$D_{55} = \frac{G_y \cdot t}{1.2}$	1278	1278	1278	MN/m

Table 9-2 Properties of orthotropic plate in Scia Engineer

9.2.2 Transformation of data

The results found in the made cuts in the orthotropic plate model are transformed to the working forces in the first ZIP girder doing the following steps:

1. Multiply the shear force and bending moments with the width of the strip (representing the first ZIP girder). Width = 1.023 m.
2. Multiply the plate torsion moments with the width of the strip (width = 1.023 m) and the longitudinal distribution factor ($\rho_{longitudinal}$ = 1.9).
3. Reduced the torsion moments, only the part of the torsion carried by the girder is needed. It appears that 97% of the torsion is carried by the ZIP-girder (not demonstrated).

9.2.3 Resulting force distributions

In Figure 9-2, Figure 9-3 and Figure 9-4 the force distributions are presented for the load case of Spanbeton and Minalu. The forces are plotted along the length of the girder.

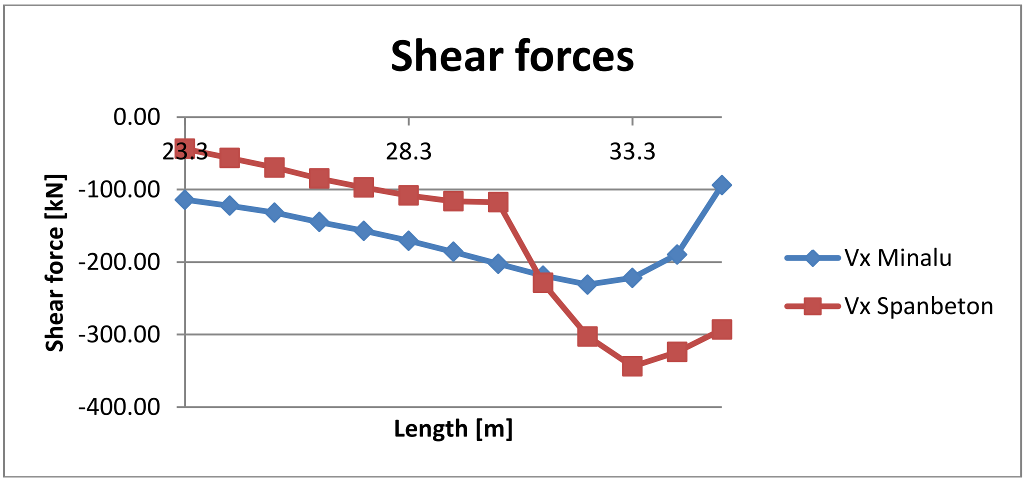

Figure 9-2 Shear force distribution determined with Scia Engineer

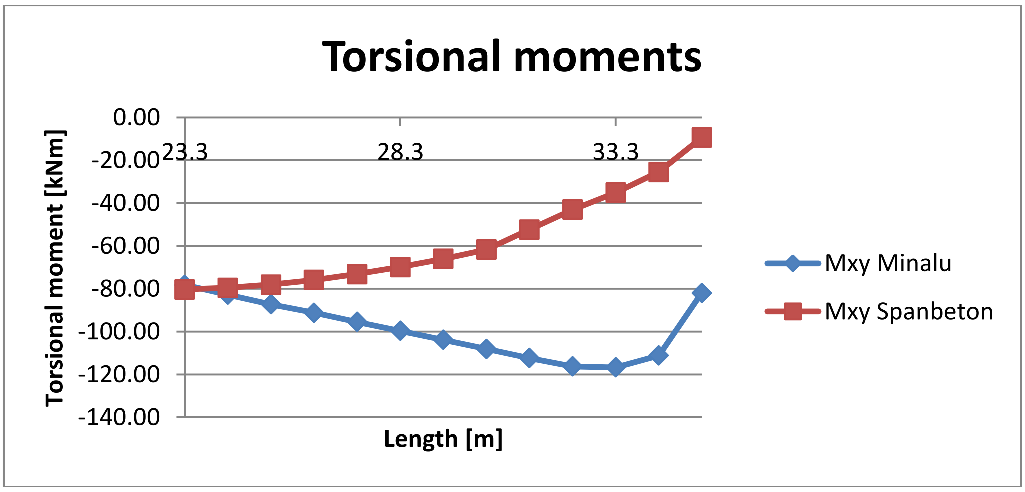

Figure 9-3 Distribution of torsional moments determined with Scia Engineer

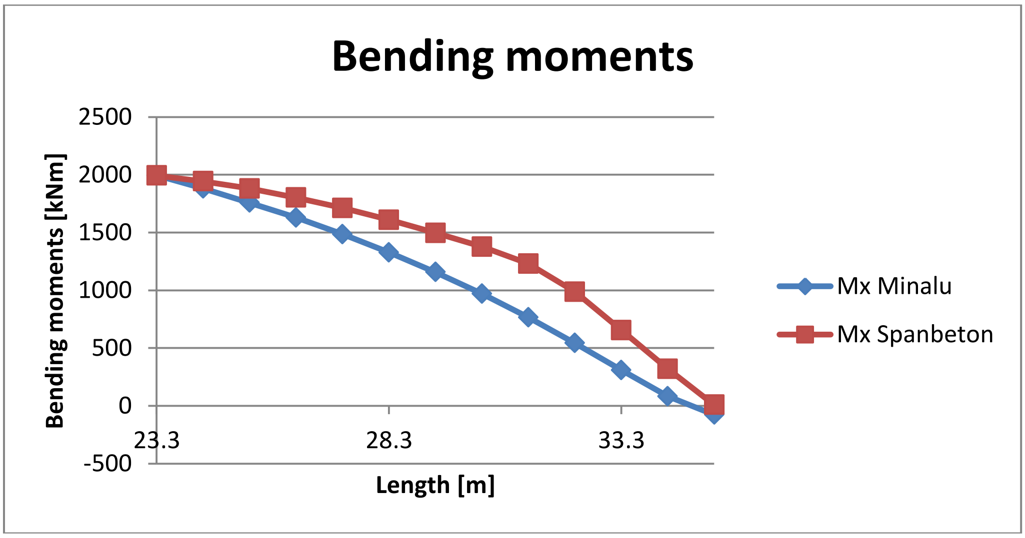

Figure 9-4 Distribution of bending moments determined with Scia Engineer

9.3 Bridge model using volume elements

This model is carried out in ATENA 3D with and without end diaphragm beam for the load case of Spanbeton and Minalu.

The shear stresses due to shear force can be determined in this model. Determine the torsional moments is more difficult because in this model the shear stresses due to torsion are not correct because there is applied only one linear element over the thickness of the web, Figure 9-5. Minalu calculates the torsional moments by integrating the stresses. In this research the known rotations are used to derive the occurring torsional moments.

9.3.1 Shear stresses due to shear force

The shear stresses due to shear force can be calculated taking the average from the indicated nodes in Figure 9-5 (which are approximately at the height of the centre of gravity).

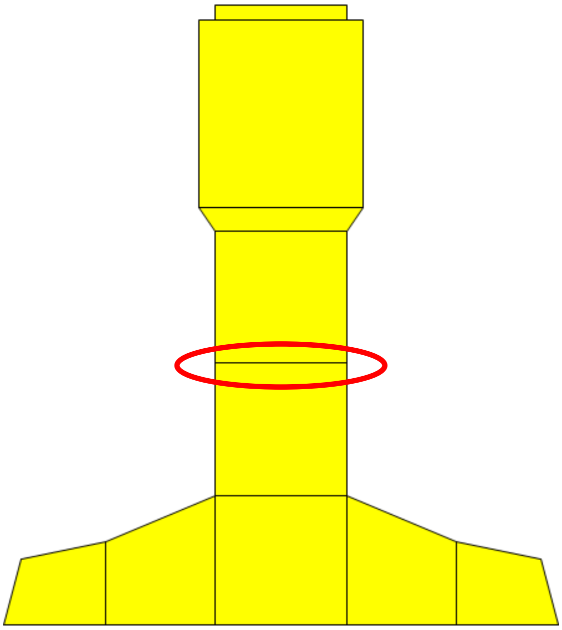

Figure 9-5 Mesh in Linear Elastic model of complete bridge

The determined shear stresses correspond well with the shear stresses calculated with the orthotropic plate model (Scia Engineer, without end diaphragm beam), Figure 9-6 and Figure 9-7.

Note: The visible peaks in the graphs are located on borders of macro-elements and have no physical meaning.

The found shear stresses from ATENA can be compared with the shear stresses from Scia. Little differences are visible between the results, this is presented in Figure 9-6 and Figure 9-7. The small differences are not investigated further.

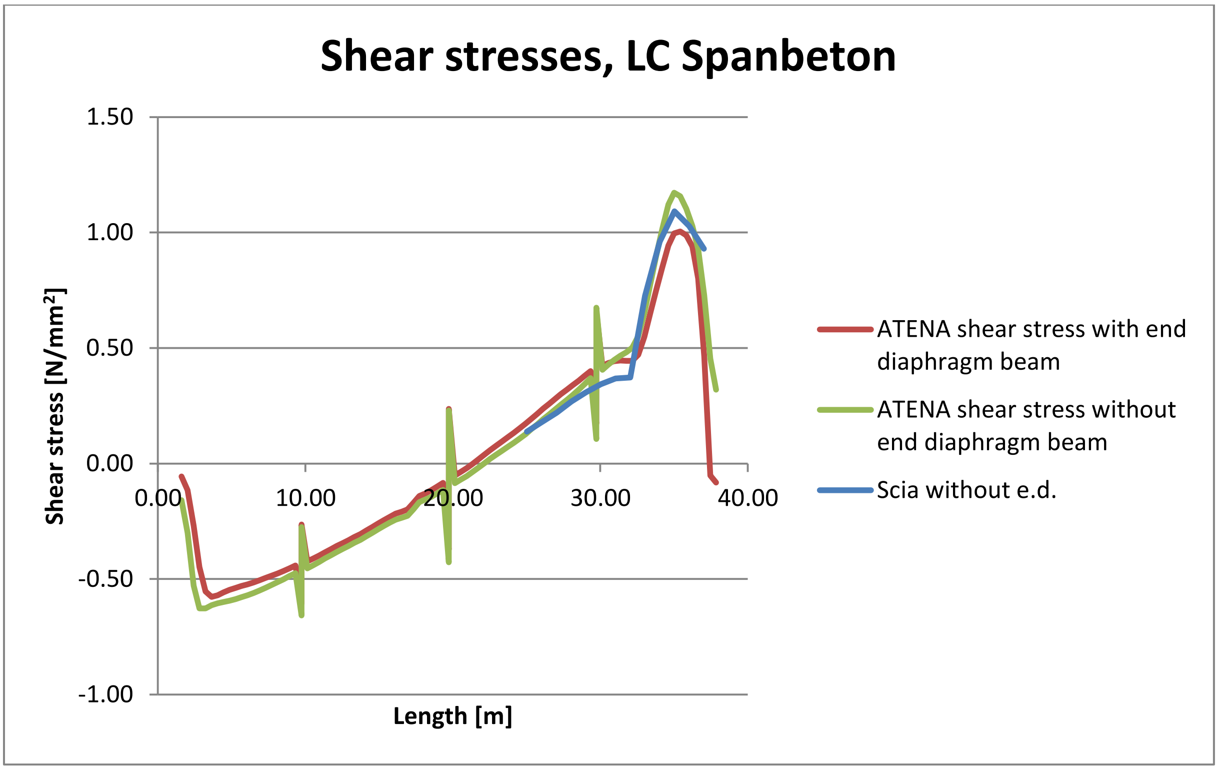

Figure 9-6 Shear stresses compared for the load case of Spanbeton

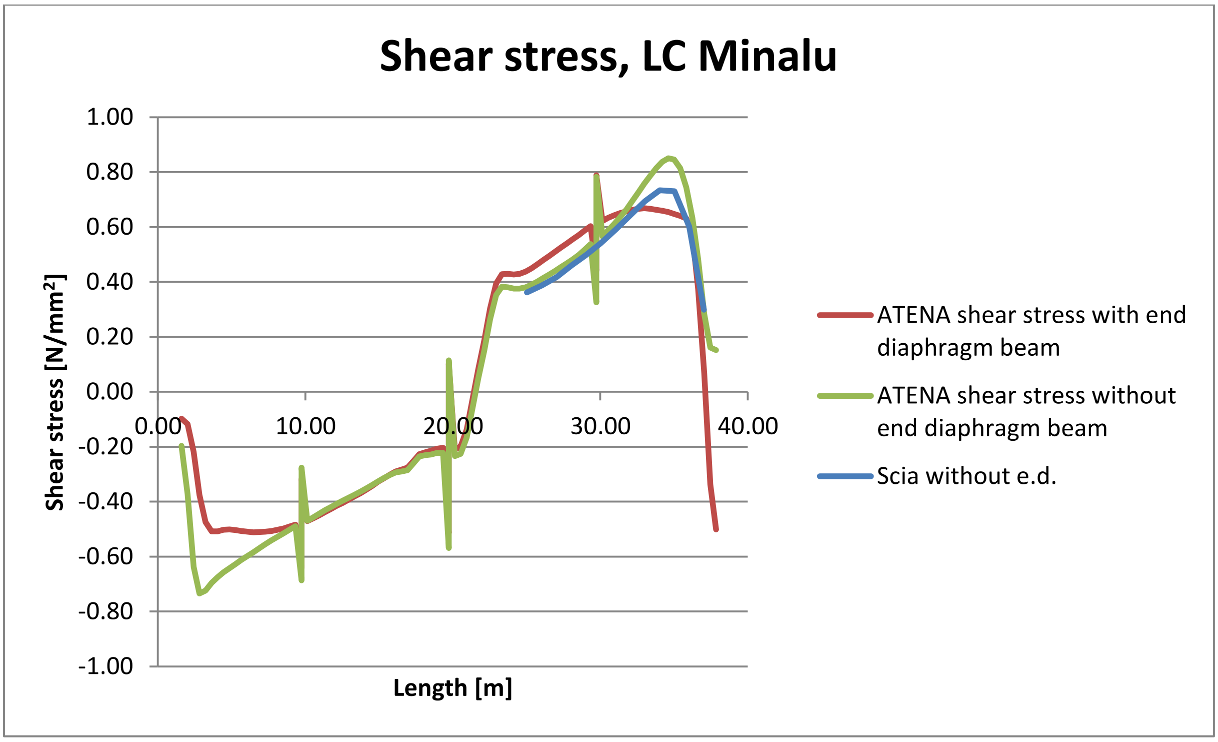

Figure 9-7 Shear stresses compared for the load case of Minalu

9.3.2 Torsional moments

The torsional moment can be calculated using the available data of the rotations. The occurring torsional moment consists of two parts, pure torsion and restrained warping. The following formula is used:

$$M_t = G \cdot I_w \cdot \frac{d\vartheta}{dx} - E \cdot C_w \cdot \frac{d^3\vartheta}{dx^3}$$

Important variables are:

$$E = 38 \cdot 10^6 \ {kN}/{m^2}$$
$$G = 15.833 \cdot 10^6 \ {kN}/{m^2}$$
$$I_w = 1.11 \cdot 10^{-2} \ m^4$$
$$C_w = 1.0 \cdot 10^{-3} \ m^6$$

The constants I_w and C_w are determined using respectively the programs Scia Engineer and ShapeBuilder.

9.3.2.1 Analysis of rotations

With Microsoft Excel the rotation curves (determined with ATENA) are estimated with an 6th order polynomial. That formulae are used to take the derivative of the rotation using Maple. The formulae are valid in the interval 0.63 < x < 35.63 meter.

In Figure 9-8, Figure 9-9, Figure 9-10 and Figure 9-11 the following components are plotted:

- Green: restrained warping [kNm]
- Blue: pure torsion [kNm]
- Red: total torsion moment [kNm]

From the figures can be observed that the torsion moment is not carried by restrained warping (normal stresses) but mainly by pure torsion (shear stresses). Only in the support area restrained warping has some influence which is largest for the model with an end diaphragm beam. When no end diaphragm is available no restrained warping is expected, but the warping that occurs is small and neglectable compared with the total occurring torsional moment, so no further investigation is done. The occurring torsional moments are higher when the end diaphragm beams are neglected. Furthermore, it can be observed that the obtuse corner attracts a lot of the torsional moments.

See appendix G for the used Maple code to determine the torsional moments.

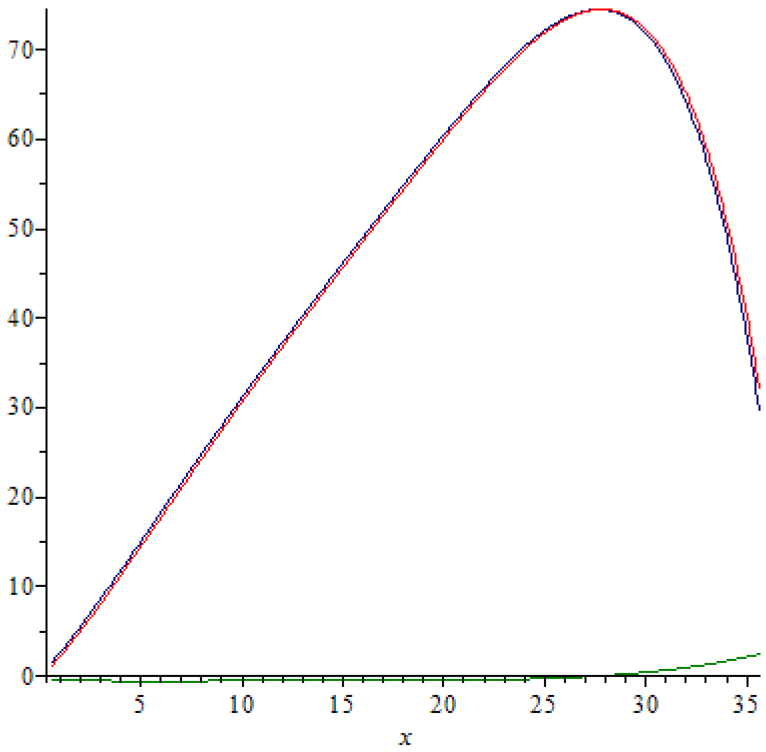

Figure 9-8 Torsional moments [kNm] for the load case of Spanbeton, without end diaphragm beam

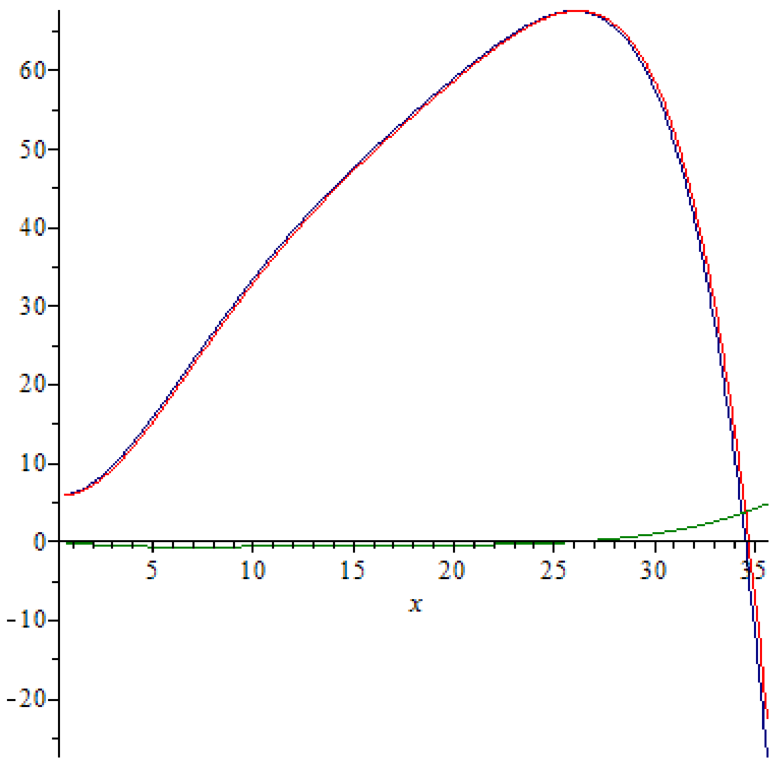

Figure 9-9 Torsional moments [kNm] for the load case of Spanbeton, with end diaphragm beam

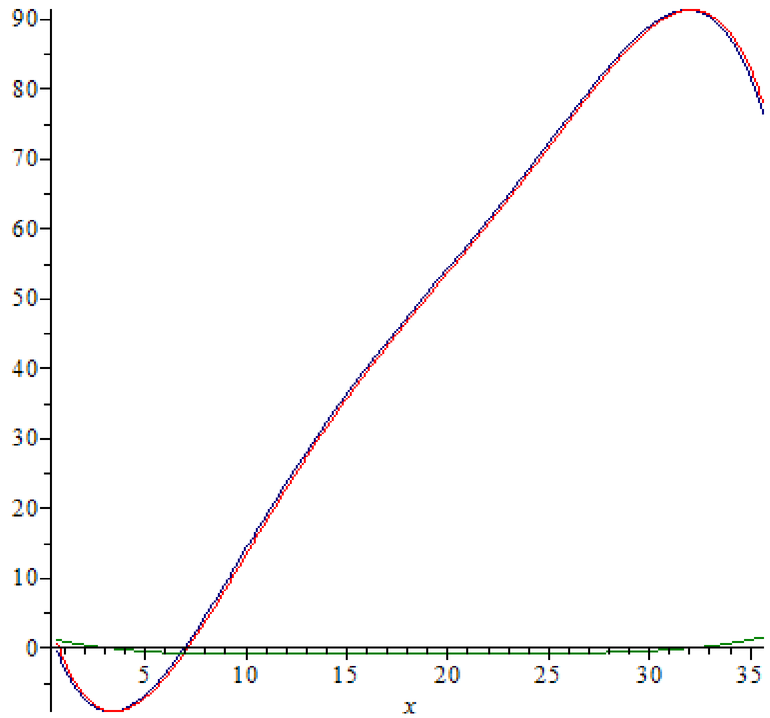

Figure 9-10 Torsional moments [kNm] for the load case of Minalu, without end diaphragm beam

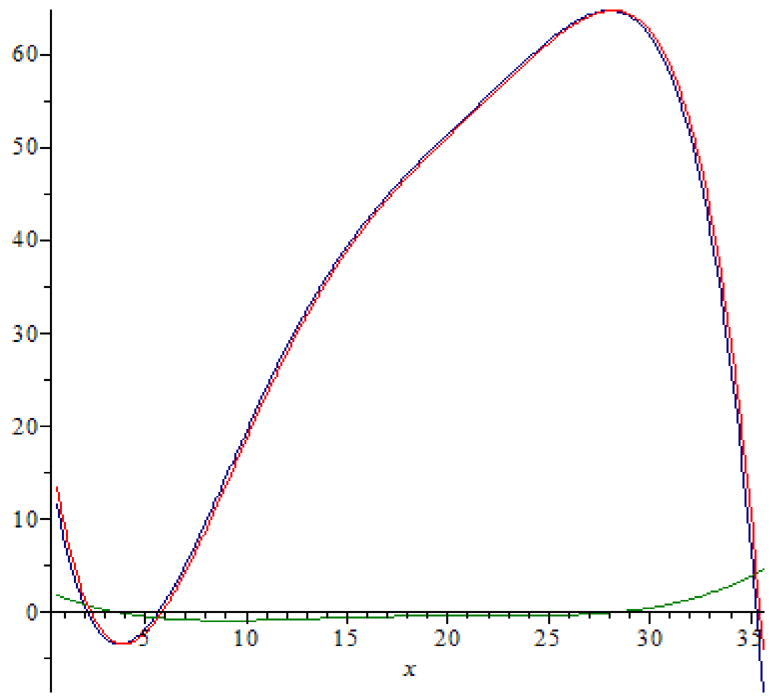

Figure 9-11 Torsional moments [kNm] for the load case of Minalu, with end diaphragm beam

9.3.2.2 Comparison with 2D orthotropic plate model

The determined torsional moments, in paragraph 9.3.2.1, can be compared with the torsional moments determined with the orthotropic plate model, in paragraph 9.2.3.

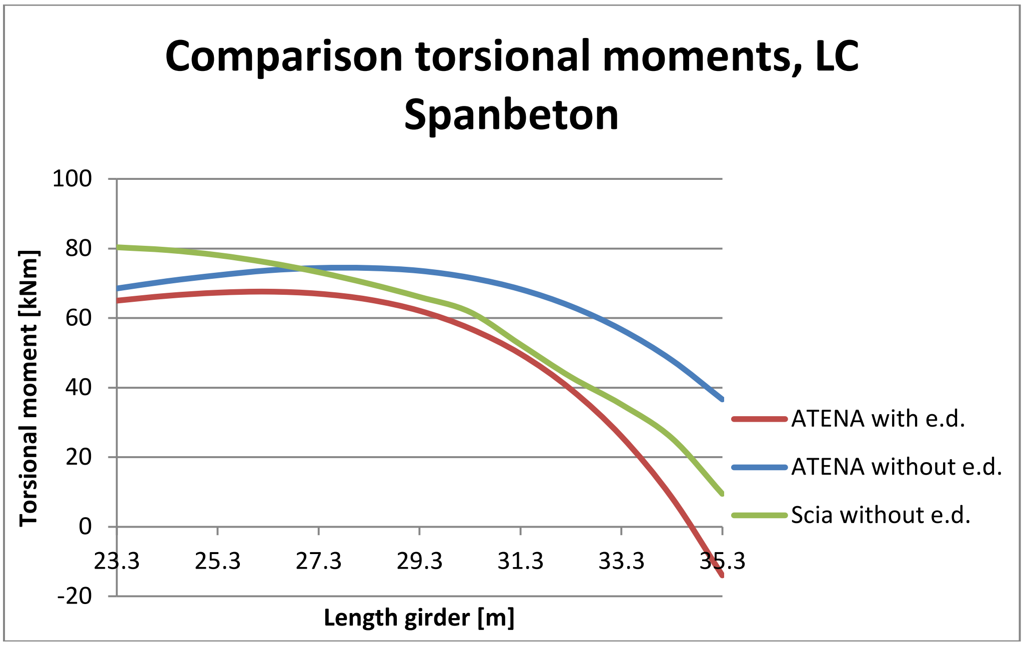

Figure 9-12 Torsional moments compared, LC Spanbeton

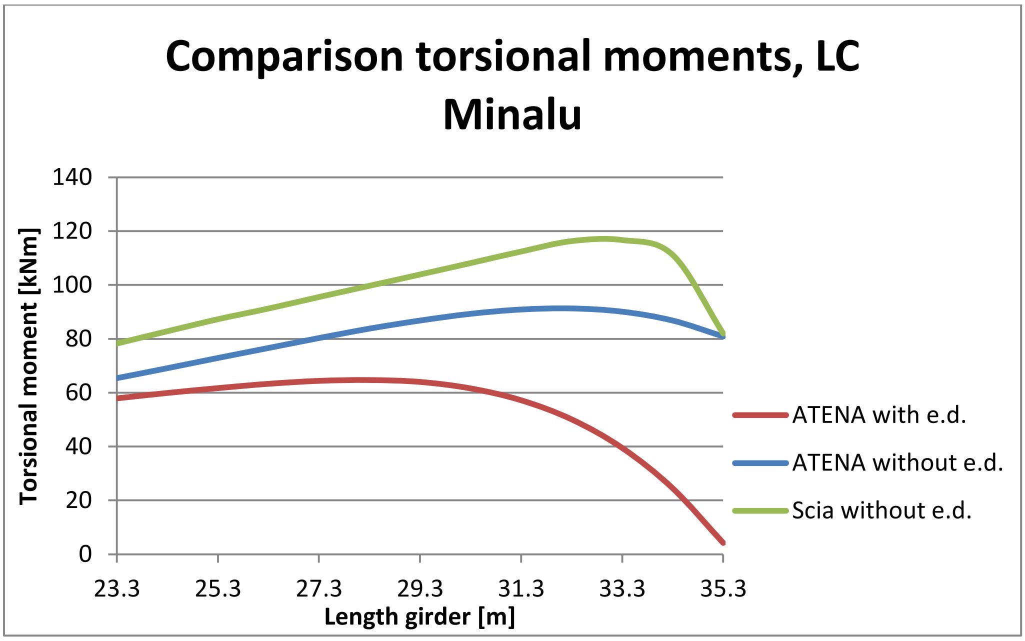

Figure 9-13 Torsional moments compared, LC Minalu

There is one direct comparison possible for the case that no end diaphragm beam is applied. The Scia and ATENA model without end diaphragm beam deviates. So for the linear elastic model a difference is found. Why this difference is found is not further investigated, the presented torsional distributions are all calculated and presented in the next chapters.

10 Evaluation of stresses

The forces from construction stage A and B are determined in chapter 8 and 9. With this knowledge the occurring stresses can be calculated.

In chapter 7 already the governing point in the cross-section is presented and explained. First the stresses in that point will be calculated based on the calculation with the orthotropic plate model. After that a calculation based on the results from the volume model is carried out. Finally at the governing location a complete cross-section is checked.

10.1 Calculation based on the orthotropic plate model of the bridge

10.1.1 Normal stresses

Normal stresses occur in the girder. Normal stresses are caused by:

- Bending moments and normal forces due to prestressing, paragraph 8.1.
- Bending moments due to own weight and the wet concrete of the fresh poured deck, paragraph 8.2.
- Bending moments due to permanent and variable loads on the deck, calculated with the orthotropic plate model, paragraph 9.2.3.

The resultant normal stresses from all these components are calculated and presented in Figure 10-1 and Figure 10-2. It is visible that no flexural cracks will occur for both load cases from 31 meter till the end of the girder. So in that region the principal stresses in an uncracked cross-section can be checked.

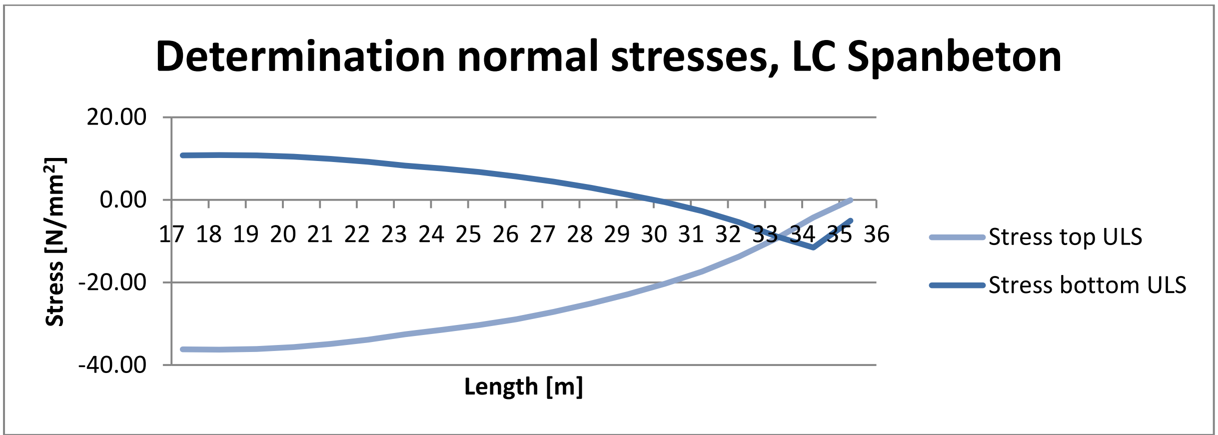

Figure 10-1 Normal stresses in top and bottom of girder, LC Spanbeton

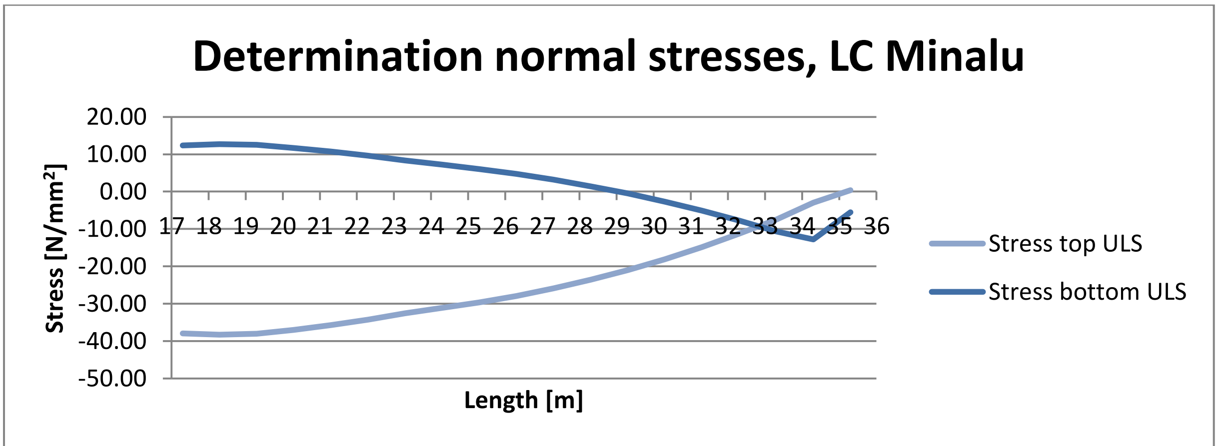

Figure 10-2 Normal stresses in top and bottom of girder, LC Minalu

10.1.2 Stresses due to permanent and variable load on deck

The occurring shear forces and torsional moments in construction stage B are presented in paragraph 9.2.3. The occurring shear stress consists out of shear stresses due to torsion and due to shear force. The calculated stresses for the elastic en plastic shear stress distribution (paragraph 7.4) are presented in Figure 10-3 and Figure 10-4. For the load case of Minalu the maximum occurring shear stress contains more shear stress due to torsion than due to shear force. For the load case of Spanbeton the opposite is the case. It is visible that both load cases have a maximum at about 33.3 meter.

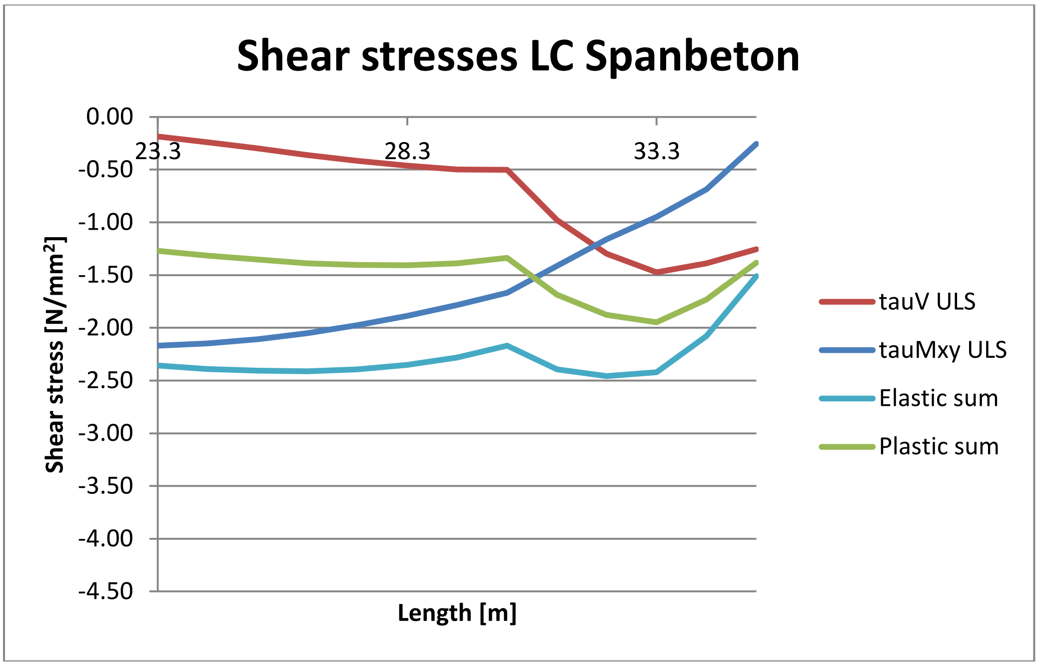

Figure 10-3 Shear stresses from construction stage B, LC Spanbeton

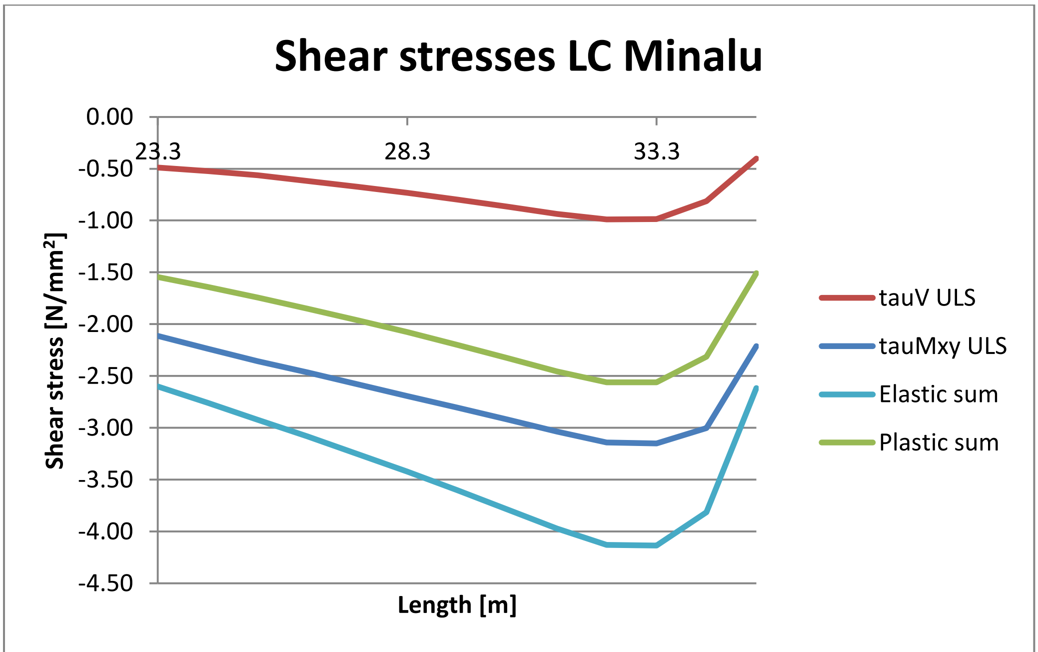

Figure 10-4 Shear stresses from construction stage B, LC Minalu

Note: The presented shear stress ‘τ_{Mxy} ULS’ is the elastic shear stress (Figure 7-2).

10.1.3 Total shear stresses

The shear stresses of construction stage A and B can be combined using the elastic or plastic sum. The calculated stresses are presented for the load case of Spanbeton and Minalu.

The following formulae are used to determine the stresses:

$$\tau_{ULS,\ \ elastic} = \tau_{V,prestressing} + \tau_{V,dead\ weight,sls} + \tau_{elastic\ sum\ construction\ stage\ B}$$

$$\tau_{ULS,\ \ plastic} = \tau_{V,prestressing} + \tau_{V,dead\ weight,sls} + \tau_{plastic\ sum\ construction\ stage\ B}$$

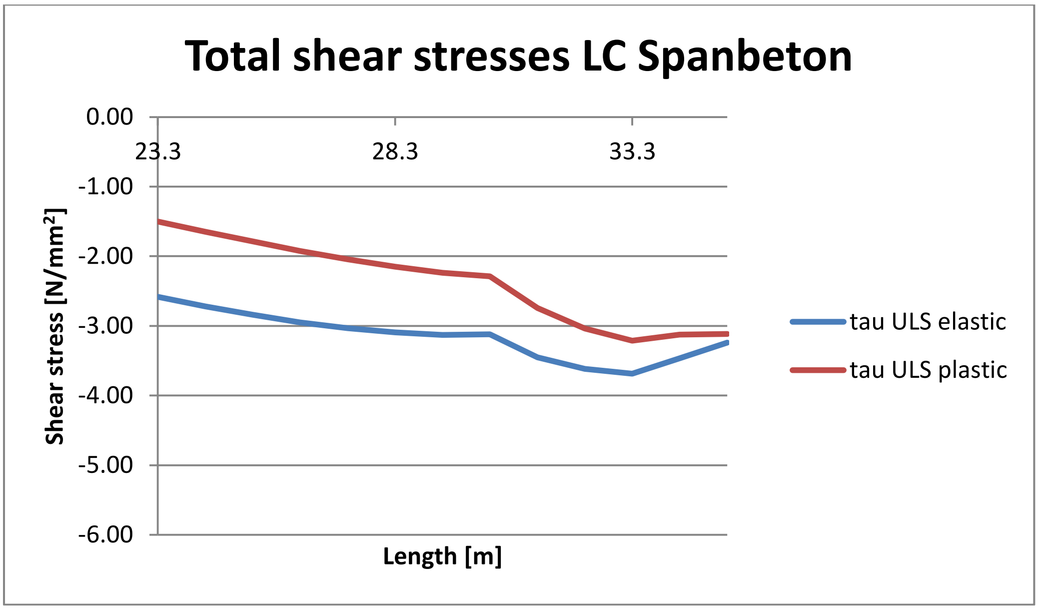

Figure 10-5 Total shear stresses in ULS, LC Spanbeton

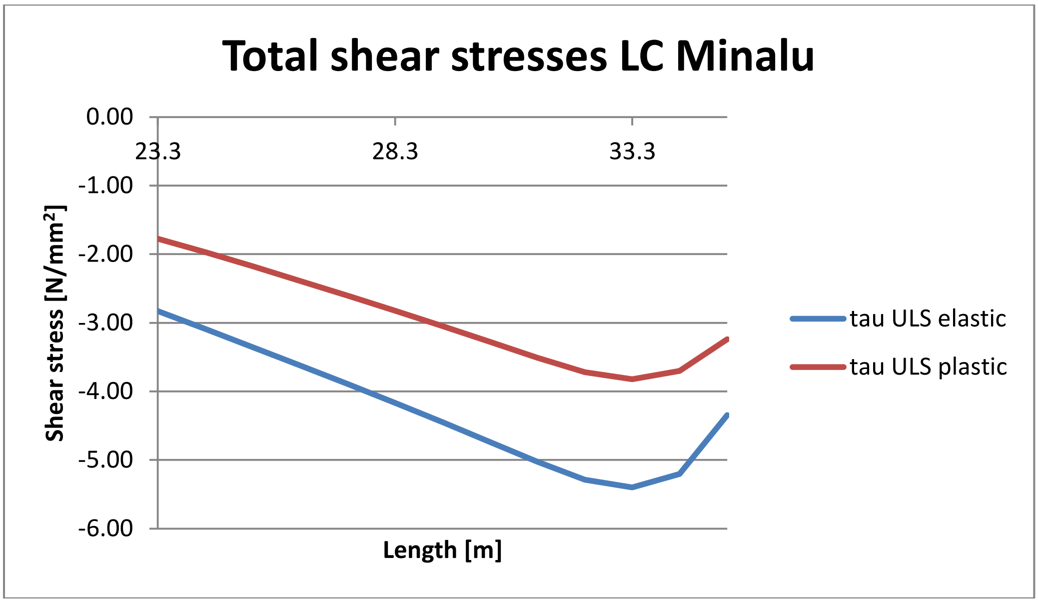

Figure 10-6 Total shear stresses in ULS, LC Minalu

Note: The maximal shear stresses due to the shear force of construction stage A and B are simply added to each other neglecting the different locations of the centres of gravity. This is not totally true but safe based on Figure 10-15.

10.1.4 Principal stresses

The combination of normal and shear stresses can be analysed using principal stresses. The formulae for principal stresses are as follows:

$$\sigma_1 = \frac{\sigma_{xx} + \sigma_{yy}}{2} + \sqrt{\left(\frac{\sigma_{xx} - \sigma_{yy}}{2}\right)^2 + \sigma_{xy}{}^2}$$

$$\sigma_2 = \frac{\sigma_{xx} + \sigma_{yy}}{2} - \sqrt{\left(\frac{\sigma_{xx} - \sigma_{yy}}{2}\right)^2 + \sigma_{xy}{}^2}$$

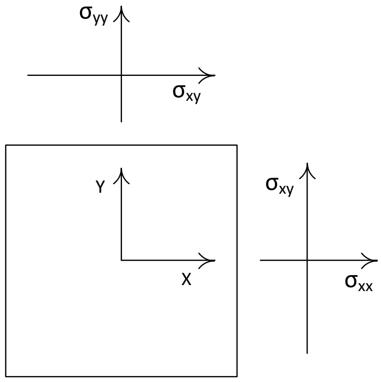

Figure 10-7 Stresses on infinitesimal element

Remember: It is assumed that the stresses in Y-direction (vertical stresses) are zero. The resulting formula for principal tension stress is in that case:

$$\sigma_1 = \frac{\sigma_{xx}}{2} + \sqrt{\frac{\sigma_{xx}{}^2}{4} + \sigma_{xy}{}^2}$$

Interesting is the location where, based on design tension strength, the concrete can bear the load without cracking. In Figure 10-8 and Figure 10-9 the principal tension stresses for the two considered load cases (Spanbeton and Minalu) are visualized. From the figures can be concluded that no cracking is expected.

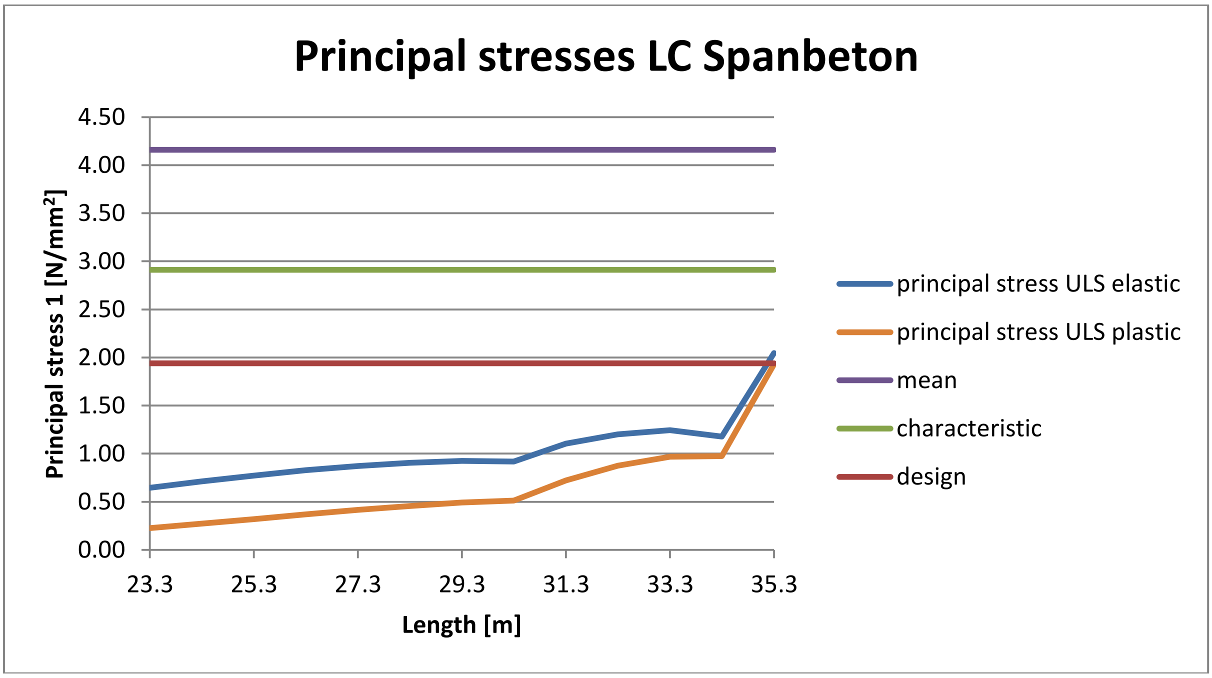

Figure 10-8 Principal stresses LC Spanbeton based on calculation with Scia Engineer without end diaphragm beam

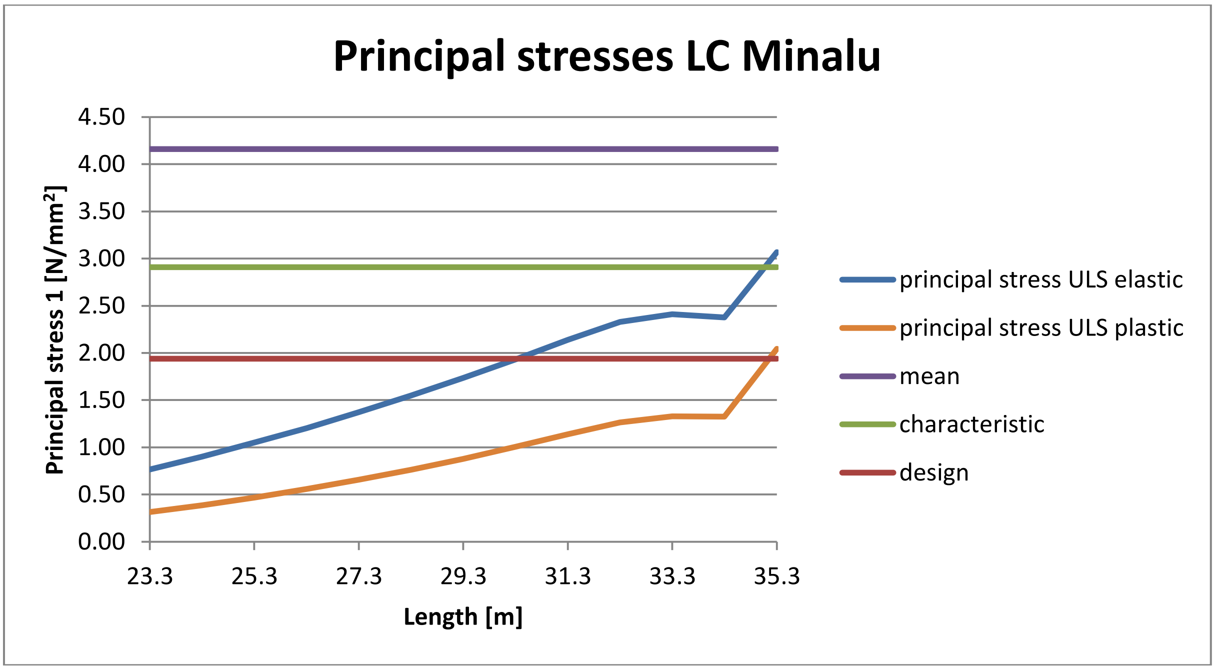

Figure 10-9 Principal stresses LC Minalu based on calculation with Scia Engineer without end diaphragm beam

10.2 Calculation based on the bridge model using volume elements

10.2.1 Principal stresses

Now the principal stresses can be calculated again using the data from the ATENA models. The data from these models can be found in paragraph 9.3. Note that stresses from construction stage A does not differ. Only the forces for construction stage B are adapted. Not the complete calculation is described again, this is already done in paragraph 10.1, only the resulting principal stresses are presented.

10.2.1.1 Model without end diaphragm beams

In the calculation the values for the shear force and torsional moment from construction stage B are changed to the values found with the ATENA model without end diaphragm beam. The principal stresses are presented in Figure 10-10 and Figure 10-11.

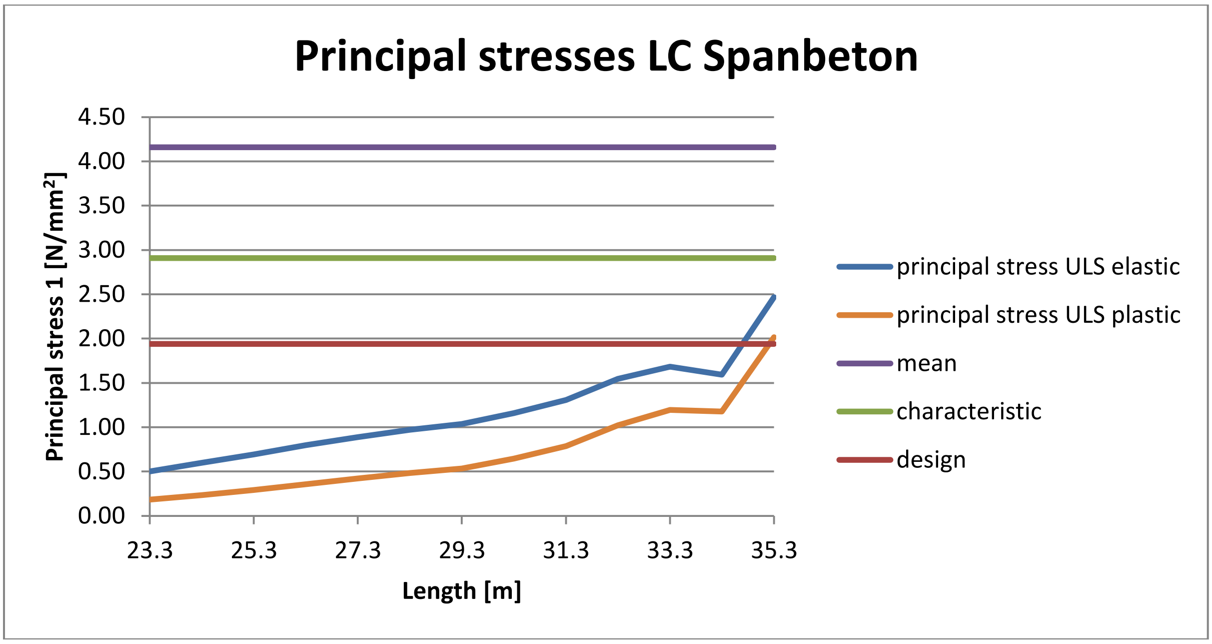

Figure 10-10 Principal stresses LC Spanbeton, based on ATENA calculation without end diaphragm beam

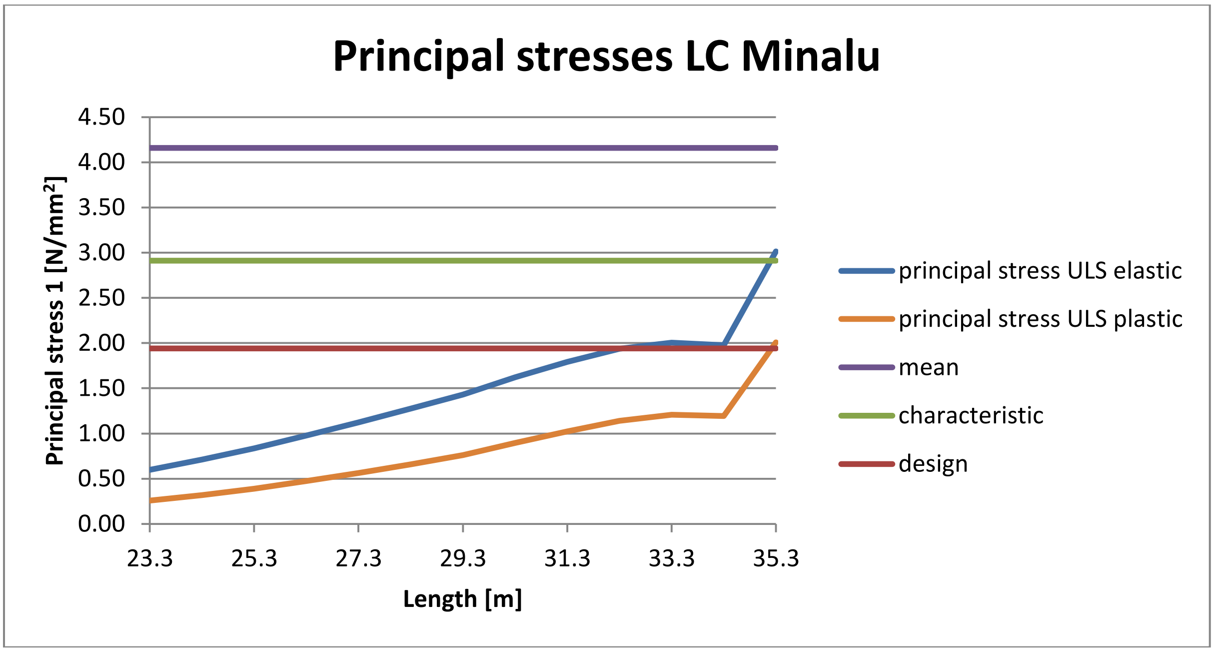

Figure 10-11 Principal stresses LC Minalu, based on ATENA calculation without end diaphragm beam

10.2.1.2 Model with end diaphragm beams

In the calculation the values for the shear force and torsional moment from construction stage B are changed to the values found with the ATENA model with end diaphragm beam. The principal stresses are presented in Figure 10-12 and Figure 10-13.

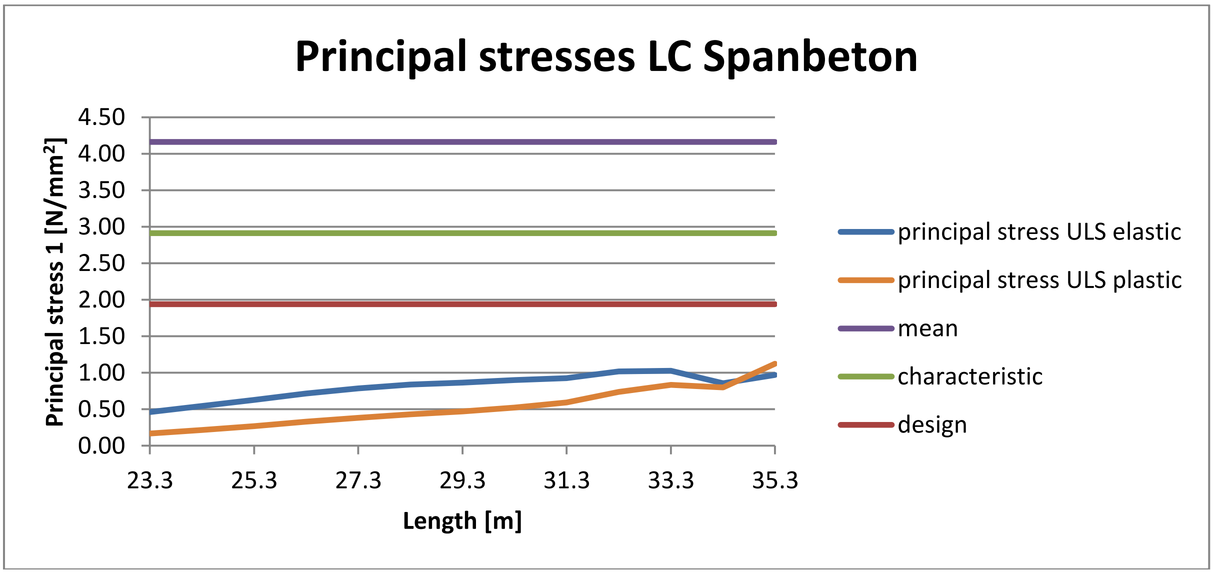

Figure 10-12 Principal stresses LC Spanbeton, based on ATENA calculation with end diaphragm beam

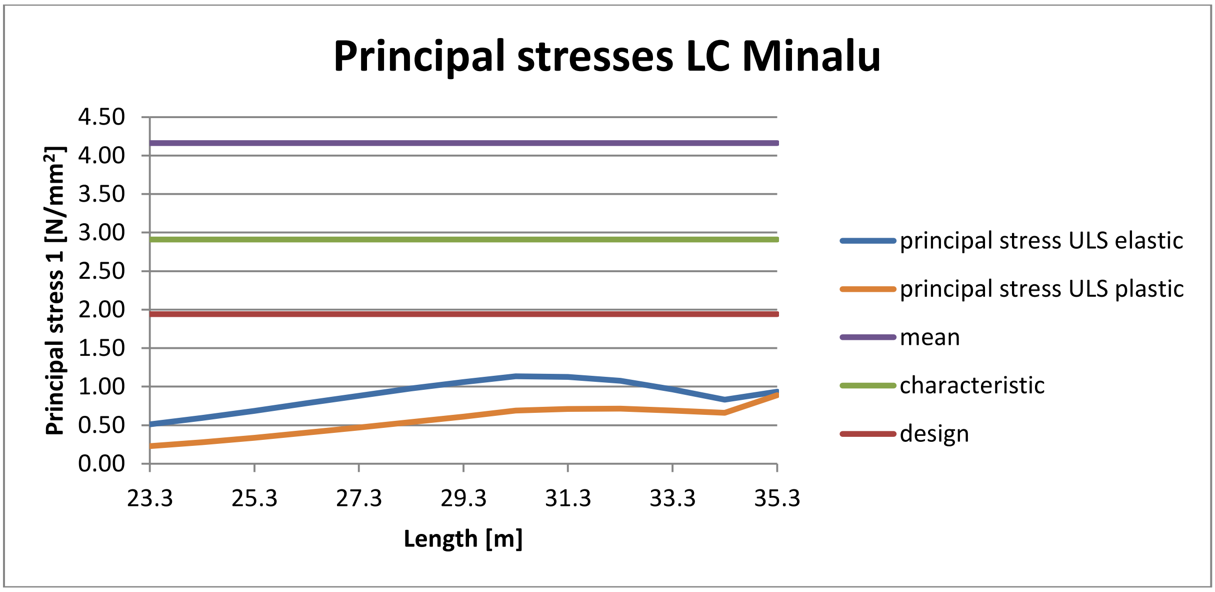

Figure 10-13 Principal stresses LC Minalu, based on ATENA calculation with end diaphragm beam

10.2.1.3 Comparison

It is visible that the principal stresses for all cases (figure Figure 10-8 till Figure 10-13) meets the criteria as formulated in paragraph 7.3, so no cracking is expected.

The presence of end diaphragm beam in the linear elastic model of the bridge decreases the stresses a lot. But Minalu already noted that large torsional moments occur in the end diaphragm beam in that situation which leads to much reinforcement and is likely to be physically impossible[10]. The real principal stresses will be in between the case with and without end diaphragm beam. It is safe make a calculation without end diaphragm beam because that produces governing principal stresses.

[10] Minalu, Kassuhun K. (2010), *Finite element modelling of skew slab-girder bridges.* Page 52.

10.3 Calculation of governing cross-section

Till now the principal stresses are checked in one point of the cross-section based on the location were maximal shear stresses will occur. But the principal stresses depends also on the normal stresses. Lower normal stresses will lead to higher principal stresses. For completeness the governing cross-section will be calculated more detailed to be sure that there is no other governing point in ULS.

When the principal stresses from the presented calculations are compared the largest are observed in Figure 10-9 for the load case of Minalu calculated with Scia Engineer. For that load case a calculation of the cross-section is performed at x=33.3 meter.

10.3.1 Normal stresses

Using the orthotropic plate model has the advantage that the longitudinal moments are calculated already, which are presented again in Figure 10-14.

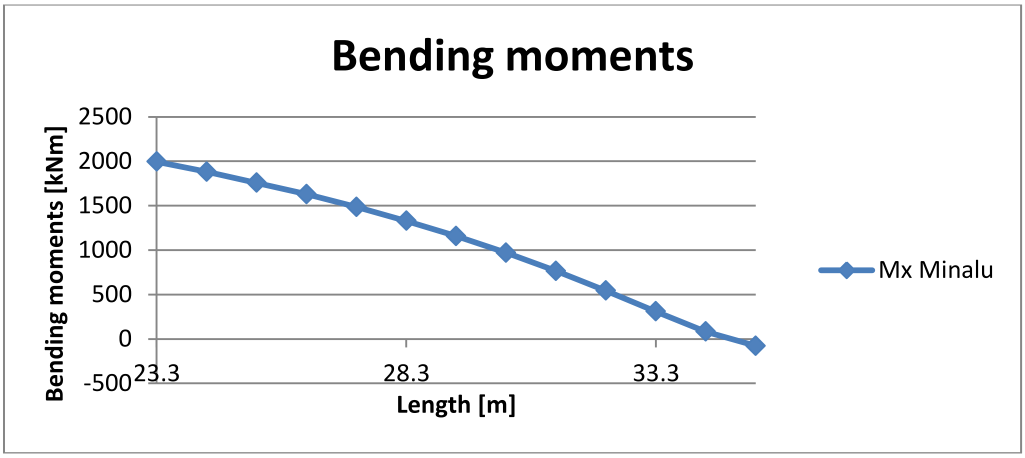

Figure 10-14 Distribution of bending moments for the LC of Minalu

The stresses are checked at x = 33.3 meter. Bending moments:

- Construction stage A (Figure 8-1 and Figure 8-2)
  - Prestressing, M = -1569 kNm
  - Dead weight and weight fresh poured concrete, M = 678 kNm
- Construction stage B, (Figure 10-14)
  - Variable and permanent load on deck, M = 308 kNm.

From this moments follow the stresses in ULS:

- Normal stress top: -7.5 N/mm^2
- Normal stress bottom: -10.6 N/mm^2

10.3.2 Shear stresses

10.3.2.1 Shear force

The shear stress distribution due to shear force can be calculated. Construction stage A and B must be calculated separately for a detailed calculation. The total occurring shear stress can be calculated taking the sum of the shear stresses from construction stage A and B. The results are presented in Figure 10-15.

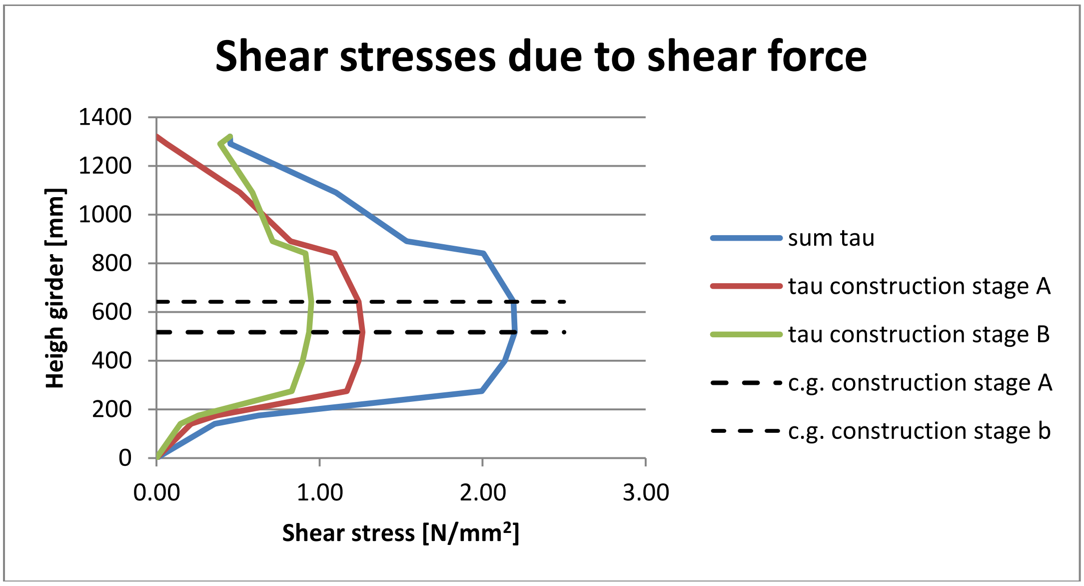

Figure 10-15 Shear stresses in cross-section

10.3.2.2 Torsion

When Figure 6-1 and Figure 6-2 are studied follows that in the thicker top part of the web the shear stresses due to torsion could be a little bit higher than at the height of the centre of gravity. However in the top part of the web the shear stresses due to shear force are relatively low. So it is a safe approximation to take a maximal torsion shear stress of 3.15 N/mm^2 (in the ULS) over the whole cross-section.

10.3.3 Principal stresses

The determined normal and shear stresses can be combined to principal stresses using the formulae, already presented in paragraph 7.4. The resulting stresses over the height of the girder are presented in Figure 10-16.

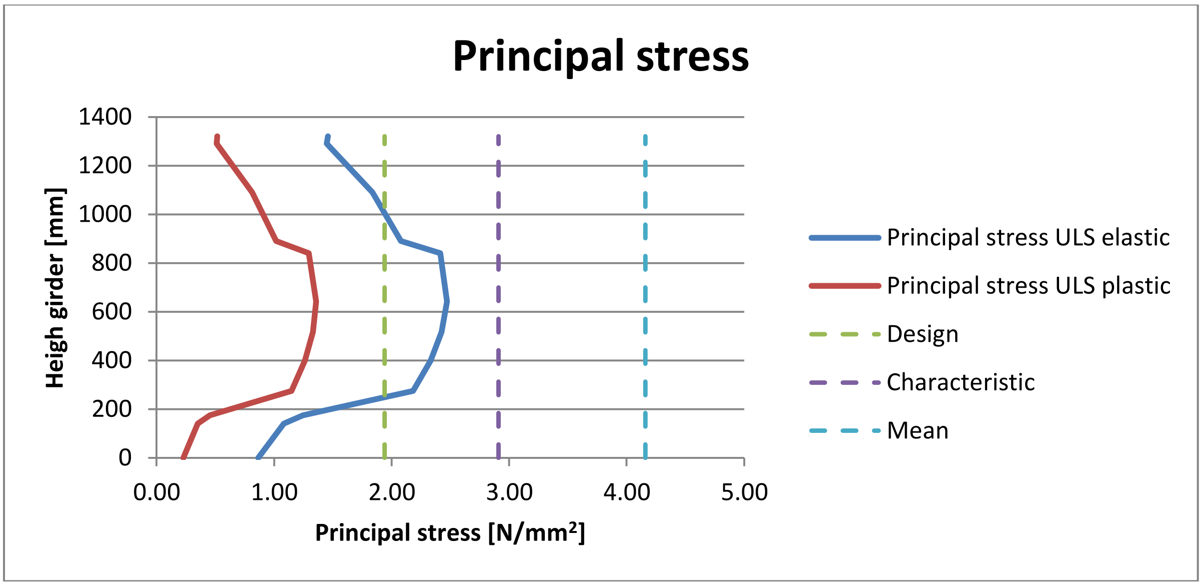

Figure 10-16 Principal stresses in cross-section

This figure can be compared with Figure 10-9. The found maxima from both figures are presented in Table 10-1. The maxima occurred in the centre of gravity of construction stage B (h=641 mm).

Shear stress distribution	Performed calculation of principal stresses		Difference
	Complete cross-section	Only at centre of gravity	
Elastic distribution	2.47 N/mm^2	2.41 N/mm^2	2.4 %
Plastic distribution	1.36 N/mm^2	1.33 N/mm^2	2.2 %

Table 10-1 Comparison calculations

There are two differences between the calculations:

1. In the calculation at the centre of gravity presented in paragraph 10.1 the maximal shear stresses from construction stage A and B are summed up while the maxima are not at the same location. The calculated shear stress is 5.40 N/mm^2 while a detailed calculation of the cross-section gives 5.34 N/mm^2, a difference of 1.2%. This is not significant compared with the next point.
2. From the calculation of the complete cross-section it is visible that taking into account the effects of the bending moments reduces the advantageous normal stresses at the considered centre of gravity. The bending moments of construction stage A reduce the normal stress in the centre of gravity of construction stage B as visualized in Figure 10-17. The normal stress reduces from -9.68 N/mm^2 to -9.08 N/mm^2, a reduction of 6%. This explains the increased principal stresses for the detailed calculation of a complete cross-section.

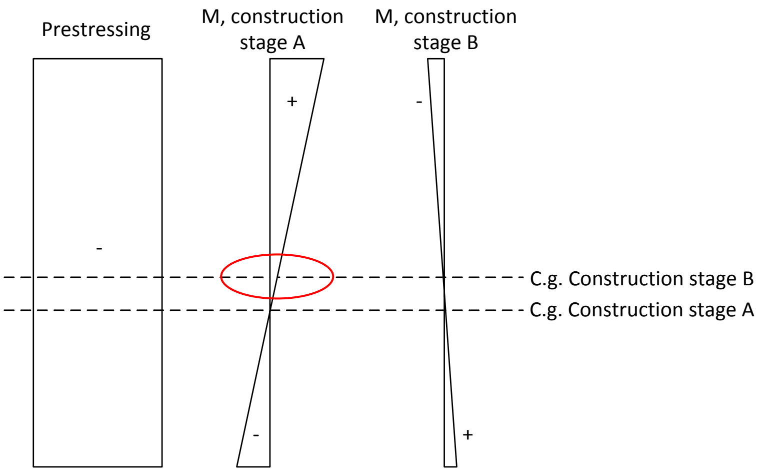

Figure 10-17 Stress diagrams for normal stresses

10.4 Conclusion

Firstly, the load case of Minalu produces the governing principal stresses. Secondly follows from the comparison of the calculations in Table 10-1 that it is valid to check the principal stresses only at the height of the centre of gravity with the presented remark. Important is that the shift of the centre of gravity has influence on the normal stress. The bending moments of construction stage A reduces the normal stress in the centre of gravity of construction B, in the calculated case the normal stresses reduces with 6% which leads to an increased principal stress. For the considered case this do not lead to other conclusions about cracking.

From the calculations can be concluded that there is a zone in the girder from about 31 – 35 meter which is uncracked in ULS. Consequently in the SLS also no cracking will occur. For the straight bridge, presented in paragraph 0, in which lower torsional moments and comparable shear forces occurs also no cracking will occur.

Conclusions

1. It is impossible to model a whole bridge with volume elements including physically non-linear behaviour. From a rough calculation it is expected that this will possibly be daily practice within eighteen years. It is possible to model a whole bridge linear elastically with coarse linear or quadratic volume elements. In this model only one coarse element is available over the thickness of the web. Shear stresses due to torsion are not calculated correctly in this coarse elements. For obtaining accurate torsion stresses at least three quadratic elements in the web thickness are needed (Chapter 4).

2. It is possible to develop an accurate physically non-linear model for one girder. In this model the cracking can be analysed. However, it is difficult to determine a realistic loading to this girder. In theory the linear elastic displacements, determined with the linear elastic model of the bridge, can be imposed to the girder. Firstly this takes a lot of time. Secondly, the local applied deformations and other imperfections lead to wrong stresses in the model. Despite these difficulties the developed model gives a good estimation of the available uncracked zone in the girder (chapter 5).

3. Using a hand calculation to determine the torsion shear stresses at the height of the centre of gravity is conservative. This calculation leads to 40% higher results. This is due to the different phi-distributions in the cross-section used in the hand calculation and the real cross-section. In the real cross-section the phi distribution is maximal in the thickened part of the web and in the flange, the shear stresses are attracted to these zones. This causes a substantial decrease of torsion shear stresses at the height of the centre of gravity. The program Scia Engineer can be used to calculate the shear stresses, a sufficient refined mesh is necessary (Chapter 6).

4. The occurring torsional moments can be determined using the rotations of the first ZIP girder, determined with the linear elastic model of the bridge. From this analysis it follows that the torsion moment is not carried by restrained warping (normal stresses) but mainly by pure torsion (shear stresses). Only in the support area restrained warping has some influence which is largest for the model with an end diaphragm beam (Chapter 7).

5. For the determination of the force distribution in the bridge an orthotropic plate model (Scia Engineer) and a volume model (ATENA 3D) can be used. Comparison of the results from these models show that the shear forces correspond reasonable. However, the torsional moments deviate substantially. This is remarkable because both models are linear elastic which should be comparable (Chapter 7).

6. In the report two load cases are investigated. Using a plastic calculation of the stresses both load cases produce comparable principal stresses. Using the elastic calculation the load case of Minalu produces governing principal stresses.

7. From the calculation of the principal stresses it follows that in the first ZIP girder of the skew bridge in ultimate limit state a large uncracked zone is available. Important is that the stresses within the bond length must be evaluated, depending on the permitted plastic redistribution (Chapter 7). Implicitly this conclusion is also valid for the serviceability limit state. For the straight bridge a comparable uncracked zone will be found because comparable shear forces, but lower torsional moments will occur compared with a skew bridge.

Recommendations

A. The project is started making a time-consuming physical non-linear finite element model. It is important to make first hand calculations and linear elastic finite elements when a similar research project is intended. When necessary a physical non-linear model can be developed.

B. The principal stresses in this research are compared with static tension strengths of concrete. The calculation of fatigue is not incorporated in this research. In the case of a fatigue calculation the tension strength is reduced but also other load configurations must be used. This calculation must be carried out to be sure that the girder also following that calculation contains a large uncracked zone.

C. The presented research can be used to reduce the amount of reinforcement in the uncracked zone to the minimum demands. From research of one bridge with particular geometric properties no general law can be derived. However, a possible procedure can be presented to check if the advantage of the uncracked zone can be used, for a bridge using ZIP girders.

   Possible procedure:

   1) First a distribution calculation must be carried out in which the torsional stiffness is not reduced. The load cases of this report must be considered as a minimum.
   2) The prestressing can be calculated using the standard procedures in serviceability limit state. Important is that no flexural cracks will occur in the top of the beam at the ends.
   3) The length of the uncracked area in ultimate limit state can be determined using the point where the bending moments cause a tension stress. It is safe to avoid any tension stress for this calculation. It is possible that for this calculation the load case for maximal bending in the girder is governing.
   4) The shear stress distribution due to torsion in the cross-section can be determined using Scia Engineer. It is conservative to do this with a simplified hand calculation. The torsion shear stresses can be calculated elastically or plastically. The shear stresses due to shear force can be calculated using the known formula. These two components can be summed up elastically or plastically.
   5) The occurring normal stress varies over the height of the girder. Important is the normal stress at the height of the centre of gravity. The height of the centre of gravity varies for a ZIP-girder and the combined system. The governing height will be somewhere in between these boundaries. When one of the centres of gravity is chosen the reduction due to the bending moments around the other centre of gravity must be incorporated (Figure 10-17). In this research the reduction of the normal stress was at most 6% due to this effect. The advantageous effect of the prestressing in the ultimate limit state must be reduced by multiplying the prestressing force with a factor 0.9.
   6) In the uncracked zone the principal stress can be calculated from the found normal and shear stresses at the governing height. When this stress is below the limits can be concluded that the girder is uncracked. The assumption to take full torsional stiffness in the orthotropic plate model is correct in this case. The minimal reinforcement for shear and torsion must be applied following the Eurocode.

Evaluation

This master project was not a straightforward process. A short description of the occurred problems is given.

Process

The first idea was a research to compressive membrane action (CMA) in ZIP bridge decks with a comparison between the situation with and without end diaphragm beam. At the start meeting a large 3D-model is discussed for a skew and a straight bridge. In this model the effects of CMA and torsion could be investigated. For that model all reinforcement must be calculated by doing a calculation of a whole bridge. Also a short literature study to the effects of CMA and torsion must be done.

When this work was finished, some months later making a large physical non-linear model was started. In the second meeting this idea was discussed further. First some attempts are done combining physically non-linear behaviour and linear elastic elements. This did not work. But it was not decided unanimously to stop making a large physical model. Dobromil Pryl, employer of Cervenka Consulting, believed that it must be possible to model this bridge physical non-linear. That was the reason to continue making the model. After some months of trial-and-error it was decided that it is not possible to make this model. In this stage it was decided to focus on torsion and forget about CMA.

Generating a good alternative was complex. A system is applied using a large linear elastic model to determine the deformations and a small physically non-linear model on which the deformations are applied. In this small physically non-linear model the effects of torsion on cracking should be visible. In the large linear elastic model no reinforcement is applied. In the small physically non-linear model only prestressing and the standard reinforcement at the ends of the girders is applied.

When the deformations were determined (a lot of work) and applied on the small physically non-linear model no torsion cracks were visible, this leads at that moment to the conclusion that in ULS no torsion cracks will occur. At that moment Van der Veen asked for an analytical calculation to be sure that the model is correct and reliable.

This analytical calculation is done using hand calculations and using the found torsional moments with a Scia orthotropic plate model and the analyses from ATENA. From this calculation follows that the load case of Minalu will give shear/torsion cracking based on the elastic distribution of stresses. After making this calculation again the ATENA small physically non-linear model was studied. That model resulted in too low shear stresses. The reason for this is that the large linear elements in the small physical non-linear model do not calculate the torsion stresses correctly. This is of course an important reason that no torsion cracks occur, so refinement of the interesting zones is of importance. So based on the calculations the models must be carried out again with refinement.

A critical reflection of the calculation of torsion stresses using the program ShapeBuilder was carried out. Doing this it was found that it is quite conservative to calculated torsion shear stresses by dividing the cross-section in rectangles. This result gives a better correspondence between the found stresses in the ATENA model and the calculated stresses.

Evaluation

Evaluating the process it is clear that lot of time is spend on preparation (making calculations) and developing a finite element model while at the end a simple calculation appeared to be sufficient to solve the problem. The most important lesson from this is for me that starting a finite element model without making some calculations is not an effective way of doing research.

When this research had to be repeated the following procedure shall be used:

1. Choose one subject from the beginning of the project.
2. Make first analytical calculations.
3. Carry out linear elastic models.
4. When necessary: carry out physical non-linear models.

Appendices

This appendices are presented in an separate document.

Appendices:

A. Literature research about Compressive membrane action.
B. Comparison calculation skew and straight bridge
C. Determination bond length following the Eurocode.
D. Determination force distribution in prestressed ZIP-girder, including effect of bond length.
E. Detailed information about used finite element model.
F. Simple method to take results from ATENA.
G. Maple sheet to determine torsion in a ZIP-girder using rotations as input.

References

1. Minalu, Kassuhun K. (2010), *Finite element modelling of skew slab-girder bridges*
2. Sengupta, dr. Amlan K. et. al. *Prestressed concrete structures*
3. Hoogenboom, P.C.J. (2010), *Aantekeningen over wringing*
4. Zia and McGee (march-april 1974), *Torsion design of prestressed concrete*, PCI Journal, page 46 – 65
5. Rangan, B. V. and Hall, A. S. (March 1975), *Design of Prestressed Concrete Beams Subjected to Combined Bending, Shear and Torsion*, ACI Journal, American Concrete Institute, Vol. 72, No. 3, page 89 – 93
6. Blauwendraad, Prof.dr.ir.J. (2006), *Plate analysis, Theory and Application.*
7. Eurocode 1991-2: *Actions on structures, traffic loads on bridges*.
8. Eurocode 1992-1-1: *Design of concrete structures, General rules and rules for buildings.*
9. Eurocode 1992-2: *Design of concrete structures, Concrete bridges design and detailing rules.*
10. ATENA 3D manuals, available on the website www.cervenka.cz

List of figures

List of tables